Control of vehicle platoons and traffic dynamics: catch-up coordination and congestion dissipation

MLADEN ČIČIĆ

Licentiate Thesis in Electrical Engineering
School of Electrical Engineering and Computer Science
KTH Royal Institute of Technology
Stockholm, Sweden 2019

KTH Royal Institute of Technology
School of Electrical Engineering and Computer Science
Department of Automatic Control
SE-100 44 Stockholm
SWEDEN

TRITA-EECS-AVL-2019:1
ISBN 978-91-7873-024-7

Akademisk avhandling som med tillstånd av Kungliga Tekniska högskolan framlägges till offentlig granskning för avläggande av teknologie licentiatexamen i elektro- och systemteknik måndag den 21 januari 2019 klockan 10:00 i sal Q2, Malvinas väg 10, Q-huset, våningsplan 2, KTH Campus, Stockholm.

Tryck: Universitetsservice US AB

Abstract

Traffic congestion is a constantly growing problem, with a wide array of negative effects on the society, from wasted time and productivity to elevated air pollution and increased number of accidents. Classical traffic control methods have long been successfully used to alleviate congestion, improving the traffic situation of many cities and highways. However, traffic control is not universally employed, because of the necessity of installing additional equipment and instating new legislation.

The introduction of connected, autonomous vehicles offers new opportunities for sensing and controlling the traffic. The data that most of the vehicles nowadays provide are already widely used to measure the traffic conditions. It is natural to consider how vehicles could also be used as actuators, driving them in a specific way so that they affect the traffic positively. However, many of the currently considered strategies for congestion reduction using autonomous vehicles rely on having a high penetration rate, which is not likely to be the case in the near future. This raises the question: How can we influence the overall traffic by using only a small portion of vehicles that we have direct control over? There are two problems in particular that this thesis considers, congestion wave dissipation and avoidance, and platoon catch-up coordination.

First, we study how to dissipate congestion waves by use of a directly controlled vehicle acting as a moving bottleneck. Traffic data can help predict disturbances and constraints that the vehicle will face, and the individual vehicles can be actuated to improve the overall traffic situation. We extend the classical cell transmission model to include the influence of a moving bottleneck, and then use this model to devise a control strategy for an actuator vehicle. By employing such control, we are able to homogenize the traffic without significantly reducing throughput. Under realistic conditions, it is shown that the average total variation of traffic density can be reduced over 5%, while the total travel time increases only 1%.

Second, we study how to predict and control vehicles catching up in order to form a platoon, while driving in highway traffic. The influences of road grade and background traffic are examined and vehicles attempting to form a platoon are modelled as moving bottlenecks. Using this model, we are able to predict how much the vehicles might be delayed because of congestion and adjust the plan accordingly, calculating the optimal platoon catch-up speeds for the vehicles by minimizing their energy consumption. This leads to a reduction of energy cost of up to 0.5% compared to the case when we ignore the traffic conditions. More importantly, we are able to predict when attempting to form a platoon will result in no energy savings, with approximately 80% accuracy.

Sammanfattning

Trafikstockning är ett ständigt växande problem, med ett brett utbud av negativa effekter på samhället, från bortkastad tid och produktivitet till ökade mängd luftföroreningar och antal olyckor. Klassiska metoder för trafik kontroll har länge använts framgångsrikt för att lindra detta problem, med förbättrad trafiksituation för många städer och motorvägar. Trafikkontrollen är emellertid inte universellt tillämpad eftersom den är beroende av ytterligare utrustning och ny lagstiftning som behöver installeras och införas.

Införandet av uppkopplade, autonoma fordon medför nya möjligheter att mäta och kontrollera trafiken. Data som de flesta fordon tillhandahåller redan idag används allmänt för att mäta trafikförhållandena. Det är naturligt att överväga hur fordon också skulle kunna användas som ställdon, genom att driva dem på ett visst sätt så att de påverkar trafiken positivt. Men många av dagens strategierna för trängselnedsättning med hjälp av autonoma fordon är beroende av att de tillämpas av en stor del av fordonen, vilket sannolikt inte kommer att bli fallet inom en snar framtid. Det väcker frågan: Hur kan vi påverka den totala trafiksituationen genom att kontrollera en liten del av fordonen? Det finns två problem specifika problem som den här avhandlingen tar hänsyn till, trängselvågsavledning och –undvikande samt koordinering av fordonståg av lastbilar.

I det första problemet studerar vi hur vi kan skingra trängselvågor med hjälp av ett direktstyrt fordon som fungerar som en rörlig flaskhals. Trafikdata kan hjälpa till att förutsäga störningar och begränsningar som fordonet kommer att stöta på, och de enskilda fordonen kan styras för att förbättra den totala trafiksituation. Vi utvidgar den klassiska cellöverföringsmodellen för att inkludera påverkan av en rörlig flaskhals och använder sedan denna modell för att utforma en kontrollstrategi för ett styrbart fordon. Genom att använda sådan styrning kan vi homogenisera trafiken utan att avsevärt minska genomströmningen. Under realistiska förhållanden visar vi att den genomsnittliga totala variationen i trafiktäthet kan minskas med över 5%, medan den totala körtiden ökar med endast 1%.

I det andra problemet studerar vi hur vi kan förutsäga och styra fordonens hastighetsprofiler vid formering av fordonståg under körning i motorvägstrafik. Påverkan av väglutning och motorvägstrafik undersöks, och fordon som försöker bilda en fordonståg modelleras som rörliga flaskhalsar. Med denna modell kan vi förutsäga förseningar på grund av trängsel och justera planen i enlighet med dessa, samt beräkna de optimala hastigheterna för fordonen genom att minimera energiförbrukningen. Detta leder till en minskning av energikostnaden på upp till 0,5% i jämförelse med fallet när vi ignorerar trafikförhållandena. Ännu viktigare är att vi kan vi förutsäga när försök att bilda ett fordonståg kommer att resultera i utebliven energibesparing, med ungefär 80% noggrannhet.

Acknowledgements

First and foremost, I would like to express my deep gratitude to my supervisor Karl Henrik Johansson for all the support, feedback, guidance, inspiration, as well as the opportunity to work on interesting research topics, that they provided. I have learned much from you, I would also like to thank my co-supervisor, Jonas Mårtensson for all the enjoyable collaboration.

There are many that I have met on this journey that I am thankful to. Special thanks to my co-authors, Kuo-Yun Liang, Li Jin and Giulia Piacentini, as well as Saurabh Amin and Antonella Ferrara. Working with you proved not only fruitful, but also fun and rewarding in more ways than one. I am also very grateful to Anton Selivanov and Mohammad Pirani for feedback and comments on the thesis, and especially to Alexander Johansson, for providing both of these in addition to help with translating the abstract—in very tropical circumstances. It was truly a pleasure working with everyone at the department, and in the oCPS and WASP programmes. To all my colleagues and comrades—far too many to name everyone here—thank you for all the collaboration, help, administrative support, enjoyable atmosphere, courses taken, lunch discussions, barbecues organized, events attended, trips shared, hikes wandered, and all the experiences experienced that have made my PhD life more pleasant.

The research leading to this thesis has received funding from the European Union's Horizon 2020 research and innovation programme, VINNOVA, the Swedish Research Council, the Swedish Foundation for Strategic Research and Knut and Alice Wallenberg Foundation. I am grateful for their support.

Last but not least, a heartfelt thanks goes to my family and friends. This whole endeavour would have been much less worthwhile, much more arduous, and much less likely to come to fruition without the support and encouragement I had from home, wherever home may be.

Mladen Čičić,
Stockholm, December 2018

Contents

Chapter 1

Introduction

INTRODUCING new communication and control technologies into vehicles and transportation infrastructure offers new possibilities to solve the growing traffic congestion problem. Even a small portion of connected collaborating autonomous vehicles on the roads can enable the traffic control centres to directly influence the traffic situation, without the need for building additional road infrastructure, or installing traffic control equipment.

This paradigm offers us a way to utilize the resources that will become available over the course of the slow, partial or complete, transition from human-driven to self-driving vehicles. It is important to understand and model the mutual influence the individual vehicles and the overall traffic have on each other. This understanding would enable us to better predict how some vehicles of interest, such as heavy-duty vehicles and platoons, will actually be able to move in traffic, as well as to develop control strategies that exploit this interdependence. This is the focus of this thesis.

The outline of this chapter is as follows. In Section 1.1 we motivate why using individual vehicles to control the traffic is a promising approach. In Section 1.2 we formulate the problems this work addresses. Lastly, Section 1.3 gives an overview of this thesis, its contents and contributions.

1.1 Motivation

Traffic congestion has been a growing problem for at least as long as there have been cars, and with ever accelerating urbanization, its gravity can only be expected to increase in the future [1]. The negative effect that it has is not limited to wasting road user's time in traffic jams, leading to decreased reliability, efficiency and quality of life. Traffic congestion also increases fuel consumption [2], and as a direct consequence, CO_2 emissions, thus contributing to air and noise pollution. Additionally, it also poses a safety hazard, since it both stresses and frustrates

Figure 1.1: Illustration of connected vehicles. Vehicles communicate with each other (V2V) and with the infrastructure (V2I).

the drivers and increases the risk for collisions due to stop-and-go traffic and low headways.

The advent of autonomous vehicles promises to change the way we think of traffic forever. This technology has the potential to greatly impact virtually all facets of traffic [3], including significantly increasing traffic safety, reducing congestion and fuel consumption, and increasing the efficiency of freight transport, to name but a few. However, many of these benefits hinge on having a high autonomous vehicles market penetration rate. For example, the reservation-based intersection control mechanism [4] outperforms conventional traffic light control with average delays that are two to three hundred times lower—but only in case all vehicles are autonomous. Including even a small number of human drivers would lead to a sharp performance deterioration, and traditional traffic lights become a preferred strategy if the portion of human drivers is significant.

A number of major car manufactures promise to have fully autonomous cars in highway driving scenarios in the early 2020s [5]. Alongside them, we can expect vehicles communicating with other vehicles and with the infrastructure (See Fig. 1.1) [6]. Even if these predictions materialize, it will take decades for the market penetration rate to become high enough for some of the benefits to become significant [7]. For example, Shladover et al. [8] estimate that we can achieve 90% higher lanes'

Figure 1.2: A phantom traffic jam in effect. Vehicles at a standstill are circled in red.

capacity if we have a 80% market penetration rate of cooperative adaptive cruise control (CACC), but with low market penetration rates around 10%, the increase in capacity drops to only 1%. Therefore, in order to successfully deal with the transition period, we have to answer the following question: "How can we influence the overall traffic by using only a small portion of vehicles that we have direct control over?" This notion of regulating the macroscopic traffic conditions by acting at a microscopic level is the centrepiece of emerging traffic control strategies.

If the traffic volume exceeds the road capacity, there is little that can be done to reduce the congestion other than rerouting some of the traffic to other roads [9]. However, if the traffic density is close to the critical density, it is possible for the actions of individual drivers to cause traffic jams. For example, an aggressive lane change can force the driver in front of which the lane changing vehicle cut in to brake. This breaking in turn forces the driver behind to break harder, and the disturbance propagates upstream, amplified until the point some car is forced to come to a full stop, and a so-called phantom traffic jam, shown in Fig. 1.2, is formed.

Figure 1.3: Heavy-duty vehicles in a platoon. Image courtesy of Scania.

Individual vehicles can, under some circumstances, also help prevent or dissipate congestion waves. The notion of “jam-busting” or “jam-absorbing” driving techniques has been discussed, not only in research [10, 11], but also in media [12]. These techniques offer guidelines to the drivers, for example to leave a large gap in front of them and drive at the average speed of the surrounding traffic. By doing this, the driver is less likely to be forced to break aggressively if another car cuts in front of them, while also leaving enough space for cars to change lanes and move towards the exit lane or merge into the mainstream from merging lanes. Although this strategy focuses on vehicle interaction at a microscopic level, we may think of extending this approach to a higher layer of control. A similar idea, but in the macroscopic traffic model with moving bottlenecks, will be explored in Chapter 4.

Automated heavy-duty vehicle platooning, shown in Fig. 1.3, is expected to enter the traffic at an accelerated pace [13]. Since these vehicles are typically moving slower than the rest of the traffic, they naturally act as moving bottlenecks. In the future, we can expect fleet management systems to employ some centralized remote control over vehicles, using vehicle-to-infrastructure (V2I) communication to enable advanced route planning [14]. Since in addition, these vehicles would send their status to the fleet management system and receive reference speed profiles to follow, this makes them an ideal candidate for in-flow traffic actuators. It is therefore important to understand how controlling these vehicles can affect the

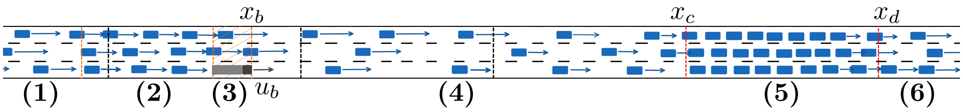

Figure 1.4: Congestion wave dissipation problem. The road can be split into six zones: (1) unaffected oncoming vehicles, (2) congestion upstream of the moving bottleneck, (3) moving bottleneck zone, (4) "starvation" zone downstream of the moving bottleneck, (5) traffic jam, and (6) vehicles discharging from the traffic jam

traffic around them, as well as how the traffic conditions could cause these vehicles to be delayed, thus enabling us to better plan their trajectories. We study how platoon coordination can take traffic conditions into account in Chapter 5.

1.2 Problem formulation

The focus of this thesis is on modelling and control of heavy-duty vehicles, platoons and the rest of traffic, as well as the interaction between them. There is a mutual influence between the individual vehicles and the surrounding traffic that in many cases cannot be ignored, and needs to be modelled. In particular, we are interested in modelling the influence that heavy-duty vehicle platoons have on other vehicles. Since these platoons consist of large vehicles that typically move slower than the rest of the traffic, they can be modelled as moving bottlenecks. The effect of moving bottlenecks can be captured either as an extension of the classical cell transmission model (CTM), or in the framework of multi-class CTM. Traffic data can help better predict disturbances and constraints that the vehicle of interest will face, and individual vehicles can be used as actuators, in order to improve the overall traffic situation. In the rest of this section, we will present these problems in more detail.

Congestion wave dissipation and avoidance problem

The traffic scenario in which we consider this problem is shown in Figure 1.4. A vehicle that we control is approaching a congestion wave stretching from $x_c(t)$ to $x_d(t)$ at time t. The congestion wave will evolve according to the traffic dynamics, with vehicles leaving from its downstream end at some rate, and new vehicles arriving at its upstream end. Effectively, the congestion wave will propagate backwards, and shrink or grow according to the difference of outflow and inflow.

The position of the vehicle is $x_b(t)$, and its speed can be controlled within some limits, $u_b(t) \in [u_{\min}, u_{\max}]$. If the controlled vehicle is slower than the surrounding traffic, it acts as a moving bottleneck and limits the traffic flow that can go past it, thus creating a zone of lower traffic density between it and the traffic jam ("starvation" zone), and also delaying some of the traffic flow that reaches the traffic jam.

By doing this, a congestion is formed upstream of the moving bottleneck, but if the vehicle is suitably controlled, this congestion will be less severe and harmful than the one in the congestion wave.

The congestion wave dissipation and avoidance problem entails calculating the controlled vehicle speed that is optimal with regard to some cost function. There are two main directions from which we can approach this problem—from the perspective of the controlled vehicle and from the perspective of the overall traffic.

From the perspective of the controlled vehicle, the goal is to avoid the traffic jam with minimum delay. This objective can be expressed as an optimization problem

$$\begin{aligned} \underset{u_b \in [u_{\min}, u_{\max}]}{\text{minimize}} \quad & \text{controlled vehicle travel time} \\ \text{subject to} \quad & \text{controlled vehicle dynamics and constraints} \\ & \text{traffic with a moving bottleneck,} \end{aligned}$$

where controlled vehicle constraints include the condition that the vehicle never enters the congestion wave.

The other option is to consider the problem from the perspective of the overall traffic, in this case optimizing some performance indices. In this case, the optimization problem is

$$\begin{aligned} \underset{u_b \in [u_{\min}, u_{\max}]}{\text{minimize}} \quad & \text{traffic performance index} \\ \text{subject to} \quad & \text{controlled vehicle dynamics and constraints} \\ & \text{traffic with a moving bottleneck.} \end{aligned}$$

In Chapter 4, we will focus on the first optimization problem, but also discuss the second. The two objectives are related and compatible, so we will show that by applying the speed at which the controlled vehicle avoids the traffic jam with minimal delay, we also improve the traffic performance.

Platoon catch-up coordination problem

Consider the simplest platoon catch-up problem, illustrated in Figure 1.5. Assume a potential platooning pair, driving along the common stretch of road, has been identified by a platooning coordinator at a higher decision layer. These two vehicles

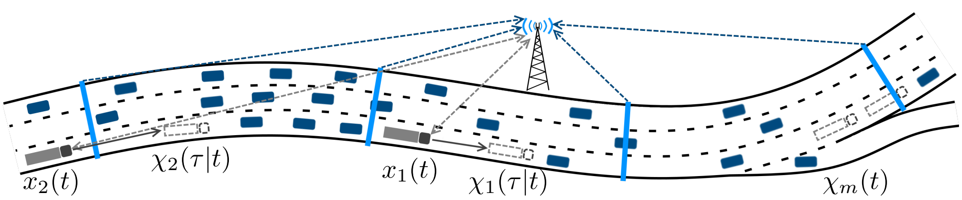

Figure 1.5: Platoon catch-up problem.

adjust their speeds so that the leader (the vehicle farther ahead, $i = 1$) drives slower than the follower ($i = 2$), so that they would meet and merge into a platoon at some point. Their state at time t is given by their positions $x_i(t)$ and their speeds $v_i(t)$, so we have that $x_1(t) > x_2(t)$ and $v_1(t) < v_2(t)$.

Considering a discrete time instant t, we define the continuous time τ so that the next time instants $t+k$ correspond to $\tau = kT$, where T is the sampling period. We can then adopt a relative coordinate system so that at time $\tau = 0$, the leading vehicle's position is $\chi_1(0|t) = \chi_0 = x_1(t) - x_2(t)$, and the following vehicle's position $\chi_2(0|t) = 0$. Time τ denotes the prediction time after the time instant t, i.e., $x_i(t+k) = \chi_i(kT|t)$, $k = 1, 2, \ldots$. The dynamics of the vehicles for $\tau > 0$ can thus be written

$$\dot{\chi}_1(\tau) = v_1(\tau),$$
$$\dot{\chi}_2(\tau) = v_2(\tau),$$

with $\chi_1(0) = \chi_0$, $\chi_2(0) = 0$.

The distance between the vehicles is $d = \chi_1 - \chi_2$. We say that the vehicles merge into a platoon at time τ_m if the distance between them is lower than some predefined distance d_p for the first time,

$$\tau_m = \min\left\{\tau | d(\tau) \leq d_p\right\}, \tag{1.1}$$

and the position of the merge as the position of the follower vehicle at the time of the merge,

$$\chi_m = \chi_2(\tau_m) = \chi_1(\tau_m) - d_p. \tag{1.2}$$

In the simplest case, vehicles attempt to drive at some constant desired speeds u_1 and u_2 until they have successfully merged into a platoon, and then proceed together driving at speed u_p.

There are two parts of this problem that we study: predicting when and where the platoon merging will occur assuming we know how vehicle speed is controlled, and calculating vehicle catch-up speeds that are optimal with regard to some metric. Both parts are covered in Chapter 5.

1.3 Thesis outline and contributions

In this section, we provide an overview of the thesis. We describe each chapter's content and contribution, and indicate the publications on which they are based.

Chapter 2 Background

In this chapter, we provide the background of the thesis. We discuss how the traffic congestion problem is addressed in the literature, and how the introduction of new technologies can change this. Using intelligent vehicles as moving bottleneck for traffic control is particularly pointed out. Finally, we discuss how platoon coordination systems can be used to fulfil this role, as well as how insights from traffic models with moving bottlenecks can be used to improve platoon operations planning.

Chapter 3 Traffic and platooning models

In this chapter, we give models of traffic and platoons, both from the literature, as well as contributed by the author.

We present the traffic models, discuss how they relate to each other, and then study how trucks and platoons can be introduced to these models as moving bottlenecks. The models from this chapter are then mostly used in the following chapters, but some are included for completeness of the overview.

This chapter is based on the author's modelling work in the following publications:

- M. Čičić and K. H. Johansson, "Traffic regulation via individually controlled automated vehicles: a cell transmission model approach," in *21st IEEE International Conference on Intelligent Transportation Systems (ITSC)*, Maui, US, 2018

- M. Čičić and K. H. Johansson, "Energy-optimal platoon catch-up in traffic in moving bottleneck framework," in *European Control Conference (ECC)*, Naples, Italy, 2019, Submitted

- L. Jin, M. Čičič, S. Amin, and K. H. Johansson, "Modeling the impact of vehicle platooning on highway congestion: A fluid queuing approach," in *Proceedings of the 21st International Conference on Hybrid Systems: Computation and Control (part of CPS Week).* ACM, 2018, pp. 237–246

Chapter 4: Congestion wave dissipation and avoidance

In this chapter, we study the potential of using individual automated vehicles to control the surrounding traffic. We consider the scenario when the automated vehicle (or platoon) acts as a moving bottleneck for the rest of the traffic. The control strategy was tested on a simulation where the controlled vehicle helping clear a congestion wave downstream, while also avoiding running into congestion itself.

This chapter is based on the control part of the publication:

- M. Čičić and K. H. Johansson, "Traffic regulation via individually controlled automated vehicles: a cell transmission model approach," in *21st IEEE International Conference on Intelligent Transportation Systems (ITSC)*, Maui, US, 2018

Chapter 5: Platoon catch-up coordination

In this chapter, we address the problem of coordinating the process of vehicles catching up and forming a platoon while driving on a highway. First we discuss predicting the vehicle trajectories during the catch-up phase, and using these predicted trajectories to estimate when and where the vehicles will merge into a platoon. Here, we use the data obtained from an experiment to learn the vehicles' control law and dynamics, and use the information about the road grade to achieve better prediction of platoon merging position. Second, we calculate optimal catch-up speeds for the vehicles attempting to form a platoon. We consider the mutual influence between the controlled vehicles and the traffic, and calculate energy-optimal catch-up speed pairs.

This chapter is based on the following publications:

- M. Čičić, K.-Y. Liang, and K. H. Johansson, "Platoon merging distance prediction using a neural network vehicle speed model," *IFAC-PapersOnLine*, vol. 50, no. 1, pp. 3720–3725, 2017
- M. Čičić and K. H. Johansson, "Energy-optimal platoon catch-up in traffic in moving bottleneck framework," in *European Control Conference (ECC)*, Naples, Italy, 2019, Submitted

Chapter 6: Conclusions and future work

Finally, in this chapter we conclude the thesis, summarizing and discussing the results, and outline some future and ongoing work, indicating some possible directions in which this work can be extended.

Contribution by the author

The order of the author names reflects the workload, where the first has the most important contribution. In all listed publications, all authors were actively involved in formulating the problems, developing the solutions, evaluating the results, and writing the paper.

Chapter 2

Background

THIS chapter provides some background on a number of topics relevant to the rest of the thesis. Since the thesis deals with control of automated vehicles and traffic, it falls within the scope of intelligent transportation systems (ITS). We give a brief overview on ITS, including established traffic control technologies as well as new technologies. One of the new approaches is microscopic actuation in macroscopic traffic, which holds the central place of this thesis. Heavy-duty vehicle platoons are a significant part of the thesis, since their interaction with the rest of the traffic follows the same mechanism that we use for actuation. Finally, the different behaviour that automated vehicles have compared to human-driven vehicles necessitates handling these two classes of vehicles separately in traffic models. These topics are discussed in this chapter.

2.1 Intelligent transportation systems

Conventionally, the problem of traffic congestion would be tackled either by increasing the capacity of the road network, by adding more lanes or new links and routes, or by reducing the number of vehicles that use the road network, using various policy approaches such as congestion pricing [19] and other incentive schemes [20]. Mitigation of excess demand typically requires costly investment in transportation infrastructure, and it may produce undesirable side-effects [21], as well as have a negative impact on the environment. Building new infrastructure is therefore a decreasingly attractive solution, and it is desirable to attempt to solve this problem by other, more cost-efficient, means.

Apart from excess demand, traffic congestion can also be caused by poor traffic management [22], or conflicts between traditional and new traffic management [23]. Although not universally employed, the traditional methods of traffic control, such as variable speed limits [24, 25, 26], ramp metering [27, 28, 29] and their combinations [30, 31, 32] have successfully been used to manage traffic systems, improve their efficiency and reduce congestions. These control strategies rely on traffic monitoring infrastructure consisting of inductive loops detectors, cameras and radars, and communicate or enforce their control actions by use of traffic lights or variable-message signs. Although the cost of installing additional equipment is much lower than the cost of expanding or building new roads, it is not negligible. Furthermore, the fact that the required equipment is fixed at certain locations reduces the flexibility of these systems, since they're only able to control the traffic flow at certain points.

These relatively old traffic control strategies are a part of the wider and newer trend of ITS [33, 34]. The new technologies include “intelligent” vehicles with varying levels of vehicle-to-vehicle and vehicle-to-infrastructure communication capabilities [35], and varying degrees of autonomy, such as those equipped with adaptive cruise control (ACC) and collaborative ACC (CACC) [36], and platooning systems [14]. In addition to reducing traffic congestion simply by virtue of being able to drive more smoothly or with lower headways [8, 17], these vehicles can be used for sensing traffic by providing floating car data [37, 38], and for controlling traffic [39, 40].

2.2 Mixed traffic models

All these traffic control strategies require at least some basic traffic model, either for testing and tuning control parameters through simulations, directly setting the parameters based on a model, or even directly calculating the control action using optimization-based control such as model predictive control (MPC). For an overview on different types of traffic models, the reader is referred to [41, 42, 43], and to [44] for a historical view.

One class of widely used traffic models are the microscopic traffic models. In these models, the traffic evolution is described through the longitudinal (car-following) and lateral (lane-changing) behaviour of each single vehicle. This high level of complexity allows microscopic traffic models to replicate real-life traffic conditions with high fidelity, at the cost of requiring numerous parameters to be properly calibrated. Car-following (or follow-the-leader) models describe how drivers follow the preceding vehicle (leader). Some of the most well-known car-following models are Gazis-Herman-Rothery model [45], Gipps model [46] and Intelligent Driver Model [47, 48]. Recently, efforts have been made to model the car-following behavior by using artificial neural networks [49], specifically aimed at capturing some emergent phenomena such as stop-and-go waves. There exist many commercial traffic simulators that use microscopic traffic models, e.g. Aimsun [50] and Vissim [51], as well as open-source traffic simulators such as SUMO [52].

The behaviour of intelligent vehicles, heavy-duty vehicles and platoons can significantly differ from the behaviour of human-driven passenger cars, at least in some specific scenarios, which motivates considering them as different flows. Driving behaviour heterogeneity in car-following models was studied in [53]. Even if all vehicles have the same driving behaviour, we might want to classify them based on their destination or route, in order to be able to correctly model their behaviour at off-ramps and diverges. Since microscopic traffic models typically allow for vehicles to have different parameters, modelling different classes of traffic in them can often be straightforward. For example, this can be done by setting different reaction times to human drivers, ACC-enabled and CACC-enabled vehicles in Improved Intelligent Driver Model, as was done in [40].

Modelling different classes of vehicles in macroscopic traffic models is more challenging, and there are numerous different approaches to choosing the parameters that will differ across the classes. In [54] the authors present a generalization of the Lighthill-Whitham and Richards (LWR) traffic flow model, with different classes having different free flow speeds, and [55] gives a multi-class gas-kinematic traffic model. The model from [56] distinguishes between different classes of traffic by allowing for different reaction times for each (with automated vehicles having a shorter reaction time than human-driven vehicles), leading to congestion wave speed that depends on the ratio of automated vehicles in traffic. Conversely, in [57], different classes of traffic are allowed separate fundamental diagrams, and traffic flow is allocated between them based on how much space they take on the road. While in [57] the space the vehicle take was a constant, in [58] a model is proposed where the personal car equivalent of heavy vehicles is dynamically depending on the speeds of the vehicles. The model given in [59] captures the overtaking and creeping behaviour, where small vehicles are able to advance even though larger vehicles are not moving. Some other notable macroscopic multi-class traffic models include [60] and [61].

2.3 Microscopic actuation in macroscopic traffic

A large portion of solutions that rely on autonomous vehicles suffer from the lack of communication and cooperation from older and less technologically advanced vehicles. However even if the ratio of intelligent vehicles is small, we can influence the surrounding traffic by using them as Lagrangian (in-flow) actuators. A notable example of this is given in [62], where one autonomous vehicle was able to dissipate and prevent emergence of stop-and-go waves, as predicted in [63]. Stop-and-go, or congestion waves, are traveling ripples in traffic density on highways, as demonstrated in circle road experiments [64] and modeled in theory [65]. Other jam-absorption driving strategies have also been proposed in the literature [10, 11].

While multi-class traffic models are appropriate for modelling the interaction of different vehicle classes, they are often unable to describe the effect individual vehicles can have on the rest of the traffic, at least in their basic form. One notable way a single vehicle can affect the overall traffic is by acting as a moving bottleneck. If a vehicle moves slower than the surrounding traffic, it affects the traffic flow by limiting the number of vehicles that can pass it. In order to model this effect, we may impose some additional local constraints on the traffic flow in the area close to the slow–moving vehicle. In the literature, moving bottlenecks have predominantly been considered in PDE traffic models [66, 67, 68, 69], but also in an experimental and empirical way [70], or in the framework of kinematic wave theory [71].

There exist a multitude of second- or higher-order models in the literature, like the Aw-Rascle-Zhang model [72], or METANET [73], which are widely used. However, introducing second-order dynamics would make the analysis and introducing moving bottlenecks much less tractable.

While moving bottlenecks are usually seen as detrimental to traffic efficiency, the prospect of controlling them for traffic regulation has attracted some attention lately. Since this is a new traffic control approach, very few published works exist on this topic as of writing of this thesis, but we can forecast much interest in this field in the near future. In [74] the authors considered an optimal control problem using the speed of the moving bottleneck as control variable and fuel consumption as the performance metric. A similar mechanism was exploited for bottleneck decongestion in [75], though here the controlled automated vehicles were not used as moving bottlenecks, but instead simply held up other vehicles in a microscopic traffic model.

2.4 Platoons in traffic

Recent years have seen an accelerated push towards heavy-duty vehicle platooning [14], with numerous projects working on it [13]. Traditionally, such platooning was primarily regarded as means of reducing the air drag acting on the vehicles [76], and thus fuel consumption, but there are also other benefits, like facilitating a higher level of automation. There has been much work done on controlling the vehicles inside a platoon [77, 78, 79, 80], and this technology is slowly transitioning from academia to industry. There are other aspects of platooning that still require more research, including how truck platoons influence traffic, how platoons should be formed, and how to make decisions on which vehicles should platoon with which other vehicles [81].

Real-time platoon formation, where vehicles attempt to form platoons en-route, is one of these open problems. Dynamic planning strategies have been proposed, with platooning coordinator matching and organizing vehicles into platoons [82]. Selected vehicles receive jointly fuel-optimal speed profiles and routes, and by following them, merge into a platoon and drive together for some time. However, this also means that, since the participating vehicles will have to deviate from their own optimal speed profiles, attempting to form a platoon entails higher fuel consumption during the catch-up and merging phase. The hope is to offset this effect by fuel savings during the time the vehicles drive in the platoon [83]. If the platoon merging is delayed due to some unpredicted disturbance [84], or if the vehicles fail to merge into a platoon, the net energy consumption could be much higher than expected, potentially leading to more fuel being spent compared to the case when the vehicles would continue driving at their individual optimal speeds. It is therefore important to have a good prediction of when the platoon merging will be completed, so as to be able to calculate predicted energy savings and make a better informed decision on whether to attempt to form a platoon at all. This problem was studied in [85] and [86], as well as in [87]. In these papers, however, the authors did consider the influence of traffic, but did not study how to compensate for it.

2.5 Summary

In this chapter we have provided a number of references relevant to the scope of the thesis. First, the ITS were discussed, along with the technological basis for implementing the different control laws that are discussed. Then, we covered the topic of modelling mixed traffic, with various model structures and distinguishing characteristics between vehicle classes. Next, we discussed how microscopic actuation can be introduced to macroscopic models, mostly using the framework of controlled moving bottlenecks. Finally, we provided some background on heavy-duty vehicle platooning. This technology is one of the first that is predicted to enter the mainstream, and could provide suitable candidates for vehicles to use as controlled moving bottlenecks. Conversely, the performance of platooning operations can be improved by also considering the influence of traffic condition in planning.

Chapter 3

Traffic and platooning models

In this chapter we discuss various traffic flow models and extend some of them to incorporate the influence of slow-moving vehicles and platoons acting as moving bottlenecks. A slow-moving vehicle in traffic forces faster moving vehicles to overtake it, restricting the road capacity at the slow-moving vehicle's position. We call this slow-moving vehicle a moving bottleneck. In particular, we are looking for traffic models that can be extended to capture the moving bottleneck phenomenon, in a way that is conducive to control design, which will be the main focus of the next two chapters.

First, we will discuss the traffic flow models that will be used, and then introduce the extensions which capture the influence of slow-moving vehicles and platoons.

3.1 Traffic models

Macroscopic models have the advantage of being relatively easy to simulate and analyse, which makes them suitable for traffic control design. For more in-depth view on traffic models, the reader is referred to [43]. Macroscopic models describe traffic by using aggregate variables such as traffic density $\rho(x, \tau)$, average traffic speed $v(x, \tau)$ and traffic flow $q(x, \tau)$, where x is the position along the road and τ time. These three variables are linked by the hydrodynamic equation,

$$q(x, \tau) = \rho(x, \tau)v(x, \tau). \tag{3.1}$$

Additionally, in a given road segment, the number of vehicles $n(\tau)$ will be a conserved quantity,

$$\dot{n}(\tau) = q_{\text{in}}(\tau) - q_{\text{out}}(\tau), \tag{3.2}$$

where $q_{\text{in}}(\tau)$ is the flow into the segment and $q_{\text{out}}(\tau)$ the flow from the segment. Note that here we use τ to denote the continuous time, and the dot operator represents derivation by τ. We use t to denote the discrete time step.

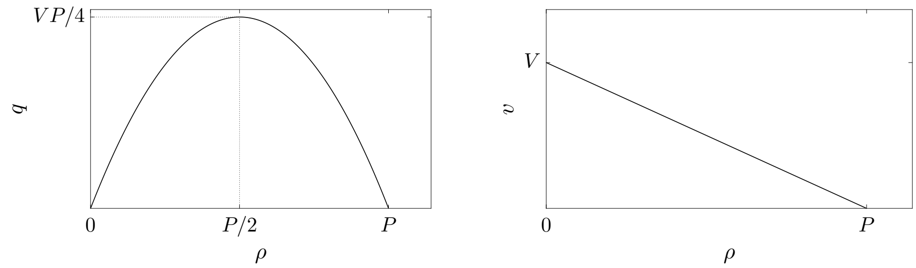

(a) Greenshields

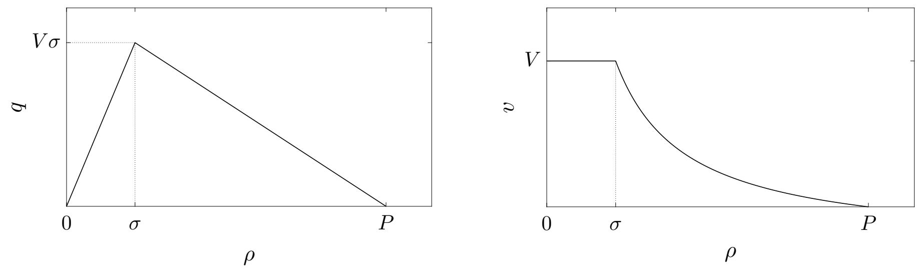

(b) Newell-Daganzo

Figure 3.1: Greenshields and Newell-Daganzo flux function and speed function.

Since here we only consider first-order models, the state of the system will be uniquely determined by the traffic density, and the average speed is given by a function, $\mathcal{V}(\rho(x,\tau))$.

The LWR model

The oldest macroscopic traffic model is the Lighthill-Whitham-Richards (LWR) model [88, 89]. Although it originated in the 50s, this model and its many extensions are still widely used. The model consists of a first-order nonlinear partial differential equation

$$\partial_\tau \rho(x,\tau) + \partial_x Q(\rho(x,\tau)) = 0. \tag{3.3}$$

It is assumed that the traffic flow $q(x,\tau)$ is given as function of $\rho(x,\tau)$,

$$q(x,\tau) = Q(\rho(x,\tau)),$$

or equivalently, that the traffic flow is given by (3.1) where the average speed is a function of $\rho(x,\tau) \in [0,P]$, where P is the maximum, jam traffic density at which the vehicles stop moving.

The function $Q(\rho)$ is known as the fundamental diagram, or the traffic flux function. The two most commonly used fundamental diagrams are the Greenshields [90] flux function and Newell-Daganzo [91, 92] (triangular or trapezoidal) flux function, shown in Fig. 3.1. In this thesis, we will use the latter.

In Greenshields fundamental diagram, traffic speed is given by

$$\mathcal{V}(\rho) = V\left(1 - \frac{\rho}{P}\right),$$

where V denotes the free flow speed, at which the vehicles would be travelling if the rest of the traffic did not affect them. Using this expression to model average traffic speed, makes the traffic flow $Q(\rho) = \rho\mathcal{V}(\rho)$ a parabolic function,

$$Q(\rho) = V\left(\rho - \frac{\rho^2}{P}\right),$$

as shown in Fig. 3.1a. Since this function is once continuously differentiable, (3.3) is a hyperbolic conservation law. This allows us to use the broad body of literature that deals with such systems (see, for example [93, 94]).

Newell-Daganzo flux function is a piecewise linear function (see Fig. 3.1b), and is given by

$$Q(\rho) = \min\left(V\rho, Q^{\max}, W(P-\rho)\right),$$

where W is the backward congestion wave propagation speed (i.e., the negative slope in congested mode, $\rho > \sigma$) and $Q^{\max}$ some maximum traffic flow. We denote by σ the critical density at which $V\sigma = W(P-\sigma)$, and take $Q^{\max} = V\sigma$, so that

$$Q(\rho) = \begin{cases} V\rho, & 0 \le \rho \le \sigma, \\ W(P-\rho), & \sigma < \rho \le P, \end{cases} \tag{3.4}$$

and the traffic speed dependence on traffic density is

$$\mathcal{V}(\rho) = \begin{cases} V, & 0 \le \rho \le \sigma, \\ W\left(\frac{P}{\rho} - 1\right), & \sigma < \rho \le P. \end{cases}$$

Note that Newell-Daganzo flux function is not continuously differentiable, but an arbitrary smoothed version of it is, so (3.3) will be a limit case of a hyperbolic conservation law.

The cell transmission model

Consider a stretch of highway between positions X_i and X_{i+1} with length $L_i = X_{i+1} - X_i$. We can describe the evolution of the number of vehicles inside this "cell", N_i according to the conservation law (3.2), with inflow and outflow depending on the surrounding traffic conditions. This is the original cell transmission model (CTM) [91, 95]. The evolution of traffic density ρ_i in cell i is then given by

$$\rho_i(t+1) = \rho_i(t) + \frac{T}{L_i}\left(\Phi_i^+(t) - \Phi_i^-(t)\right), \quad i = 1, \dots N. \tag{3.5}$$

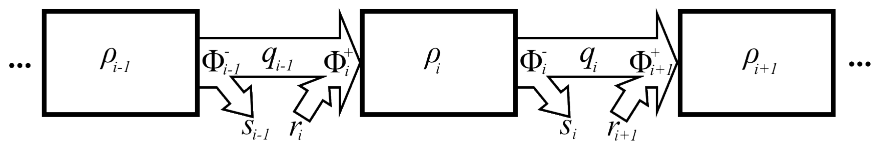

Figure 3.2: A representation of CTM.

Here T is the time step, N the number of cells, and $\Phi_i^+(t)$ and $\Phi_i^-(t)$ are the total flow during one time step into cell i, and out of cell i, respectively, given by

$$\Phi_i^+(t) = q_{i-1}(t) + r_i(t),$$
$$\Phi_i^-(t) = q_i(t) + s_i(t),$$

where q_i is the flow from cell i to cell $i+1$, $r_i(t)$ is the flow entering cell i from the on-ramp, and $s_i(t)$ flow exiting cell i through the off-ramp (see Fig. 3.2). We require T to be short enough so that the Courant-Friedrichs-Lewy condition is satisfied, $V \leq L/T$.

For now, we will assume that all cells are of same length, $L_i = L$ and consider a section that has no on- or off-ramps, $s_i(t) = r_i(t) = 0, i = 1, \ldots, N$. The CTM then reduces to

$$\rho_i(t+1) = \rho_i(t) + \frac{T}{L_i}\left(q_{i-1}(t) - q_i(t)\right), \quad i = 1, \ldots N. \tag{3.6}$$

We can determine $q_i(t)$ as a minimum between a "demand" (sending) function of cell i and "supply" (receiving) function of cell $i+1$,

$$q_i(t) = \min\left(D_i(t), S_{i+1}(t)\right), \tag{3.7}$$

where

$$\begin{aligned} D_i(t) &= \min\left(V_i\rho_i(t), Q_i^{\max}\right), \\ S_i(t) &= \min\left(W_i(P_i - \rho_i(t)), Q_i^{\max}\right). \end{aligned} \tag{3.8}$$

In order to make the model consistent with the LWR model with Newell-Daganzo flux function, we set the congestion wave speeds to $W_i = V_i\frac{\sigma_i}{P_i - \sigma_i}$, so that $V_i\sigma_i = W_i(P_i - \sigma_i)$, and set $Q_i^{\max} = V_i\sigma_i$. Notice that the demand and supply functions can also be written as a function of minimum and maximum, respectively, of ρ and σ,

$$D(\rho, \sigma) = Q(\min(\rho, \sigma)),$$
$$S(\rho, \sigma) = Q(\max(\rho, \sigma)),$$

with parameters specific to the cell for which they are calculated, $V = V_i$, $W = W_i$, $\sigma = \sigma_i$ and $P = P_i$.

We can handle the boundaries of the model by separately defining either the flow into the first cell $q_0(t)$ and out of the last cell $q_N(t)$, or boundary traffic densities $\rho_0(t)$ and $\rho_{N+1}(t)$.

PDE interpretation of the CTM

Although in its original formulation [91] it was conceived as a distinct model, the CTM has been shown [96] to be equivalent to a Godunov (finite volume) discretization of the LWR model, assuming all parameters are the same for all cells, $\sigma_i = \sigma$, $P_i = P$, $V_i = V$, $W_i = W$.

Godunov discretization of (3.3) corresponds to taking piecewise constant initial conditions for $\rho(x, \tau)$,

$$\rho(x,0) = \begin{cases} \rho_0(t), & x \leq X_1, \\ \rho_1(t), & X_1 \leq x < X_2, \\ \quad\vdots & \quad\vdots \\ \rho_i(t), & X_i \leq x < X_{i+1}, \\ \quad\vdots & \quad\vdots \\ \rho_N(t), & X_N \leq x < X_{N+1}, \\ \rho_{N+1}(t), & X_{N+1} \leq x, \end{cases} \tag{3.9}$$

where $\rho_0(t)$ and $\rho_{N+1}(t)$ are the boundary conditions, $\rho(x,0) = \rho_0(t), x < X_1$, and $\rho(x,0) = \rho_{N+1}, x > X_N + L$, solving the initial values problem for time up to $\tau = T$. As stated earlier, we use τ to denote the continuous time in PDE models and t to denote the discrete time step in CTM.

We can then obtain average cell traffic density at the next time step $\rho(t+1)$ by averaging the solution of the PDE $\rho(x,T)$ over the interval corresponding to each cell, (X_i, X_{i+1}). The reader is referred to [94] for more details on handling hyperbolic conservation laws.

Since the flux function (3.4) is piecewise linear, the solution of (3.3), $\rho(x,\tau)$, will be piecewise constant in x for every τ, and it can be calculated exactly by solving Riemann problems for the cell interfaces.

The Riemann problem is the Cauchy problem (problem of finding a solution to a PDE given initial conditions) in the particular case when the initial conditions are given as

$$\rho(x,0) = \begin{cases} \rho_-, & x < 0, \\ \rho_+, & x > 0. \end{cases} \tag{3.10}$$

This corresponds to assuming we have a cell interface at $x = 0$ and looking at the evolution of traffic density around it. The solution of this problem will be a self-similar function of form $\rho(x,\tau) = f(x/\tau)$. If $\rho_- = \rho_+$, the initial conditions are not discontinuous, and the solution will stay constant. Otherwise, the solution can either be a shock or a rarefaction wave. A shock is a solution of form

$$\rho(x,\tau) = f(x/\tau) = \begin{cases} \rho_-, & x/\tau < \lambda \\ \rho_+, & x/\tau > \lambda, \end{cases}$$

where $\lambda = \Lambda(\rho_-, \rho_+)$ is the Rankine-Hugoniot transition speed between ρ_- and ρ_+,

$$\Lambda(\rho_-, \rho_+) = \frac{Q(\rho_+) - Q(\rho_-)}{\rho_+ - \rho_-}.$$

We call such a moving discontinuity a wavefront or a front. A rarefaction wave is a solution of the form

$$\rho(x,\tau) = f(x/\tau) = \begin{cases} \rho_-, & x/\tau \le \alpha, \\ r(x/\tau), & \alpha \le x/\tau < \beta, \\ \rho_+, & x/\tau > \beta, \end{cases}$$

where $r(x/\tau)$ is a monotonic function related to the lower convex envelope of Q if $\rho_- < \rho_+$ or the upper concave envelope of Q if $\rho_- > \rho_+$.

In the particular case of Newell-Daganzo flux function (3.4), the solution to the Riemann problem ((3.3), (3.10)) will consist of one or two wavefronts radiating from the discontinuity, depending on the density upstream of the cell interface, ρ_- and downstream, ρ_+. In case we have a congestion upstream $\rho_- > \sigma$, and free flow downstream $\rho_+ \le \sigma$, the solution will be a rarefaction wave, with two wavefronts,

$$\rho(x,\tau) = \begin{cases} \rho_-, & x < -W\tau \\ \sigma, & -W\tau < x < V\tau, \\ \rho_+, & x > V\tau, \end{cases}$$

as shown in Fig. 3.3c. Otherwise, the solution will be a shock, consisting of one wavefront,

$$\rho(x,\tau) = \begin{cases} \rho_-, & x < \Lambda(\rho_-, \rho_+)\tau, \\ \rho_+, & x > \Lambda(\rho_-, \rho_+)\tau, \end{cases}$$

corresponding to Fig. 3.3a, Fig. 3.3b or Fig. 3.3d, depending on ρ_- and ρ_+. We will be using the style of the upper figures to describe the evolution of solutions in space and time.

The overall solution to (3.3),(3.4) for initial conditions (3.9) can be acquired by solving a composite Riemann problem, i.e., solving a Cauchy problem with piecewise constant initial conditions through solving Riemann problems for all discontinuities in initial conditions (cell interfaces), evolving the solutions in time until some wavefronts originating from these interfaces collide, and then solving the new Riemann problems that thus appear. This procedure is known as front tracking, and since the flux function Q is piecewise-linear, it will yield exact solutions for all $\tau > 0$. In case the flux function is not piecewise-linear, front tracking can still be applied, but the flux function needs to be approximated with a piecewise-linear function.

The multi-class CTM

Multi-class traffic models are often inspired by the introduction of autonomous and connected vehicles, but can also provide a useful tool for capturing uncertainties

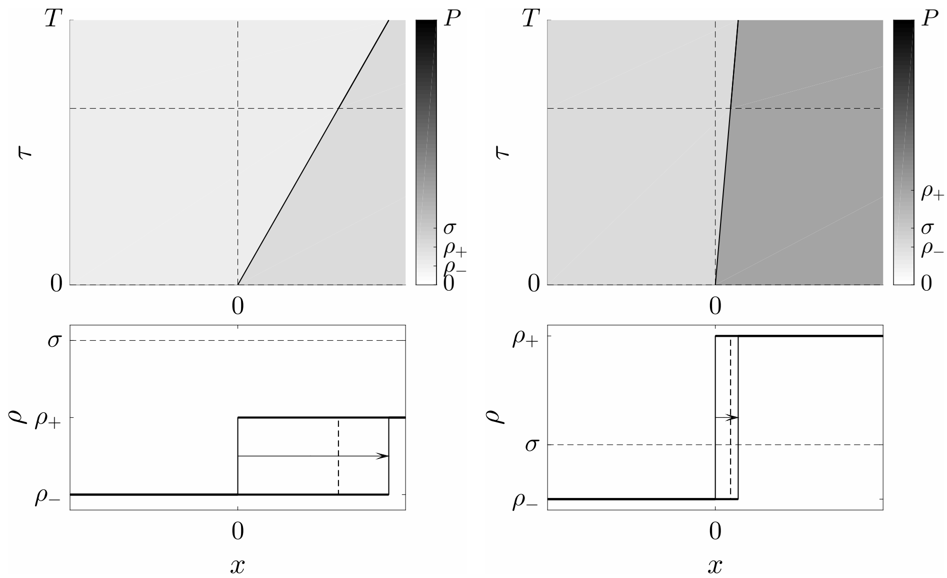

(a) Free flow to free flow (b) Free flow to congested

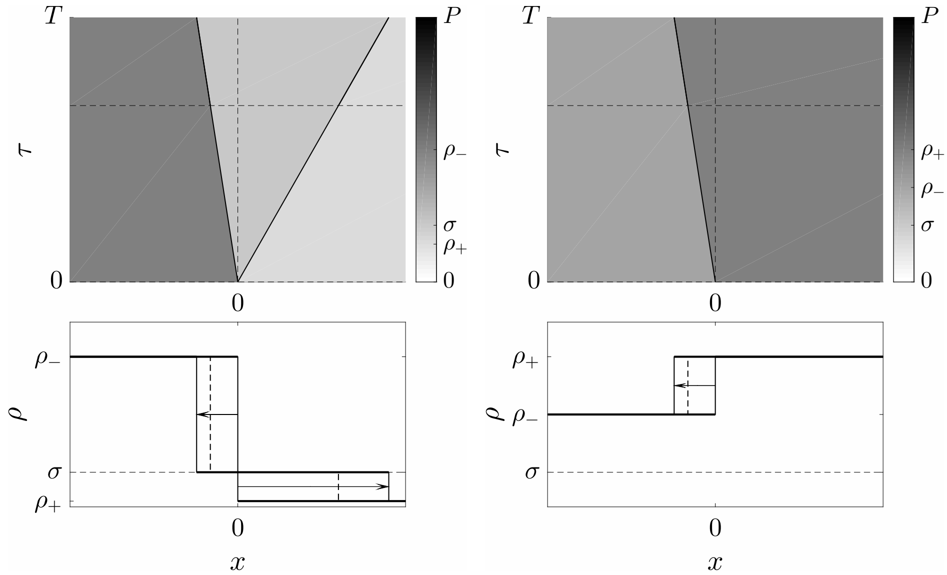

(c) Congested to free flow (d) Congested to congested

Figure 3.3: Riemann problem solutions for the four cases of initial conditions. The solutions for densities $\rho(x, \tau)$ are shown color-coded, with space on x-axis and time on y-axis, and on lower figures, we show three snapshots of the solution with space on x-axis and traffic density on y-axis. The direction in which the wavefronts travel over time is indicated with an arrow.

in the flow model. Introducing two (or more) classes of traffic, for example the 'rabbits' and the 'slugs', can also be seen as a simple way of defining a second-order (or higher-order) traffic model, where the conserved quantities would be the total traffic density and the ratio of vehicles of one class in it. The multi-class cell transmission model (MCCTM) we use here is similar to the model introduced in [61], with proportional priority allocated to all vehicle classes.

Let $\mathcal{K}$ be the set of vehicle classes $\kappa \in \mathcal{K}$. Although the traffic consists of various types of vehicles, we commonly express all their contribution to the overall traffic density in passenger car equivalents. The traffic density of vehicles of class κ in cell i at time t will be denoted $\rho_i^\kappa(t)$. We allow each of the classes to have a distinct free flow speed $U_i^\kappa(t)$ in every cell and at every time instant. Furthermore, we allow the vehicles of each class to have a different, possibly time-varying headway ratio $h_i^\kappa(t)$ in every cell. This headway ratio describes how much total space a vehicle of class κ takes on the road, compared with some baseline value for which the critical and jam densities σ and P were calculated. We can let $h_i^\kappa(t)$ depend on the surrounding traffic conditions, or on some external input. Typically, for human-driven vehicles, we fix $U_i^\kappa(t) = V$ and $h_i^\kappa(t) = 1$. The effective traffic density is defined as

$$\bar{\rho}_i^\kappa(t) = \rho_i^\kappa(t) h_i^\kappa(t),$$

indicating the density of regular passenger cars that would have the same effect on the rest of the traffic. Essentially, by $\bar{\rho}_i^\kappa(t)$ we denote the aggregate contribution to the overall congestion level from class κ vehicles that the other vehicles perceive, and it reflects the total road space these vehicles take.

For example, suppose class a represents platooning autonomous vehicles, while class b represents the 'background' traffic that consists of human-driven vehicles. Vehicles of class a are able to safely maintain much shorter headway times than vehicles of class b, so if we assume that characteristic densities are calculated for human-driven vehicles, this would mean that $h_i^a(t) < 1$ and $h_i^b(t) = 1$. The total traffic density

$$\rho_i(t) = \sum_{k \in \mathcal{K}} \rho_i^k(t)$$

will then differ from the total effective traffic density

$$\bar{\rho}_i(t) = \sum_{k \in \mathcal{K}} \rho_i^k(t) h_i^k(t) = \sum_{k \in \mathcal{K}} \bar{\rho}_i^k(t).$$

Same as in the single-class case (3.5), the evolution of cell traffic densities for each class is given by

$$\rho_i^\kappa(t+1) = \rho_i^\kappa(t) + \frac{T}{L_i} \left(\Phi_i^{+\kappa}(t) - \Phi_i^{-\kappa}(t) \right).$$

Assuming again that the cells are of same length and that there are no on- or off-ramps, we have

$$\rho_i^\kappa(t+1) = \rho_i^\kappa(t) + \frac{T}{L}\left(q_{i-1}^\kappa(t) - q_i^\kappa(t)\right),$$

and the traffic flow is again given by

$$q_i^\kappa(t) = \min(D_i^\kappa(t), S_{i+1}^\kappa(t)).$$

However, the demand and supply functions of each class will now also depend on vehicles of other classes, due to shared road capacity. We write the demand function

$$D_i^\kappa(t) = U_i^\kappa(t)\rho_i^\kappa(t)\min\left(\frac{V\sigma_i}{\sum\limits_{k\in\mathcal{K}} U_i^k(t)\bar{\rho}_i^k(t)}, 1\right), \tag{3.11}$$

and the supply function

$$S_i^\kappa(t) = \frac{\rho_{i-1}^\kappa(t)}{\bar{\rho}_{i-1}(t)}\min\left(W(P_i - \bar{\rho}_i(t)), V\sigma_i\right). \tag{3.12}$$

It is easy to verify that in case we only have one class $\mathcal{K} = \{a\}$ and $U_i^a(t) = V$, $h_i^a(t) = 1$, expressions (3.11) and (3.12) simplify to (3.8).

Another benefit of using the MCCTM is that it gives us a way of precisely defining flows of off-ramps or diverging links. Instead of assuming that a fraction of all vehicles leaves the mainstream, we can now distinguish vehicles with different destinations as members of different classes. Let i_r be a cell with an off-ramp or a diverge (denoted (1) and (2) in Fig. 3.4, respectively), where vehicles of classes $\mathcal{K}_{i_r} \subset \mathcal{K}$ exit the mainstream. We may then write

$$\begin{aligned}
\Phi_{i_r}^{-\kappa}(t) &= q_{i_r}^\kappa(t) + r_{i_r}^\kappa(t),\\
r_{i_r}^\kappa(t) &= \begin{cases}\min\left(D_{i_r}^\kappa(t), S_{i_r+1}^\kappa(t), S_{j,i_r}^\kappa(t)\right), & \kappa \in \mathcal{K}_{i_r},\\ 0, & \kappa \in \mathcal{K}\setminus\mathcal{K}_{i_r},\end{cases}
\end{aligned}$$

where

$$S_{j,i_r}^\kappa(t) = \frac{\rho_{i_r}^\kappa(t)}{\sum\limits_{\kappa\in\mathcal{K}_{i_r}}\bar{\rho}_{i_r}^\kappa(t)}\min\left(W(P_j - \bar{\rho}_j(t)), V\sigma_j\right), \tag{3.13}$$

is the supply of the first cell j of the link that the traffic flow from cell i_r diverges into. Alternatively, if vehicles leave the highway via an off-ramp in cell i_r, we may replace (3.13) with

$$S_{r,i_r}^\kappa(t) = \frac{\rho_{i_r}^\kappa(t)}{\sum\limits_{\kappa\in\mathcal{K}_{i_r}}\bar{\rho}_{i_r}^\kappa(t)}Q_{r,i_r}^{\max}.$$

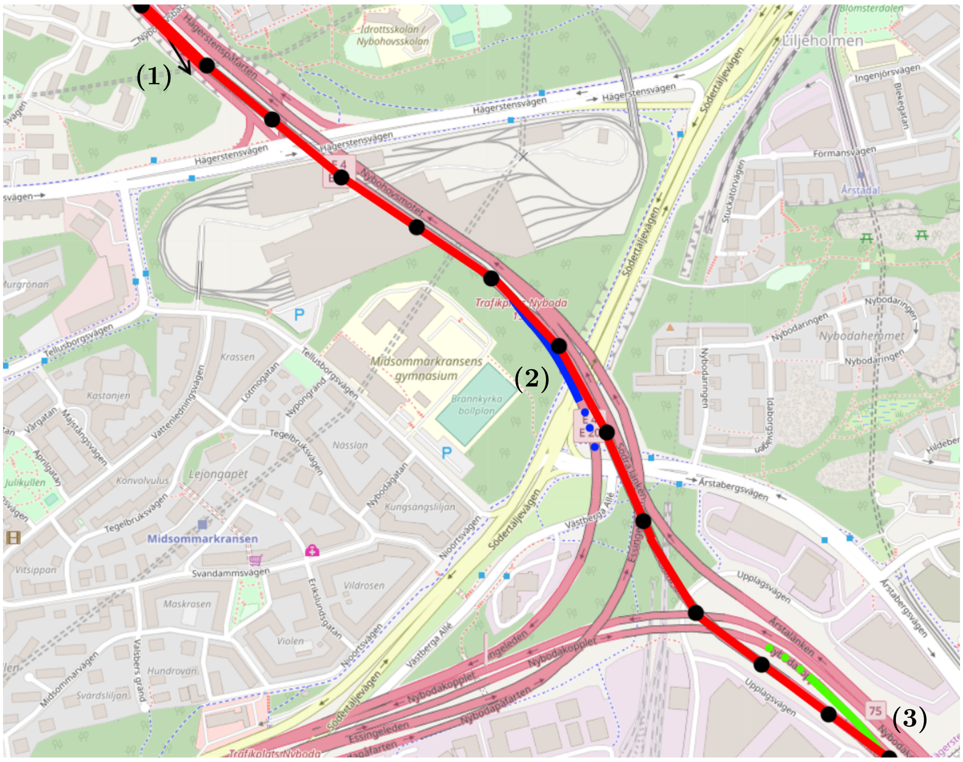

Figure 3.4: Map of Trafikplats Nyboda with an overlay illustrating an arrangement of cells, off-ramps, diverges and merges for modelling traffic originating from Essingeleden and bound for Södra länken eastwards. The mainstream is shown in red, with black circles indicating cell boundaries. At (1) there is an off-ramp, at (2) a portion of the mainstream diverges westwards (shown in blue), and at (3) the mainstream traffic merges with the traffic from another link (shown in green). Imagery taken from OpenStreetMap.

Finally, we update $q^{\kappa}_{i_r}(t)$ accordingly,

$$q^{\kappa}_{i_r}(t) = \begin{cases} \min(D^{\kappa}_{i_r}(t), S^{\kappa}_{i_r+1}(t)), & \kappa \in \mathcal{K} \setminus \mathcal{K}_{i_r}, \\ 0, & \kappa \in \mathcal{K}_{i_r}. \end{cases}$$

For multiple links merging, we will assume proportional allocation of road capacity. Let i be the cell the links are merging into and $\mathrm{Pre}(i)$ the set of preceding cells, from which traffic flows into cell i (denoted (3) in Fig. 3.4). Then we may write

$$\Phi^{+\kappa}_i(t) = \sum_{j \in \mathrm{Pre}(i)} q^{\kappa}_j(t),$$

$$q_j^\kappa(t) = \min\left(D_j^\kappa(t), S_{i,j}^\kappa(t)\right), \qquad j \in \mathrm{Pre}(i),$$

$$S_{i,j}^\kappa(t) = \frac{\rho_j^\kappa(t)}{\sum\limits_{\iota\in\mathrm{Pre}(i)} \bar{\rho}_\iota(t)} \min\left(W(P_i - \bar{\rho}_i(t)), V\sigma_i\right), \qquad j \in \mathrm{Pre}(i),$$

and all other equations remain unchanged.

3.2 Platoon and moving bottleneck models

Broadly speaking, there are two ways we can model moving bottleneck, as shown in Figure 3.5. The first approach is to consider it a moving traffic flow constraint, i.e. a reduction of road capacity at the moving bottleneck's position, and not explicitly count the slow vehicle acting as a moving bottleneck a part of the overall traffic density. The second approach is to represent the slow moving vehicles through their density, and model interactions between vehicles moving at different speeds in some cell-based model.

In this section we introduce the moving bottleneck into the CTM, using the first approach, and model platoons, which can act as moving bottlenecks, in MCCTM using the second approach. We will first address this effect in the LWR model and describe the Riemann problems that arise from its treatment. Then, we apply a Godunov-like scheme to obtain traffic flow updates in the CTM, in order to incorporate moving bottlenecks into it. Finally, we will describe how a platoon acting as a moving bottleneck can be modelled in MCCTM.

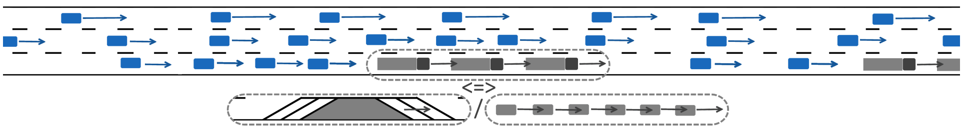

Figure 3.5: A platoon of trucks acting as a moving bottleneck and two ways of representing this phenomenon.

Moving bottlenecks in the LWR model

Assume we have a vehicle (or a platoon of vehicles) in traffic, at position $\chi_b(\tau)$, moving at speed u_b that is lower than the speed of the surrounding traffic $\mathcal{V}(\rho(\tau, \chi_b(\tau)_+))$, and thus acting as a moving bottleneck. We can model this phenomenon by imposing additional constraints on the LWR model. This yields a PDE-ODE strongly coupled system [66], with the traffic conditions evolution described by a scalar conservation law with a moving flux constraint, and the motion of the moving bottleneck described by an ordinary differential equation,

$$\partial_\tau \rho(x,\tau) + \partial_x Q(\rho(x,\tau)) = 0,$$

$$
\begin{aligned}
&Q(\rho(\chi_b(\tau),\tau)) - \dot{x}_b(\tau)\rho(\chi_b(\tau),\tau) \le Q_\beta^{\max}(\dot{\chi}_b(\tau)),\\
&\dot{\chi}_b(\tau) = \min\left(u_b, \mathcal{V}(\rho(\chi_b(\tau)_+,\tau))\right).
\end{aligned}
$$

Here $\chi_b(\tau)$ is the position of the moving bottleneck, u_b its desired speed and $Q_\beta^{\max}$ maximum flow past the bottleneck. The maximum flow is obtained by studying the problem in the reference frame of the moving bottleneck,

$$
Q_\beta^{\max}(\dot{\chi}_b(\tau)) = \max_{0\le\rho\le P} Q_b(\rho) - \dot{\chi}_b(\tau)\rho,
$$

as shown in Figure 3.6b.

This formulation is equivalent to using a different flow model in the zone of the moving bottleneck. Let the flux function in this zone, $Q_b(\rho)$, be of the same form as (3.4), with different parameters,

$$
Q_b(\rho) = \begin{cases} V_b\rho, & \rho \le \sigma_b,\\ W_b(P_b-\rho), & \rho > \sigma_b, \end{cases}
$$

where $W_b = W\frac{V_b}{V}$. An example of flux functions $Q(\rho)$ and $Q_b(\rho)$ is shown in Figure 3.6a.

In order to model the capacity reduction in presence of a bottleneck, we introduce a new parameter $\beta \in [0,1]$ that describes the severity of the bottleneck. Density parameters σ and P are reduced to

$$
\begin{aligned}
\sigma(x_b) &= \sigma_b = \sigma(1-\beta),\\
P(x_b) &= P_b = P(1-\beta).
\end{aligned}
$$

Since it depends on the behaviour of drivers, we would have to experimentally determine β, but in general, it can be taken to be close to the portion of the road that the moving bottleneck takes. For example, if one of two lanes is blocked, we

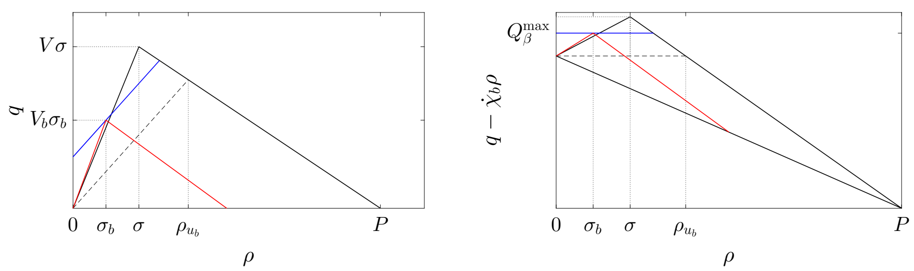

(a) Fixed reference frame (b) Moving bottleneck reference frame

Figure 3.6: Flux functions $Q(\rho)$ (solid black) and $Q_b(\rho)$ (red) for $V_b > V$ in fixed and moving bottleneck reference frame.

can set $\beta = 0.5$, or we might choose a somewhat higher value to capture additional "friction" effects.

Furthermore, we allow the free flow speed at the position of the bottleneck V_b to differ from the free flow speed elsewhere, possibly even as a function of u_b. This enables us to model the overtaking behaviour in more detail, with $V_b > V$ indicating eagerness, and $V_b < V$ indicating reluctance to overtake. To ensure that the Rankine-Hugoniot condition can be satisfied at moving bottleneck interfaces, we also need $u_b \leq V_b \leq \frac{V - u_b\beta}{1-\beta}$. As with β, V_b depends on driver behaviour, and would have to be experimentally determined. We make the standing assumption that V_b is constant, $V_b > V$ and $u_b \leq \frac{V}{\beta} - \frac{V_b(1-\beta)}{\beta}$. If we let V_b depend on u_b, we can use this function $V_b(u_b)$ to capture any bottleneck diagram [97], i.e. a curve whose tangents with slope u_b we intersect with $Q(\rho)$ to obtain traffic densities upstream and downstream of a moving bottleneck.

To model the influence the moving bottleneck has on the surrounding traffic, we solve two Riemann problems, one for its head (downstream end) and one for its tail (upstream end). We denote the traffic density upstream of the bottleneck as ρ_- and downstream ρ_+, and the traffic density in the bottleneck zone as ρ_b.

First, we define some helper functions,

$$
\begin{aligned}
r_f(\rho_b, u_b) &= \frac{Q_b(\rho_b) - u_b\rho_b}{V - u_b}, \\
r_c(\rho_b, u_b) &= \frac{WP - Q_b(\rho_b) + u_b\rho_b}{W + u_b}, \\
r_f^{-1}(\rho, u_b) &= \frac{Q(\rho) - u_b\rho}{V_b - u_b}, \\
r_c^{-1}(\rho, u_b) &= \frac{W_bP_b - Q(\rho) + u_b\rho}{W_b + u_b},
\end{aligned}
$$

that give us intersections between the flux function $Q(\rho)$ ($Q_b(\rho)$) and a line with slope u_b originating from $(\rho_b, Q_b(\rho_b))$ $((\rho, Q(\rho)))$ respectively. It is easy to check that $r_{f,c}^{-1}(r_{f,c}(\rho, u_b), u_b) = \rho$ and $r_{f,c}(r_{f,c}^{-1}(\rho, u_b), u_b) = \rho$. Note that for $V_b = V$ and $\rho_b \leq \sigma_b$, $r_f(\rho_b, u_b) = \rho_b$, so it does not depend on u_b.

The Riemann problems for the moving bottleneck boundaries can be written as

$$
\begin{aligned}
\partial_\tau\rho + \partial_x\left(Q_\pm(\rho, x, \tau)\right) &= 0, \\
Q_\pm(\rho, u_b, x, \tau) &= \begin{cases} Q_-(\rho), & x < u_b\tau, \\ Q_+(\rho), & x > u_b\tau, \end{cases} \\
\rho(x, 0) &= \begin{cases} \rho_-, & x < 0, \\ \rho_+, & x > 0. \end{cases}
\end{aligned}
$$

Example solutions to Riemann problems for moving bottleneck head and tail for all traffic density cases are given in Figure 3.7.

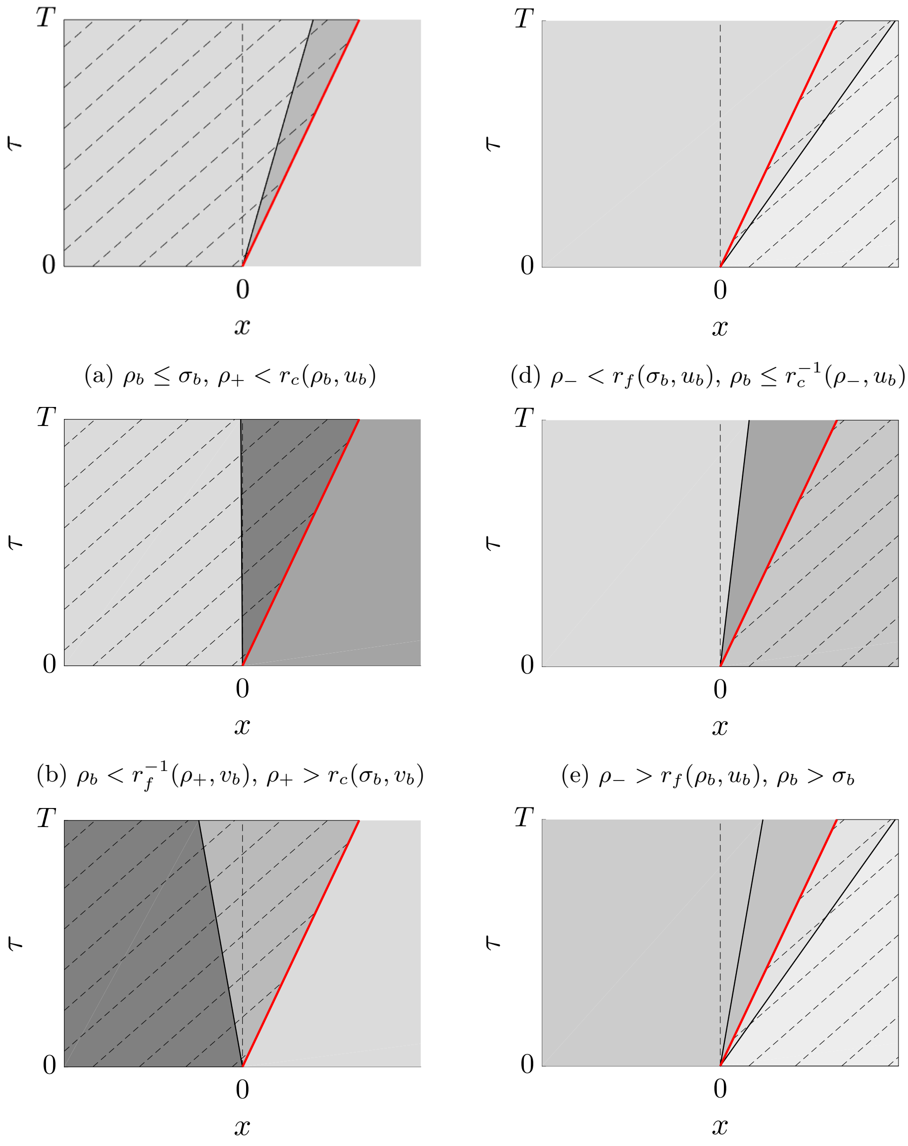

(a) $\rho_b \leq \sigma_b$, $\rho_+ < r_c(\rho_b, u_b)$

(b) $\rho_b < r_f^{-1}(\rho_+, v_b)$, $\rho_+ > r_c(\sigma_b, v_b)$

(c) $r_f(\rho_b, u_b) < \rho_+ < r_c(\rho_b, u_b)$

(d) $\rho_- < r_f(\sigma_b, u_b)$, $\rho_b \leq r_c^{-1}(\rho_-, u_b)$

(e) $\rho_- > r_f(\rho_b, u_b)$, $\rho_b > \sigma_b$

(f) $\rho_- > r_f(\rho_b, u_b)$, $\rho_b \leq \sigma_b$

Figure 3.7: Solutions for all cases of Riemann problems for moving bottleneck head (a-c) and tail (d-f). Denser traffic is shown darker, and the bottleneck zone is shown hatched.

Consider first the Riemann problem for the moving bottleneck head. In this case, we have $Q_-(\rho) = Q(\rho)$, $Q_+(\rho) = Q_b(\rho)$ and $\rho_- = \rho_b$ and the Riemann problem corresponding to it is

$$\begin{aligned}\partial_\tau \rho + \partial_x \left(Q_+(\rho, u_b, x, \tau)\right) &= 0,\\ Q_+(\rho, u_b, x, \tau) &= \begin{cases} Q_b(\rho), & x < u_b\tau,\\ Q(\rho), & x > u_b\tau,\end{cases}\\ \rho(x,0) &= \begin{cases}\rho_b, & x<0,\\ \rho_+, & x>0.\end{cases}\end{aligned}$$

We control the movement of the bottleneck, so the transition speed between the zones where different models are valid has to be equal to its speed u_b. The Rankine-Hugoniot condition for the discontinuity, $u_b(\rho_+ - \rho_b) = Q(\rho_+) - Q_b(\rho_b)$, can only hold for $\rho_+ = r_f(\rho_b, u_b)$ or $\rho_+ = r_c(\rho_b, u_b)$ (equivalently, $\rho_b = r_f^{-1}(\rho_+, u_b)$ or $\rho_b = r_c^{-1}(\rho_+, u_b)$). In this case, the entropy solution is simply

$$\rho(x,\tau) = \begin{cases}\rho_b, & x < u_b\tau,\\ \rho_+, & x > u_b\tau.\end{cases}$$

Otherwise, the entropy solution will, depending on ρ_b and ρ_+, have one or two additional wavefronts. These solutions are:

- If $\rho_b \le \sigma_b$ and $\rho_+ < r_c(\rho_b, u_b)$,

$$\rho(x,\tau) = \begin{cases}\rho_b, & x < u_b\tau,\\ r_f(\rho_b,u_b), & u_b < x < \Lambda(r_f(\rho_b,u_b),\rho_+)\tau,\\ \rho_+, & x > \Lambda(r_f(\rho_b,u_b),\rho_+)\tau.\end{cases}$$

- If $\rho_b < r_f^{-1}(\rho_+, v_b)$ and $\rho_+ > r_c(\sigma_b, v_b)$,

$$\rho(x,\tau) = \begin{cases}\rho_b, & x < \Lambda_b(\rho_b, r_c^{-1}(\rho_+,v_b))\tau,\\ r_c^{-1}(\rho_+,v_b), & \Lambda_b(\rho_b, r_c^{-1}(\rho_+,v_b))\tau < x < v_b\tau,\\ \rho_+, & x > v_b\tau,\end{cases}$$

  where $v_b = \min(u_b, \mathcal{V}(\rho_+))$. If $\mathcal{V}(\rho_+) < u_b$, the speed of both the platoon head and tail are set to $\mathcal{V}(\rho_+)$.

- If $r_f(\rho_b, u_b) < \rho_+ < r_c(\rho_b, u_b)$,

$$\rho(x,\tau) = \begin{cases}\rho_b, & x < W_b\tau,\\ \sigma_b, & W_b\tau < x < u_b\tau,\\ r_f(\rho_b,u_b), & u_b\tau < x < V\tau,\\ \rho_+, & x > V\tau.\end{cases}$$

We have a similar situation for the Riemann problem for the moving bottleneck tail (upstream end). Now, $Q_-(\rho) = Q_b(\rho)$, $Q_+(\rho) = Q(\rho)$ and $\rho_+ = \rho_b$, and the Riemann problem is

$$\begin{aligned} \partial_\tau \rho + \partial_x \left(Q_-(\rho, x, \tau)\right) &= 0, \\ Q_-(\rho, u_b, x, \tau) &= \begin{cases} Q(\rho), & x < u_b\tau, \\ Q_b(\rho), & x > u_b\tau, \end{cases} \\ \rho(x, 0) &= \begin{cases} \rho_-, & x < 0, \\ \rho_b, & x > 0. \end{cases} \end{aligned}$$

Again, we have three cases of the entropy solution, depending on ρ_b and ρ_+:

- If $\rho_- < r_f(\sigma_b, u_b)$ and $\rho_b \leq r_c^{-1}(\rho_-, u_b)$,

$$\rho(x, \tau) = \begin{cases} \rho_-, & x < u_b\tau, \\ r_f^-1(\rho_-, u_b), & u_b < x < \Lambda(\rho_-, \rho_b)\tau, \\ \rho_b, & x > \Lambda(\rho_-, \rho_b)\tau. \end{cases}$$

- If $\rho_- > r_f(\rho_b, u_b)$ and $\rho_b > \sigma_b$,

$$\rho(x, \tau) = \begin{cases} \rho_-, & x < \Lambda(\rho_-, r_c(\rho_b, u_b))\tau, \\ r_c(\rho_b, u_b), & \Lambda(\rho_-, r_c(\rho_b, u_b))\tau < x < u_b\tau, \\ \rho_b, & x > u_b\tau. \end{cases}$$

- If $\rho_- > r_f(\rho_b, u_b)$ and $\rho_b \leq \sigma_b$,

$$\rho(x, \tau) = \begin{cases} \rho_b, & x < W\tau, \\ r_c(\sigma_b, u_b), & W\tau < x < u_b\tau, \\ \sigma_b, & u_b\tau < x < V_b\tau, \\ \rho_b, & x > V_b\tau. \end{cases}$$

Incorporating moving bottlenecks into the CTM

Having described the effect of the moving bottleneck in the LWR model framework, we can now apply a similar Godunov-like scheme to calculate the effects of the moving bottleneck on traffic flows of adjacent cells. If $X_i \leq x_b(t) < X_i + L$, where $x_b(t)$ is the position of the moving bottleneck at time t, the moving bottleneck is in cell i and $i_b(t) = i$. For compactness, we will omit writing the time step for all CTM-related variables wherever the time step is obvious. We may write the resulting flows as

$$q_i = \min(V\rho_{i_b}, V\sigma, W(P - \rho_{i_b+1})) + \Delta q_{b,i}.$$

Assume the moving bottleneck in cell i_b is the only one in the road stretch considered. Since it only affects traffic flows through the interfaces of the cell it is currently in (i.e. from cell $i_b - 1$ to i_b and from cell i_b to $i_b + 1$), we will have $\Delta q_{b,i} = 0$ for all $i \notin \{i_b - 1, i_b\}$. Therefore the resulting model will be the same as the already described standard CTM (3.6)–(3.7) for $i \neq i_b$, $i \neq i_b - 1$.

In order to correctly describe the behaviour of the moving bottleneck and the effect it has on the surrounding traffic, we need to augment the cell transmission model with three additional states, the position of the moving bottleneck $x_b(t)$, the traffic density directly upstream of it $\rho_{b-}(t)$ and the traffic density in the moving bottleneck zone $\rho_b(t)$. The second and third additional states are necessary in order to properly model the flow of traffic past the bottleneck [68], effectively splitting the cell i into three parts. We will keep $\rho_i(t)$ as a state and instead, calculate the traffic density downstream of the bottleneck so that

$$\rho_i(t) = \frac{(x_b - l_b - X_{i_b})\rho_{b-} + l_b \rho_b + (X_{i_b+1} - x_b)\rho_{b+}}{L},$$

where l_b is the length of the bottleneck in question. If there are multiple bottlenecks fully or partially in the same cell, splitting the cell and calculating traffic densities in its different segments is done in a similar way, starting from the cell's upstream end and calculating traffic densities towards its downstream end so that they still average to $\rho_i(t)$.

We obtain $\Delta q_{b,i_b-1}(t)$ and $\Delta q_{b,i_b}(t)$, as well as updates $x_b(t+1)$, $\rho_{b-}(t+1)$ and $\rho_b(t+1)$ by solving the composite Riemann problem

$$\begin{gathered}
\partial_\tau \rho + \partial_x \left(Q(\rho, u_b, x, \tau) \right) = 0, \\
Q(\rho, u_b, x, \tau) = \begin{cases} Q(\rho), & x \notin \left(\chi_b(\tau) - l_b, \chi_b(\tau)\right), \\ Q_b(\rho), & x \in \left(\chi_b(\tau) - l_b, \chi_b(\tau)\right), \end{cases} \\
\dot{\chi}_b(\tau) = \min\left(u_b, \mathcal{V}(\rho(\tau, \chi_b(\tau)_+))\right),
\end{gathered} \tag{3.14}$$

with initial conditions

$$\begin{gathered}
\rho(x, 0) = \begin{cases} \rho_{i_b-1}, & x < X_{i_b}, \\ \rho_{b-}, & X_{i_b} < x < x_b - l_b, \\ \rho_b, & x_b - l_b < x < x_b, \\ \rho_{b+}, & x_b < x < X_{i_b+1}, \\ \rho_{i_b+1}, & x > X_{i_b+1}, \end{cases} \\
\chi_b(0) = x_b,
\end{gathered} \tag{3.15}$$

for τ up to T. The solution is easily obtained through front tracking, successively solving Riemann problems as described in sections 3.1 and 3.2. An example of a solution is shown in Figure 3.8.

If there are multiple moving bottlenecks, we either solve (3.14) with initial conditions (3.15) for each one if there is at least one cell between them, or include

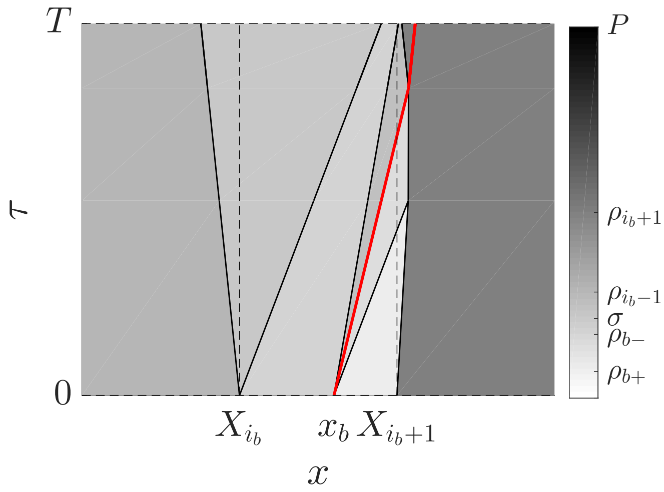

Figure 3.8: Front tracking solution example for $\tau \in [0, T]$ and $l_b \approx 0$. Note that the moving bottleneck slows down when it enters the dense traffic from cell i_{b+1}.

both of them in a larger composite Riemann problem. For example, for the situation shown in Figure 3.9, the initial conditions would be

$$\rho(x,0) = \begin{cases} \rho_{i_b-1}, & x < X_{i_{b,1}}, \\ \rho_{b-,1}, & X_{i_{b,1}} < x < x_{b,1} - l_{b,1}, \\ \rho_{b,1}, & x_{b,1} - l_{b,1} < x < x_{b,1}, \\ \rho_{b+,1}, & x_{b,1} < x < X_{i_{b,1}+1}, \\ \rho_{b-,2}, & X_{i_{b,1}+1} < x < x_{b,2} - l_{b,2}, \\ \rho_{b,2}, & x_{b,2} - l_{b,2} < x < x_{b,2}, \\ \rho_{b+,2}, & x_{b,2} < x < X_{i_{b,1}+2}, \\ \rho_{i_b+2}, & x > X_{i_{b,1}+2}. \end{cases}$$

In this case, one moving bottleneck is in cell $i_{b,1}$ and a second one in cell $i_{b,1} + 1 = i_{b,2}$, so we need to include cells $i_{b,1} - 1$ through $i_{b,1} + 2$ into the problem. Here we assumed that the moving bottlenecks are truck platoons, and that the follower catches up with the leader and merges into one platoon. If the tail of one and head of another bottleneck collide, we say that those two bottlenecks have merged, and take their speed to be the speed of the leader bottleneck.

Formally, we may write the updated traffic model that incorporates moving

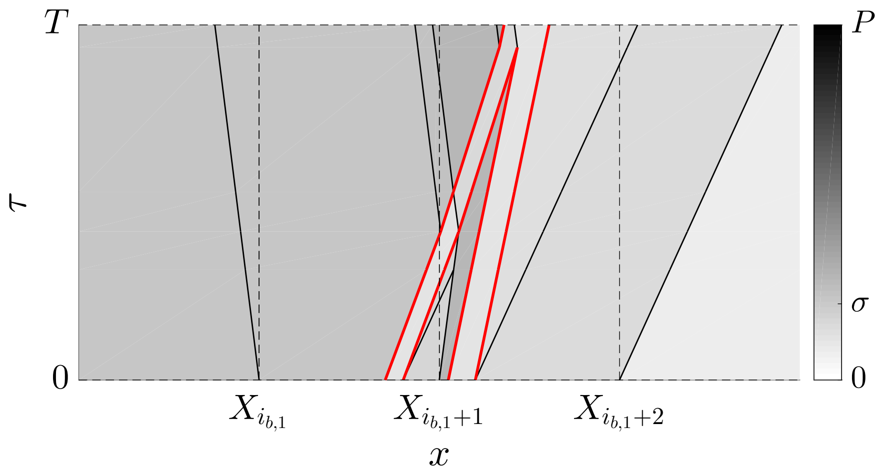

Figure 3.9: Front solution example of two platoons merging. Note that the follower platoon slows down when it enters the denser traffic from cell $i_{b,1}+1$, originating from the leader platoon. The two moving bottlenecks merge into one before $\tau = T$.

bottlenecks as

$$
\begin{aligned}
&\rho_i(t{+}1) = \rho_i(t) + \frac{T}{L}\left(q_{i-1}(t) - q_i(t)\right), \\
&q_i(t) = \min\left(V\rho_i(t), V\sigma, W(P - \rho_{i+1}(t))\right) + \Delta q_{b,i}(t), \\
&\begin{bmatrix} \Delta q_b(t) \\ x_b(t+1) \\ \rho_{b-}(t+1) \\ \rho_b(t+1) \end{bmatrix} = \mathcal{P}\left(\rho(t), x(t), u(t), \rho_{b-}(t), \rho_b(t)\right),
\end{aligned}
\tag{3.16}
$$

where by $\mathcal{P}$ we encapsulate the procedure of calculating Δq_b and new values for x_b, $\rho_{b\text{-}}$ and ρ_b from the solution of (3.14) with initial conditions (3.15) at $\tau = T$.

For ease of presentation, consider the case where there is only one moving bottleneck. Then we may calculate the updates $\Delta q_{b,i_b}(t)$ and $\Delta q_{b,i_b-1}(t)$ as

$$
\begin{aligned}
\Delta q_{b,i_b} &= \frac{1}{T}\int_{X_{i_b+1}}^{X_{i_b+2}} \rho(x,T) - \tilde{\rho}(x,T)dx, \\
\Delta q_{b,i_b-1} &= \frac{1}{T}\int_{X_{i_b-1}}^{X_{i_b}} \rho(T,x) - \tilde{\rho}(x,T)dx.
\end{aligned}
\tag{3.17}
$$

Here by $\tilde{\rho}(x,T)$ we denote the solution of the composite Riemann problem with no moving bottlenecks and for initial conditions

$$\tilde{\rho}(x,0) = \begin{cases} \rho_{i_b-1}, & x < X_{i_b}, \\ \rho_{i_b}, & X_{i_b} < x < X_{i_b+1}, \\ \rho_{i_b+1}, & x > X_{i_b+1}. \end{cases}$$

Since this solution can be expressed explicitly, integrals of $\tilde{\rho}(x,T)$ can easily be calculated as

$$\frac{1}{T}\int\limits_{X_{i_b+1}}^{X_{i_b+2}} \tilde{\rho}(x,T)dx = \max\left(\Lambda(\min(\rho_{i_b},\sigma),\rho_{i_b+1}),0\right)\left(\rho_{i_b+1} - \min(\rho_{i_b},\sigma)\right),$$

$$\frac{1}{T}\int\limits_{X_{i_b-1}}^{X_{i_b}} \tilde{\rho}(x,T) = \min\left(\Lambda(\rho_{i_b-1},\max(\rho_{i_b},\sigma)),0\right)\left(\rho_{i_b-1} - \max(\rho_{i_b},\sigma)\right).$$

Finally, the new position of the bottleneck is

$$x_b(t+1) = \chi_b(T), \tag{3.18}$$

and the new traffic density upstream of it

$$\rho_{b-}(t+1) = \frac{\int\limits_{X_{i_b(t+1)}}^{\chi_b(T)-l_b} \rho(x,T)dx}{\chi_b(T) - l_b - X_{i_b(t+1)}}, \tag{3.19}$$

and inside the bottleneck zone

$$\rho_b(t+1) = \frac{\int\limits_{\chi_b(T)-l_b}^{\chi_b(T)} \rho(x,T)dx}{l_b}. \tag{3.20}$$

In case we have merging moving bottlenecks, we also need to keep track of their number and their lengths.

To summarize, the model we propose is an extended version of CTM (3.6)–(3.7), which can be written as (3.16). Traffic flow updates for cells adjacent to the moving bottleneck are calculated according to (3.17). To properly model the dynamics of the moving bottleneck, we require adding two additional states (3.18), (3.19) and (3.20), whose updates are obtained from the solution of the composite Riemann problem. The proposed model is simple and tractable, as well as consistent with the PDE moving bottleneck traffic models. This approach also allows extensions to other PDE traffic models and different traffic phenomena, such as police cars, as well as enables traffic control design using the speed of the moving bottleneck as control variable and cell traffic densities as measurements.

Platoons and moving bottlenecks in the MCCTM

Although it is often driven by the need to classify automated and human-driven vehicles separately, MCCTM in its basic form is not suitable for modelling the behaviour of platoons. The main reason is that by discretizing the spatial coordinate, we lose information about the exact position of the platoon head and tail. Let platooning vehicles belong to class a and background traffic to class b, and let the platoon move at speed $u_p \in [U_{\min}, U_{\max}]$. Note that simply setting $U_i^a(t) = u_p$ in cells where the platoon is would not be sufficient, since it would not maintain crisp boundaries of the platoon, as some vehicles would diffuse to the next cell. For example, for a one cell long platoon travelling at $u_p = V/2$, we would have

$$
\begin{aligned}
\rho_i^a(0) &= \rho_p, & \rho_{i+1}^a(0) &= 0, & \rho_{i+2}^a(0) &= 0,\\
\rho_i^a(1) &= \frac{\rho_p}{2}, & \rho_{i+1}^a(1) &= \frac{\rho_p}{2}, & \rho_{i+2}^a(1) &= 0,\\
\rho_i^a(2) &= \frac{\rho_p}{4}, & \rho_{i+1}^a(2) &= \frac{\rho_p}{2}, & \rho_{i+2}^a(2) &= \frac{\rho_p}{4},
\end{aligned}
$$

where the correct behaviour would be

$$
\rho_i^a(2) = 0, \; \rho_{i+1}^a(2) = \rho_p, \quad \rho_{i+2}^a(2) = 0.
$$

We can deal with this problem by allowing cell interfaces to move [98], or by independently remembering the platoon position. However, if we assume that platooning control works to maintain constant headways between the vehicles, so that the density of platooned vehicles is ρ_p, the position of the platoon head will be encoded in the traffic density of the cell it is in. Then we may use the cell speeds $U_i^a(t)$ to correctly model the behaviour of platoons.

Denote by $i_h^p(t)$ and $i_t^p(t)$ the cells in which the platoon head and tail are at time t respectively, and by $x_h^p(t)$ and $x_t^p(t)$ their exact positions. Since the platoon moves at speed u_p, $x_h^p(t+1) = x_h^p(t) + u_p T$ and $x_t^p(t+1) = x_t^p(t) + u_p T$. Under perfect spacing regulation, the densities of platooning vehicles would be

$$
\rho_i^a(t) = \begin{cases} 0, & i < i_t^p(t) \vee i > i_h^p(t),\\ \rho_p \frac{x_t^p(t) - X_{i_t^p(t)+1}}{L}, & i = i_t^p(t),\\ \rho_p, & i_t^p(t) < i < i_h^p(t),\\ \rho_p \frac{x_h^p(t) - X_{i_h^p(t)}}{L}, & i = i_h^p(t). \end{cases} \tag{3.21}
$$

Then by setting

$$
U_i^a(t) = \begin{cases} V, & i < i_t^p(t),\\ V \frac{\rho_p}{\rho_i^a(t)} - \left(V - U_{i+1}^a(t)\right) \frac{\rho_{i+1}^a(t)}{\rho_i^a(t)}, & i_t^p(t) \le i < i_h^p(t),\\ V - (V - u_p) \frac{\rho_p}{\rho_{i_h}^a(t)}, & i = i_h^p(t),\\ 0, & i > i_h^p(t), \end{cases} \tag{3.22}
$$

the traffic densities will both converge to (3.21) and evolve according to it, thus correctly modelling the behaviour of the platoon. Note that in case $\rho_i(t) = \rho_p$, $i_t^p(t) < i < i_h^p(t)$, we have $U_i^a(t) = u_p$, $i_t^p(t) < i < i_h^p(t)$. This approach only works if there are at least $n_{\min}^p = \rho_p L$ vehicles (or passenger car equivalents) inside a platoon.

Let the remainder of traffic consist of human-driven vehicles of class b, $U_i^b(t) = V$, and $\sigma_i = \sigma$. Under (3.22), the maximum class b traffic density flowing past the platoon will be $\rho^b_{i_p^h(t)+1}(t) = \sigma - \rho_p$. This is exactly the same result as we get for the maximum traffic density flowing past the moving bottleneck in the model described in Section 3.2 if we take $V_b = V$, which shows that, while in free flow, the two models are functionally equivalent.

3.3 Summary

There are many models we may use to capture the behaviour of highway traffic. Due to their relative simplicity, macroscopic traffic models are widely used for traffic control design. In this chapter, we described the two most well-known macroscopic traffic models, the CTM and the LWR model. These two models were shown to be equivalent, since the CTM can be seen as a discretization of LWR. This fact was used to extend the classical CTM to include the theoretical results in moving bottleneck modelling from PDE (LWR) models. By doing this, we were able to introduce new ways of controlling traffic into the well-established model.

Another interesting extension of the CTM that we discussed is the Multi-class CTM. Having multiple classes of vehicles enables us to both model some traffic phenomena with higher fidelity, and also design and analyse control strategies that only act on a (potentially very small) subset of vehicles on the road. In this way, we may, for example, consider more advanced variable speed limit control, model platoons or accurately describe the routes the vehicles take.

Chapter 4

Congestion wave dissipation and avoidance

This chapter deals with the problem of stop-and-go wave avoidance dissipation, here assumed to be caused by a temporary reduction of road capacity. In contrast to some previous solutions that used variable speed limits (notable example being SPECIALIST [99]) or used autonomous vehicles in ring road traffic [62], we propose using a controlled automated vehicle acting as a moving bottleneck. We are using the moving bottleneck extension of the CTM described in Section 3.2.

In Section 4.1 we give a more detailed formulation of the congestion wave avoidance and dissipation problem, including some traffic performance metrics that will be evaluated. The control law is then derived by analytically solving the optimization problem under some assumptions in Section 4.2, which are then verified by simulations in Section 4.3.

4.1 Congestion wave dissipation and avoidance problem

As outlined in Section 1.2, there are two ways we can look at this problem. The first approach is from the perspective of the controlled vehicle, in which case we focus on congestion wave avoidance, i.e. calculating the constant speed at which the vehicle avoids the traffic jam with minimum delay. The second approach is to look at the problem from the perspective of the overall traffic, focusing instead on congestion wave dissipation and using the controlled vehicle just as an actuator in order to optimize traffic performance indices. In both cases, the mutual influence between the controlled vehicle and the rest of the traffic is given by model (3.16).

The control objective for the first approach can be expressed as an optimization problem

$$
\begin{aligned}
\underset{u_b}{\text{minimize}} \quad & t_f \\
\text{subject to} \quad & x_b(t_f) \geq X_f \\
& u_{\min} \leq u_b \leq u_{\max} \\
& \text{Traffic and moving bottleneck model (3.16)} \\
& \rho_{i_b(k)}(k) \leq \rho_j
\end{aligned}
$$

where we assume that the speed of the moving bottleneck u_b will remain constant, and all constraints have to be satisfied for $k = t, t+1, \ldots, t_f$. We say that a cell i is in traffic jam at time t if $\rho_i(t) > \rho_j$, where $\rho_j > \sigma$ is some predefined density. Here we will set ρ_j to the traffic density at which the average traffic speed is equal to the automated vehicle's maximum speed $u_{\max}$,

$$\mathcal{V}(\rho_j) = u_{\max}.$$

Note that ρ_j is not the jam density, which we denote P.

Since reducing the speed of the controlled vehicle both causes it to reach the congestion wave later and the congestion wave to be dissipated sooner (in case $V_b \neq V$, otherwise the congestion wave is dissipated at the same rate in this model), it is not hard to find the analytical solution, and there is no need to apply numerical methods.

In case we take the second approach, we no longer constrain the controlled vehicle not to enter congestion. Instead, we optimize some cost function J_{tr} consisting of one or more traffic performance indices,

$$
\begin{aligned}
\underset{u_b}{\text{minimize}} \quad & J_{\text{tr}} \\
\text{subject to} \quad & x_b(t_f) \geq X_f \\
& u_{\min} \leq u_b \leq u_{\max} \\
& \text{Traffic and moving bottleneck model (3.16).}
\end{aligned}
$$

One of the most used traffic performance indices is the *Total Travel Time* (TTT) [veh h], which represents the time spent in the highway mainstream segment by all vehicles in the considered time horizon, and can be calculated as

$$\text{TTT} = \int_0^{\tau_{\text{end}}} \int_{X_1}^{X_{\text{end}}} \rho(x,\tau) \mathrm{d}x \mathrm{d}\tau = \sum_{t=0}^{t_{\text{end}}} \sum_{i=1}^{N} \rho_i(t) T L.$$

Some other performance indices that are commonly used are the *Total Travel Distance* (TTD) [veh km], which is the total distance covered by all vehicles in the considered time horizon, calculated as

$$\text{TTD} = \int_0^{\tau_{\text{end}}} \int_{X_1}^{X_{\text{end}}} Q\left(\rho(x,\tau)\right) \mathrm{d}x \mathrm{d}\tau = \sum_{t=0}^{t_{\text{end}}} \sum_{i=1}^{N} q_i(t) T L,$$

and the *Mean Speed* (MS) [km/h] of the vehicles travelling in the considered highway segment in the considered time horizon,

$$\mathrm{MS} = \frac{\mathrm{TTD}}{\mathrm{TTS}}.$$

Based on the mean speed, it is straightforward to calculate the *Average Travel Time* (ATT) [h],

$$\mathrm{ATT} = \frac{X_{\mathrm{end}} - X_1}{\mathrm{MS}}.$$

Note that because of the simple traffic model and set-up, it is possible to have very different traffic situations for which these indices are the same. In order to distinguish these situations, we need to consider some additional metrics. Another performance index that will be considered here is based on the *Total Variation* (T.V.) of traffic density,

$$\mathrm{T.V.}(\rho(x,\tau)) = \sup \sum_j \left|\rho(x_j,\tau) - \rho(x_{j-1},\tau)\right|,$$

which in case of CTM simplifies to

$$\mathrm{T.V.}(\rho(t)) = \sum_{i=2}^{N} \left|\rho_i(t) - \rho_{i+1}(t)\right|.$$

We will therefore consider the *Average Total Variation* (ATV),

$$\mathrm{ATV} = \sum_{t=0}^{t_{\mathrm{end}}} \sum_{i=2}^{N} \frac{\left|\rho_i(t) - \rho_{i+1}(t)\right|}{t_{\mathrm{end}}},$$

as a measure of traffic homogeneity, where lower ATV (higher homogeneity) is preferable to higher ATV (lower homogeneity).

Consider for example two different initial conditions for $\rho(x,\tau)$,

$$\rho(x,0) = \begin{cases} 0, & x < 0, \\ \sigma, & 0 < x < L, \\ 0, & x > L, \end{cases} \tag{4.1}$$

and

$$\rho(x,0) = \begin{cases} 0, & x < L/2, \\ 2\sigma, & L/2 < x < L, \\ 0, & x > L, \end{cases} \tag{4.2}$$

shown in Figure 4.1. If we look at the segment $[0,L]$ and time interval $[0,T]$, these two examples will have the same TTT, but the second one has higher ATV, which makes it less desirable than the first one.

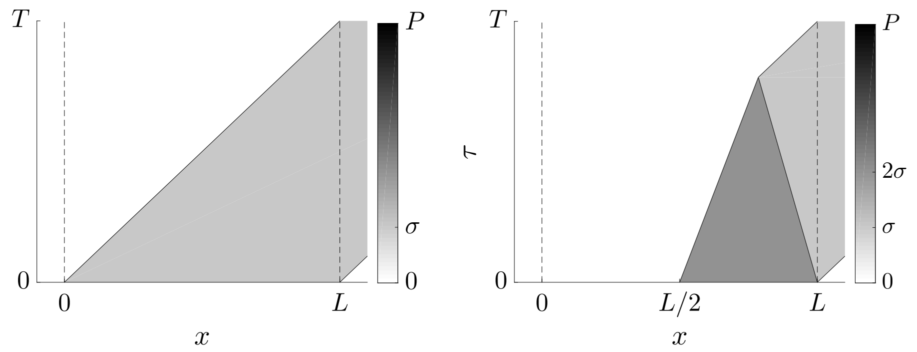

(a) Initial conditions (4.1)

(b) Initial conditions (4.2)

Figure 4.1: Example of two situations with the same TTT, but different ATV.

4.2 Controlled moving bottleneck

In this section we derive a control law for moving traffic jam dissipation and avoidance. We are using the speed of controlled automated vehicle $u_b(t)$ as a control variable, and assuming that we know cell traffic densities $\rho_i(t)$ and that the vehicle attempts to move at constant speed until the congestion downstream of it has dissipated. For readability, (t) will be omitted.

We denote by x_b, x_c, and x_d the positions of the automated vehicle, traffic jam tail and traffic jam head, respectively, and by ρ the vector of cell traffic densities. The traffic jam encompasses a number of cells, $x_c = X_{i_c}$, $x_d = X_{i_d}$, with $\rho_i > \rho_j$, $i = i_c, \ldots, i_d$.

The speed of the automated vehicle will be controlled as

$$u_b = \mathcal{U}(x_b, x_c, x_d, \rho),$$

within some limits, $u_b \in [u_{\min}, u_{\max}]$. The control law $\mathcal{U}$ is a static mapping from its arguments to u_b. It is calculated in real-time by considering the updated states. It is hard to specify $\mathcal{U}$ explicitly, but it can be calculated in a simple way by using front tracking. The calculation of $\mathcal{U}$ will be described in the remainder of this section, and is illustrated in Figure 4.2. A representation of the control loop is shown in Figure 4.3.

Due to the simplicity of the underlying traffic model, we do not need to explicitly solve the optimization problem to know the form of the solution. When there is no traffic jam ahead of the controlled vehicle, it can continue driving at its default desired speed, which is equal to its maximum speed $u_{\max}$. However, while there exists a traffic jam downstream of the controlled vehicle, it can reduce its speed, thus giving the traffic jam more time to dissipate. By doing this, it also restricts the flow of traffic at its position, by acting as a moving bottleneck, helping dissipate the traffic jam faster. We calculate and apply some constant controlled automated vehicle speed u_b so that the congestion downstream of it is cleared as soon as possible and, if feasible, so that the vehicle avoids the traffic jam with minimum delay. Since the vehicle's speed is constrained to be higher than some minimum speed $u_b > u_{\min}$, this might not always be possible, in which case the vehicle will move at its minimum speed until it has passed the traffic jam.

For the vehicle to avoid the traffic jam with minimum delay, at some $\tau = \tau_c$, we need

$$\chi_b(\tau_c) = \chi_c(\tau_c) = \chi_d(\tau_c). \tag{4.3}$$

Here we denote by χ_* the predicted evolution of x_* in PDE framework. We assume that the congestion head will move at some constant speed λ_d,

$$\chi_d(\tau) = x_d + \lambda_d \tau, \quad \chi_d(0) = x_d.$$

While the reduction of capacity is still in effect, this speed will be $\lambda_d = 0$, and afterwards, while the traffic jam is being discharged, $\lambda_d = -W$. For the position of the controlled vehicle, we have

$$\chi_b(\tau) = x_b + u_b \tau, \quad \chi_b(0) = x_b.$$

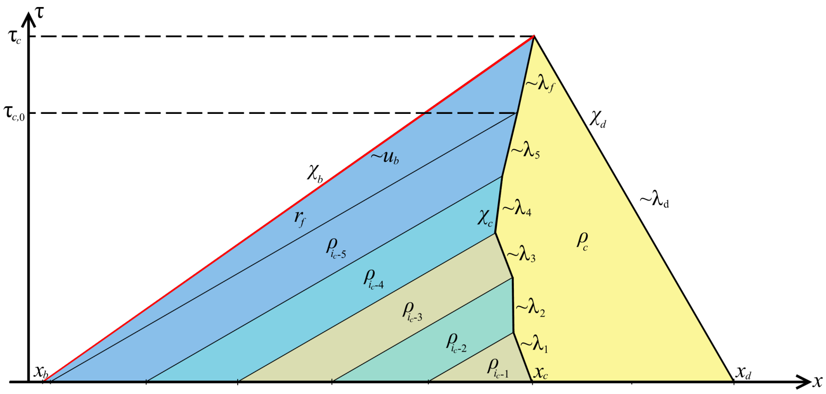

Figure 4.2: Front tracking calculation of $u_b(t)$.

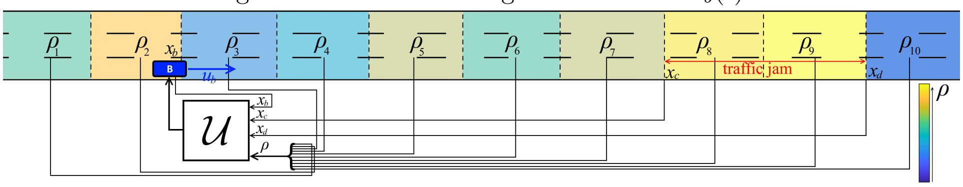

Figure 4.3: Control loop example. Cell traffic densities ρ_i are color-coded (warmer is higher density).

From (4.3), we can calculate the dependence of τ_c on u_b,

$$\tau_c(u_b) = \frac{x_d - x_b}{u_b - \lambda_d}, \tag{4.4}$$

and for the position of the traffic jam tail at $\tau = \tau_c$ we write

$$\chi_c(\tau_c) = x_c + \Delta\chi_c(\rho, u_b).$$

The dynamics of $\chi_c(\tau)$ are hard to describe in closed form, but we may calculate $\Delta\chi_c$ by the composite Riemann problem for initial conditions

$$\rho(x,0) = \begin{cases} r_f(\sigma_b, u_b), & x \le x_b, \\ \rho_i, & x \in [x_i, x_{i+1}), x_c > x > x_b, \\ \rho_c, & x > x_c, \end{cases}$$

by front tracking for $\tau \in [0, \tau_c]$. Note that here we model the influence of the moving bottleneck by formally taking the initial traffic density to be equal to $r_f(\sigma_b, u_b)$ everywhere upstream of it. This also assumes that the demand from upstream of the moving bottleneck is always higher than the moving bottleneck capacity. Otherwise, this method will overestimate the time it takes for the traffic jam to dissipate.

Then, we can write

$$\begin{aligned} \Delta\chi_c(\rho, u_b) &= \Delta\chi_{c,0}(\rho) + \Delta\chi_{c,u_b}(u_b), \\ \Delta\chi_{c,0}(\rho) &= \sum_{j=1}^{i_c - i_b} \lambda_j \Delta\tau_j, \\ \Delta\chi_{c,u_b}(u_b) &= \frac{x_c - x_b + \Delta\chi_{c,0}(\rho) - \tau_{c,0}(\rho) u_b}{u_b - \lambda_f(u_b)} \lambda_f(u_b), \end{aligned}$$

where

$$\begin{aligned} \lambda_j &= \Lambda\left(\rho_{i_c - j}, \rho_c\right), \\ \Delta\tau_j &= \begin{cases} \frac{L}{V - \lambda_j}, & i_c - j > i_b, \\ \frac{(i_b+1)L - x_b}{V - \lambda_j}, & i_c - j = i_b, \end{cases} \\ \tau_{c,0}(\rho) &= \sum_{j=1}^{i_c - i_b} \Delta\tau_j, \\ \lambda_f(u_b) &= \Lambda(r_f(\sigma_b, u_b), \rho_c). \end{aligned}$$

Substituting (4.4), we calculate u_b so that

$$x_c + \Delta\chi_{c,0}(\rho) + \Delta\chi_{c,u_b}(u_b) = x_b + \frac{u_b(x_d - x_b)}{u_b - \lambda_d}.$$

The above closed form solution is applied at each time t until there is no more congestion ahead of the controlled vehicle. If u_b is calculated to be less than $u_{\min}$ or greater than $u_{\max}$, we apply these extreme values instead.

The optimality of u_b can especially easily be shown for $V_b = V$, since in that case, as long as u_b is low enough so that the vehicle avoids the congestion wave, it does not affect the time when the congestion wave is completely dissipated. For $\tau \in [0, \tau_{c,0})$, the inflow to the congestion wave depends on the initial conditions of the traffic between the controlled vehicle and the congestion wave, so the choice of u_b can only affect what happens after $\tau_{c,0}$. Letting $V_b = V$ yields $r_f(\sigma_b, u_b) = \sigma_b$, the difference between inflow to and outflow from the congestion wave is $V(\sigma_b - \sigma) = -V\sigma\beta$, and the congestion wave is dissipated at

$$\tau_c = \tau_{c,0} + \frac{(\chi_d(\tau_{c,0}) - \chi_c(\tau_{c,0}))\,\rho_c}{V\sigma\beta}.$$

Selecting maximum u_b so that $\chi_b(\tau_c) \leq \chi_d(\tau_c)$ satisfies the congestion wave avoidance constraints and leads to minimum t_f.

4.3 Simulation Results

We tested the control law in simulations. The simulation scenario in question is as follows:

1. $t < t_0$: The traffic is in free flow, with heterogeneous traffic density. The controlled automated vehicle is moving at speed $u_{\max}$.

2. $t_0 \leq t < t_1$: A traffic jam is caused by blocking the road at position $x_d(t_0)$. The automated vehicle is acting as a moving bottleneck, and its speed is controlled so that the traffic jam is cleared as soon as possible.

3. $t \geq t_1, x_b(t) \leq x_d(t)$: The blockage is removed and the traffic jam is being resolved. The automated vehicle's speed is controlled so that it helps dissipate and avoids the traffic jam with minimum delay.

4. $x_b(t) > x_d(t)$: The vehicle has passed the traffic jam and it continues at speed $u_{\max}$.

The simulation results for $u_{\max} = 80$ km/h are shown on Figure 4.4. Warmer colors represent higher traffic density and the traffic jam is outlined in dashed red line. The trajectory of the controlled automated vehicle is represented by full red line. The parameters of the fundamental diagram we used were $V = 110$ km/h, $\sigma = 45$ veh/km, $P = 210$ veh/km and we take ρ_j so that $\mathcal{V}(\rho_j) = u_{\max}$. The parameters of the moving bottleneck are $\beta = 0.5$ and $V_b = 110$ km/h.

The reduction of capacity happens at $t_0 = 0.1$ and lasts for 15 minutes. During this time, the capacity at $x_d = 40$ is reduced to 30%. The minimum and maximum speeds of the controlled vehicle are taken to be $u_{\min} = 50$ km/h and $u_{\max} = 100$ km/h. We compare three cases:

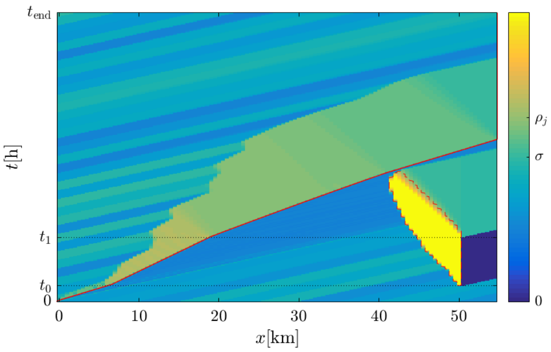

(a) Controlled

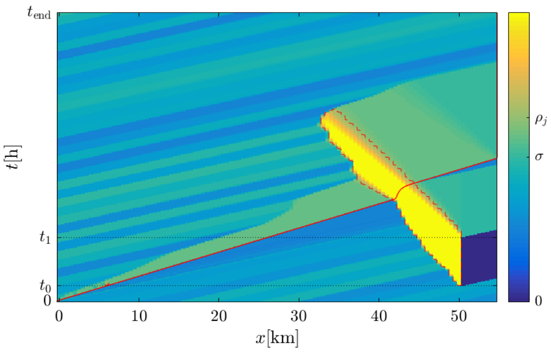

(b) Fast

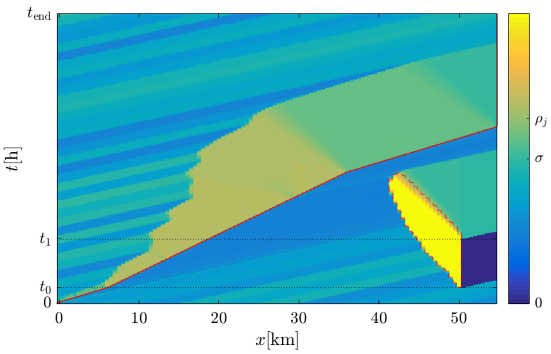

(c) Slow

Figure 4.4: Traffic densities and moving bottleneck trajectories for the three cases.

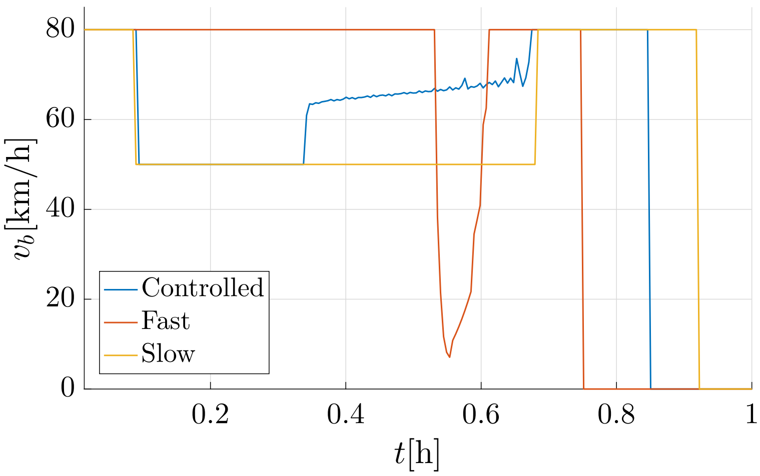

Figure 4.5: Controlled vehicle speeds for the three cases.

1. Case 1 (Controlled moving bottleneck): The vehicle is controlled according to the control law from Section 4.2.

2. Case 2 (Fast moving bottleneck): The vehicle does not reduce its speed, and continues at $u_{\max}$ until it is forced to slow down by entering the traffic jam.

3. Case 3 (Slow moving bottleneck): The vehicle reduces its speed to $u_{\min}$ until there is no longer any traffic jam ahead of it.

We can see that by implementing such control strategy, the controlled vehicle avoids the traffic jam with little delay, while also helping resolve it faster. In second case, the controlled vehicle does traverse the road segment the fastest out of the three cases, but it does not help clear the traffic jam, and is forced to sharply reduce its speed while inside the congestion, as shown on Figure 4.5. In case the vehicle reduces its speed to $u_{\min}$, it helps resolve the traffic jam, but it is unnecessarily delayed.

The achieved average travel times for the three scenarios are ATT = 0.5913 h for case 1, ATT = 0.5900 h for case 2, and ATT = 0.6048 h case 3. We can see that applying the control law from Section 4.2 results in almost no increase in ATT compared to the fast moving bottleneck case, and we see an increase in ATT in the slow moving bottleneck case due to it to causing unnecessary additional congestion. Total variations of traffic density for the three cases are shown in Figure 4.6. Although it caused a (very) slight increase in ATT, we see that the controlled moving bottleneck is able to decrease the ATV of traffic density, thus having a calming effect on the overall traffic without impeding the throughput.

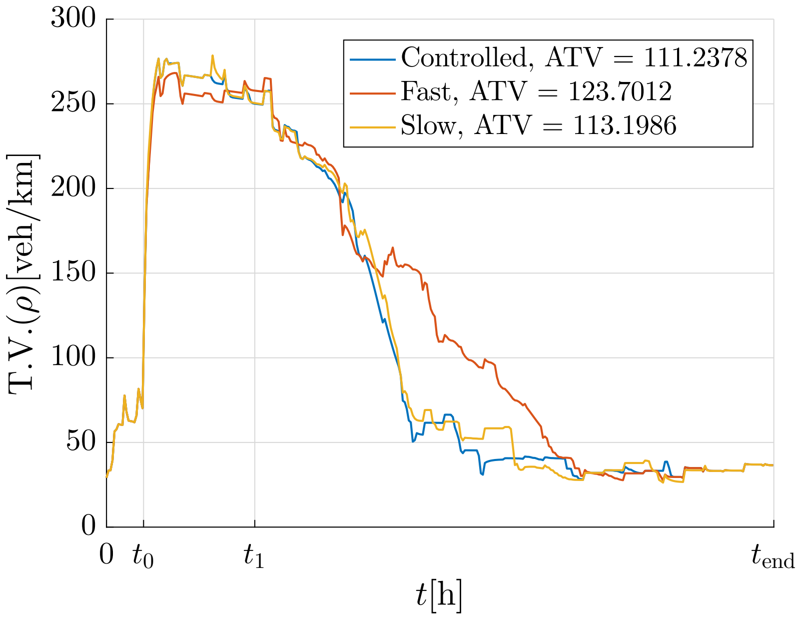

Figure 4.6: Total variation of traffic density for the three cases.

We examined the average influence this control law has on the surrounding traffic, through 100 simulation runs for randomly generated background traffic in the range $[\sigma/2, \sigma]$ and three different values for $u_{\max}$. As performance metric, we considered the ATT (results are shown on Figure 4.7 and in Table 4.1) and the ATV results are shown on Figure 4.8 and in Table 4.2.

We can see that employing the described control law leads an improvement in traffic conditions, in addition to ensuring more desirable conditions for the controlled automated vehicle. The ATT for this case is only very slightly higher than in the case of a fast moving bottleneck, while the ATV is lower. In the slow moving bottleneck case, although we avoid entering the traffic jam with the controlled vehicle, the ATT is increased due to a drop in throughput, and the ATV is comparable to than in the controlled case. Note that the control law was not explicitly derived in order to minimize ATT or ATV, so we might get even greater reduction by using optimization-based control.

4.4 Summary

In this chapter we considered the possibility of using automated vehicles acting as moving bottlenecks for congestion wave dissipation and avoidance. The problem was approached from the perspective of the controlled automated vehicle, and the

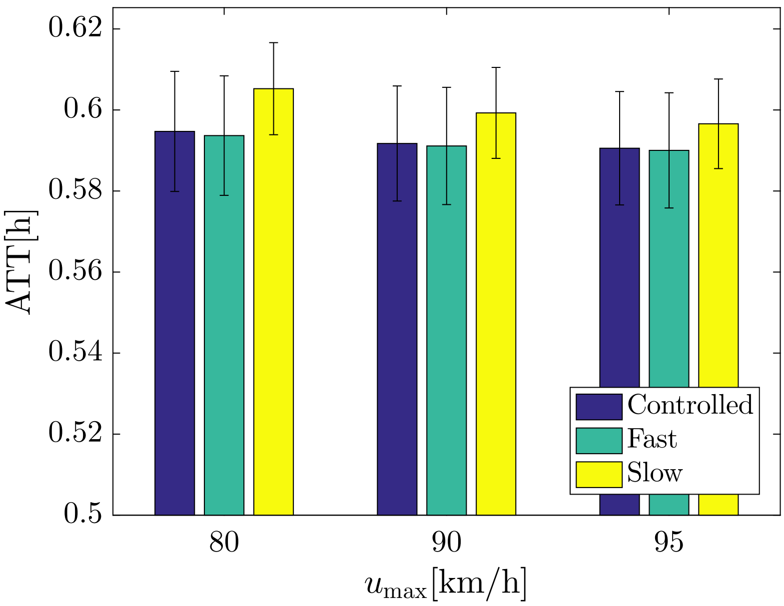

Figure 4.7: Average travel times in hours comparison.

Table 4.1: Average travel times. Without delays, $ATT_0 = 0.5$ h

$u_{\max}$[km/h]	Controlled	Fast	Slow
80	0.5931	0.5905	0.5894
90	0.5923	0.5900	0.5889
95	0.6026	0.5972	0.5949

control objective was minimizing its vehicle delay and avoiding the traffic jam. This led to an optimization problem with controlled vehicle speed as the control variable, to which we gave an analytical solution under some assumptions.

The control law designed in this way was shown to achieve good results, successfully avoiding the traffic jam at low delay. By applying this control, the overall traffic conditions were also improved in terms of homogeneity, with only a very small decrease in throughput and total travel time.

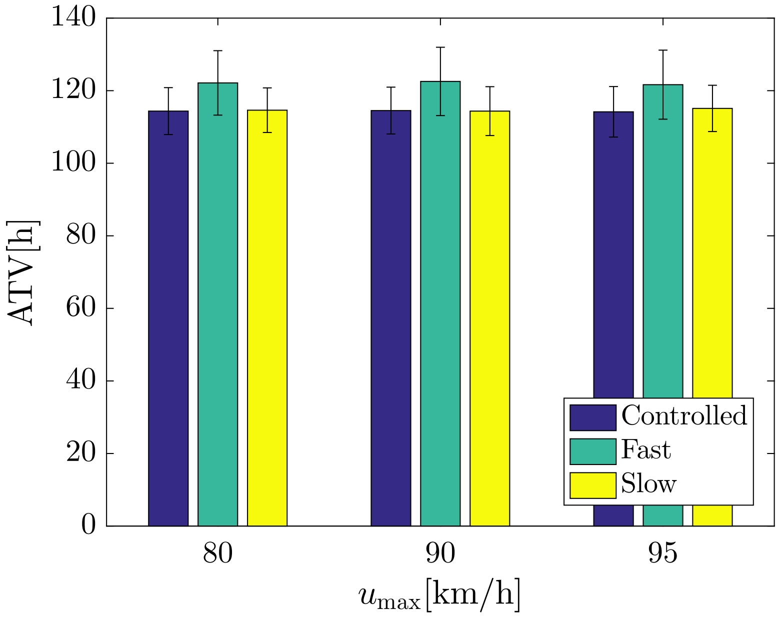

Figure 4.8: Average total variations of traffic density comparison.

Table 4.2: Average total variations of traffic density

$u_{\max}$[km/h]	Controlled	Fast	Slow
80	113.6694	120.4884	114.9623
90	114.0927	120.6848	114.4940
95	113.2028	119.5922	115.1994

Chapter 5

Platoon catch-up coordination

In this chapter we discuss the problem of platoon catch-up coordination, i.e. how vehicles starting from different positions on the road should adapt their speeds so that they form a platoon en-route. Most proposed large-scale platooning solutions involve a layered control architecture [100]. On the higher layer, platooning coordinator plans the transport assignments and optimizes vehicle routes, including identifying and managing potential platoons. On the middle layer, vehicles receive their routes and generate their speed profiles, which the lower layer control is tasked to follow. Platoon catch-up control is handled on the middle layer. There are two approaches we can take in studying this problem.

The first sub-problem pertains to predicting the vehicle trajectories during the catch-up phase. Here we assume that some control laws are governing the motion of the vehicles, and apply it to vehicle and environment models in order to predict when and where platoon merging will occur. These control laws can be learned from experimental data, depending on the deviation of vehicles' speeds from their reference values and road grade at their position.

The second sub-problem is designing an optimal control law for platoon catch-up. The case when only the varying road grade and engine power constraints are considered is well known in the literature as the look-ahead vehicle control problem [101, 102] In contrast, we consider the influence of traffic, and calculate energy-optimal catch-up speed pairs taking the interaction between the trucks and the surrounding traffic into account.

We will first give the model of vehicles used in this chapter in Section 5.1, then in Section 5.2 describe reasons we might deviate from the desired catch-up speeds, and finally deal with the two sub-problems in detail in Sections 5.3 and 5.4.

5.1 Vehicle model

While the two sub-problems studied in this chapter have different goals, they will share the basic simplified model of vehicle longitudinal dynamics. Since in this chapter we consider control at a higher level than the level of a single vehicle, a simple vehicle model will be used. The reader is referred to [103] for more detailed vehicle models. By applying Newton's second law of motion, the dynamics of vehicle i can be expressed as

$$\begin{aligned} m_i \dot{v}_i &= F_{t,i} - F_{b,i} - F_{a,i}(v_i, d_i) - F_{r,i} - F_{g,i}(\alpha(x_i)), \\ \dot{x}_i &= v_i, \end{aligned} \tag{5.1}$$

where x_i is the vehicle's longitudinal position, v_i the vehicle speed and m_i the vehicle mass. The vehicle is actuated through controlling the traction force $F_{t,i}$, and the braking force $F_{b,i}$, either by a human driver or some form of cruise control. Two resistive forces are considered, roll resistance $F_{r,i}$ and aerodynamic drag $F_{a,i}(v_i, d_i)$. The road grade at position x is denoted by $\alpha(x)$, and the gravitational force acting on the vehicle in the opposite direction of its movement,

$$F_{g,i}(\alpha(x_i)) = m_i g \sin\left(\alpha(x_i)\right).$$

The aerodynamic drag $F_{a,i}$ is major component of the resistive force acting on a large vehicle. Based on the vehicle's speed v_i and the distance to its preceding vehicle in a platoon d_i, the aerodynamic drag is modelled as

$$F_{a,i}(v_i, d_i) = \frac{1}{2}\rho_a A_a c_D \phi(d_i) v_i^2 = k_a v_i^2 \phi_a(d_i),$$

where $\phi_a(d)$ is positive, monotonically increasing and goes to 1 as d goes to infinity.

Assuming we have a platoon of n_p vehicles with constant headway d between them yields the resistive force acting on the platoon leader $F_{a,l}(u) = k_a v_p^2$ and on followers $F_{a,f}(u) = k_a v_p^2 \phi_f$, $\phi_f = \phi_a(d) < 1$. Here $v_i = v_p$ since all vehicles drive at the same speed in order to maintain constant headway. Then the total aerodynamic resistance acting on the whole platoon can be written as $F_{a,p}(v_p) = k_a v_p^2 \phi_p$, where $\phi_p = \phi_l + (n_p - 1)\phi_f$ is the total air drag coefficient of the platoon. Platooning always reduces the total air drag, i.e. air drag coefficients of single vehicles would be $\phi_1 = \phi_2 = 1$, while the total air drag coefficient of the platoon consisting of those vehicles would be approximately $\phi_p \approx 1.7$, assuming the intervehicular distance is 20 m [76].

Since the road grade is given as a function of the position, it can be beneficial to rewrite (5.1) to the form with position as the independent variable and time as dependent variable. Since $v_i > 0$, $x_i(t)$ is a bijection and we can write $t_i(x)$ as its inverse, i.e. the time when vehicle i is at the position x. Then (5.1) is uniquely rewritten as

$$m_i v_i \frac{\mathrm{d}v_i}{\mathrm{d}x} = F_{t,i} - F_{b,i} - F_{a,i}(v_i, d_i) - F_{r,i} - F_{g,i}(\alpha(x)). \tag{5.2}$$

5.2 Deviations from nominal platoon catch-up

Consider the simple platoon catch-up problem as formulated in Section 1.2. If both vehicles would be able to keep their desired speeds, $v_1(\tau) = u_1$ and $v_2(\tau) = u_2$ for

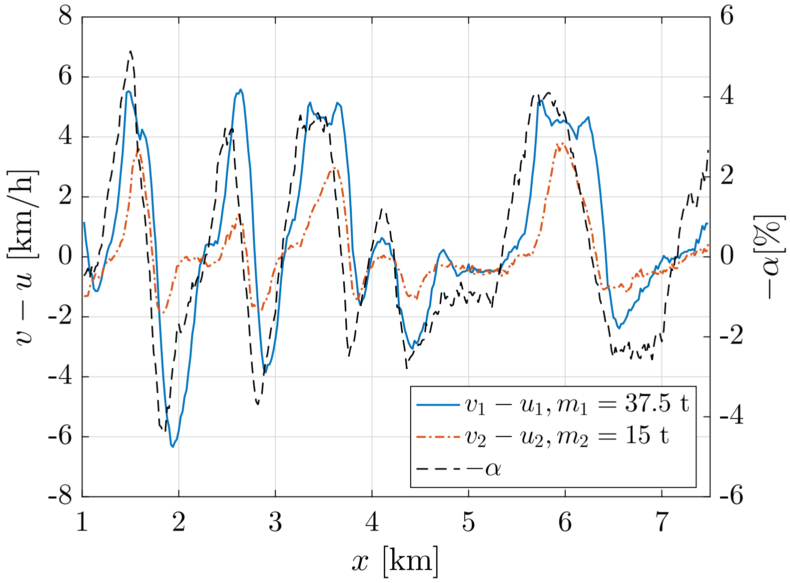

Figure 5.1: Deviation from the desired speed due to varying road grade for two trucks with different masses and negative road grade.

$0 \leq \tau \leq \tau_m$, their merging time and position would be

$$\begin{aligned} \tau_m &= \frac{\chi_0 - d_p}{u_2 - u_1}, \\ \chi_m &= u_2 \frac{\chi_0 - d_p}{u_2 - u_1}. \end{aligned} \tag{5.3}$$

However, even if the vehicles' desired speeds are constant, they will often be forced to deviate from them. Due to their large mass, the gravitational force affects trucks much more than it affects passenger cars. Heavy vehicles will often need to reduce their speed in order to tackle even small uphill slopes, even when driving at full power, and they need to brake or coast on downhill slopes in order to keep speed within safe bounds. A comparison of speed deviation from the nominal for the two trucks of different weight is shown in Fig. 5.1.

The surrounding traffic will also have an effect on the vehicles attempting to catch-up and merge into a platoon. Although when traffic is in free flow, trucks typically drive at a lower speed than the passenger cars, the same might not hold in case of congestion. This is particularly important for the case of platoon catch-up, since here the slower moving leader vehicle can act as a moving bottleneck, in turn worsening the traffic situation upstream of it. Traffic density and average traffic speed upstream of the moving bottleneck moving at speed u_1 are $r_c(\sigma_b, u_1)$ and $\mathcal{V}(r_c(\sigma_b, u_1))$, respectively. If the follower vehicle's desired speed is higher than this average traffic speed $u_2 > \mathcal{V}(r_c(\sigma_b, u_1))$, it is likely that the follower vehicle will be forced to reduce its speed and follow the overall traffic.

5.3 Platoon merging distance prediction based on the road grade

The first subproblem considered in this chapter is predicting how long it will take two trucks to form a platoon while driving on a highway at set cruise speeds, considering only the influence of varying road grade. In order to model this influence on the vehicle speed, we can either use a cruise control model, if available, or identify the dependence from data. Here, we used the experimental data from [84] to train a model that we then use to predict the evolution of vehicle speed. We then integrate the predicted vehicle speed profiles to calculate a prediction of when and where the platoon merge will occur. A significant advantage of speed prediction based merge distance prediction is that it gives us a prediction of the vehicle positions during the whole catch-up phase. This means that a disturbance that will change the platoon merging time can be detected immediately, by comparing the current vehicle positions, acquired from the GPS system, with their predicted values. When such a disturbance is identified, the prediction can be recalculated taking into account the updated information. Additionally, the new information can be used to re-plan desired vehicle speed profiles in order to compensate for the disturbance.

The prediction of platoon merge time and position can therefore be written exactly the same as (1.1) and (1.2), but using the predicted vehicle speeds $\hat{v}_i$ instead of the real speeds v_i. We use the hat to indicate predictions. The predicted positions of vehicles are

$$\begin{aligned} \frac{\mathrm{d}\hat{\chi}_1(\tau|t)}{\mathrm{d}\tau} &= \hat{v}_1(\tau|t), \\ \frac{\mathrm{d}\hat{\chi}_2(\tau|t)}{\mathrm{d}\tau} &= \hat{v}_2(\tau|t), \end{aligned} \tag{5.4}$$

where $\tau > 0$ is the relative time for the prediction calculated at (discrete) time instant t, i.e. $\hat{\chi}_i(\theta T|t)$ is a prediction of $x_i(t+\theta)$ and T is the sampling period. The predicted distance is $\hat{d}(\tau|t) = \hat{\chi}_1(\tau|t) - \hat{\chi}_2(\tau|t)$. The predicted platoon merging time and position are given by

$$\begin{aligned} \hat{\tau}_m(t) &= \min\left\{\tau \geq 0 \,\middle|\, \hat{d}(\tau|t) \leq d_p \right\}, \\ \hat{\chi}_m(t) &= \hat{\chi}_2(\hat{\tau}_m(t)|t). \end{aligned} \tag{5.5}$$

Vehicle speed prediction models

We will first discuss two simple speed prediction models, and then give the neural network speed model proposed in [18] in more detail. Finally, we describe how the proposed models were trained from data.

Constant average speed models:

The simplest vehicle speed prediction model assumes that both vehicles perfectly follow their reference speeds, assuming there are no disturbances. In that case, vehicle speed predictions are taken to be constant $\hat{v}_1 = u_1$, $\hat{v}_2 = u_2$, and platoon merging time and distance predictions are the same as (5.3), i.e.

$$\begin{aligned} \hat{\tau}_m(t) &= \frac{\chi_0(t) - d_p}{\hat{v}_2 - \hat{v}_1}, \\ \hat{\chi}_m(t) &= \hat{v}_2 \frac{\chi_0(t) - d_p}{\hat{v}_2 - \hat{v}_1}, \end{aligned} \tag{5.6}$$

where $\hat{v}_1 = u_1$ and $\hat{v}_2 = u_2$.

However, as already discussed, due to the changing road grade, traffic conditions and other exogenous effects, vehicle speeds will change. It has already been shown that even if there is no influence of traffic, even the mean speed deviation will be different for different vehicles (Fig. 5.1). Therefore, the prediction can be improved by incorporating mean speeds $\hat{v}_1 = \bar{v}_1$ and $\hat{v}_2 = \bar{v}_2$ in (5.6) as speed predictions during the catch-up phase for the training set of the given experiment scenario.

Road grade moving average speed model:

Better results can be obtained by modelling the vehicle speed deviation from its nominal value as a piecewise linear function of the moving average of road grade $\bar{\alpha}(x)$,

$$\hat{v}_i^{\alpha}(x) = u_i + u_i \cdot \begin{cases} k_{i,\alpha_+} \bar{\alpha}(x) & \bar{\alpha}(x) \geq 0 \\ k_{i,\alpha_-} \bar{\alpha}(x) & \bar{\alpha}(x) < 0. \end{cases} \tag{5.7}$$

An example of measured and modelled vehicle speeds are shown in Fig. 5.2. Note that the speed prediction for each vehicle is now given as a function of position, regardless of the vehicles' measured speed. We use different coefficients for positive and negative grades because the vehicles are affected differently by uphill and downhill slopes, and the distance over which we average road grade is determined empirically.

Neural network speed model:

Finally, the vehicle speed prediction proposed in [18] is based on learning the net propulsive force model and applying it in the dynamic equations (5.1) or (5.2). If we group air drag resistance $F_{a,i}$ and roll resistance $F_{r,i}$ with the traction force $F_{t,i}$ and braking force $F_{b,i}$ into $F_{p,i} = F_{t,i} - F_{b,i} - F_{a,i} - F_{r,i}$, this net propulsive force can be treated as the control action of the cruise controller, applied to overcome keep the vehicle speed close to its reference value. The cruise controller can adjust

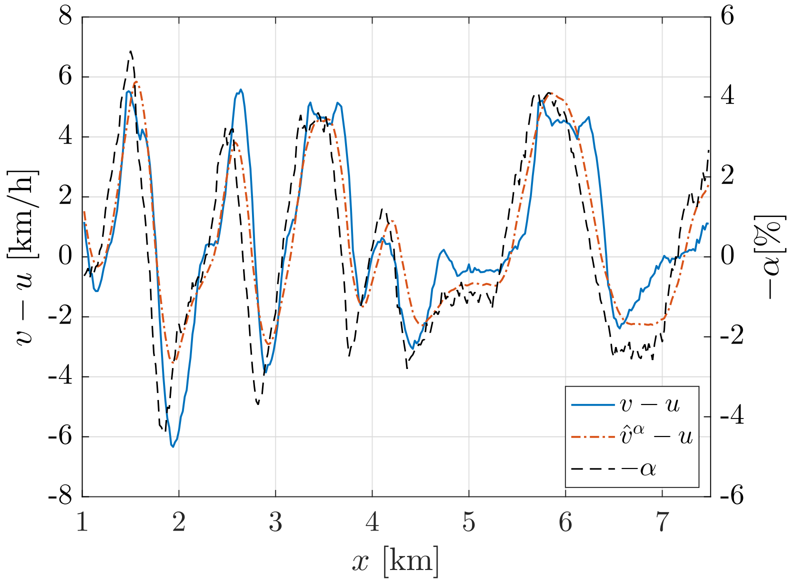

Figure 5.2: Actual and predicted deviation from the desired speed u using speed prediction model (5.7) and negative road grade.

the traction force, within the constraints imposed by maximum engine torque, so the propulsive force will also be manipulated within constraints that also take the resistive forces into account. Then, the speed dynamics of vehicle i (5.1) simplifies to

$$m_i \dot{v}_i = F_{p,i} - m_i g \sin(\alpha(x_i)).$$

We assume that $F_{p,i}$ will be a function of vehicle speed deviation from its reference speed, and of road grade at its position, $F_{p,i}(v_i - u_i, \alpha(x_i))$. Then the speed prediction can be written as

$$\begin{aligned}
\frac{\mathrm{d}\hat{v}_i(\tau|t)}{\mathrm{d}\tau} &= \frac{F_{p,i}\left(\hat{v}_i(\tau|t) - u_i(t), \alpha\left(\chi_i(\tau|t) + x_2(t)\right)\right)}{m_i} - g \sin\left(\alpha\left(\hat{\chi}_i(\tau|t) + x_2(t)\right)\right), \\
\frac{\mathrm{d}\hat{\chi}_i(\tau|t)}{\mathrm{d}\tau} &= \hat{v}_i(\tau|t),
\end{aligned}$$

with initial conditions $\hat{\chi}_1(0|t) = \chi_0(t)$, $\hat{\chi}_2(0|t) = 0$, and $\hat{v}_i(0|t) = v_i(t)$. Alternatively, taking position as the independent variable, we have

$$\begin{aligned}\frac{\mathrm{d}\hat{v}_i(x|t)}{\mathrm{d}x} &= \frac{1}{\hat{v}_i(x|t)}\left(\frac{F_{p,i}\left(\hat{v}_i(x|t) - u_i(t), \alpha(x)\right)}{m_i} - g\sin\left(\alpha(x)\right)\right),\\ \frac{\mathrm{d}\hat{\tau}_i(x|t)}{\mathrm{d}x} &= \frac{1}{\hat{v}_i(x|t)}\end{aligned}$$

with initial conditions $\hat{\tau}_1(\chi_0|t) = 0$ or $\hat{\tau}_2(0|t) = 0$, and again $\hat{v}_i(0|t) = v_i(t)$. Now, the function

$$\frac{F_{p,i}\left(\hat{v}_i(x|t) - u_i(t), \alpha(x)\right)}{m_i} = \hat{v}_i(x|t)\frac{\mathrm{d}\hat{v}_i}{\mathrm{d}x}(x|t) + g\sin\left(\alpha(x)\right) \tag{5.8}$$

can be learned from data. Using this model, we can predict vehicle speed for the whole length of the road of interest.

In order to do this, we will first need to discretize this model. Consider equally spaced points along the road, $X_k = kL$, where the road segment length L is small enough to capture the dynamics of the system, but large enough so that $L > Tv_{\max}$, i.e., vehicles do not pass through segments of length L in less than T. Then, to each X_k along the vehicle trajectory, for both vehicles i, we assign

$$\begin{aligned}\tau_{i,k} &= \min\left\{\tau | x_i(\tau) > X_k\right\},\\ v_{i,k} &= \frac{\int_{\tau_{i,k}}^{\tau_{i,k+1}} v_i(\tau)\mathrm{d}\tau}{\tau_{i,k+1} - \tau_{i,k}},\end{aligned}$$

where $\tau_{i,k}$ is the time vehicle i enters segment $[X_k, X_{k+1}]$, and $v_{i,k}$ its average speed in the segment. The road grade α_k is also taken as average road grade over the road segment $[X_k, X_{k+1}]$. Since road grades will typically be less than 5%, we can approximate $\sin(\alpha) \approx \alpha$.

Discretizing (5.8) by integration and taking this approximation, we get

$$\frac{F_{p,i}\left(v_{i,k-1} - u_i, \alpha_{k-1}\right)}{m_i} = \frac{v_{i,k}^2 - v_{i,k-1}^2}{2L} + g\alpha_{k-1}. \tag{5.9}$$

It turns out that (5.9) can be learned using a feedforward neural network, as will be described in the next subsection. Once the model for $F_{p,i}$ is available, the discrete prediction model for vehicle speed becomes

$$\hat{v}_{i,k+1} = 2L\sqrt{\hat{v}_{i,k}^2 + \frac{F_{p,i}\left(\hat{v}_{i,k} - u_i, \alpha_k\right)}{m_i} - g\alpha_k}, \tag{5.10}$$

and $\hat{v}_i(\tau|t)$ can be written as

$$\hat{v}_i(\tau|t) = \hat{v}_{i,k}, \quad \hat{\tau}_{i,k} \le \tau < \hat{\tau}_{i,k+1}, \tag{5.11}$$

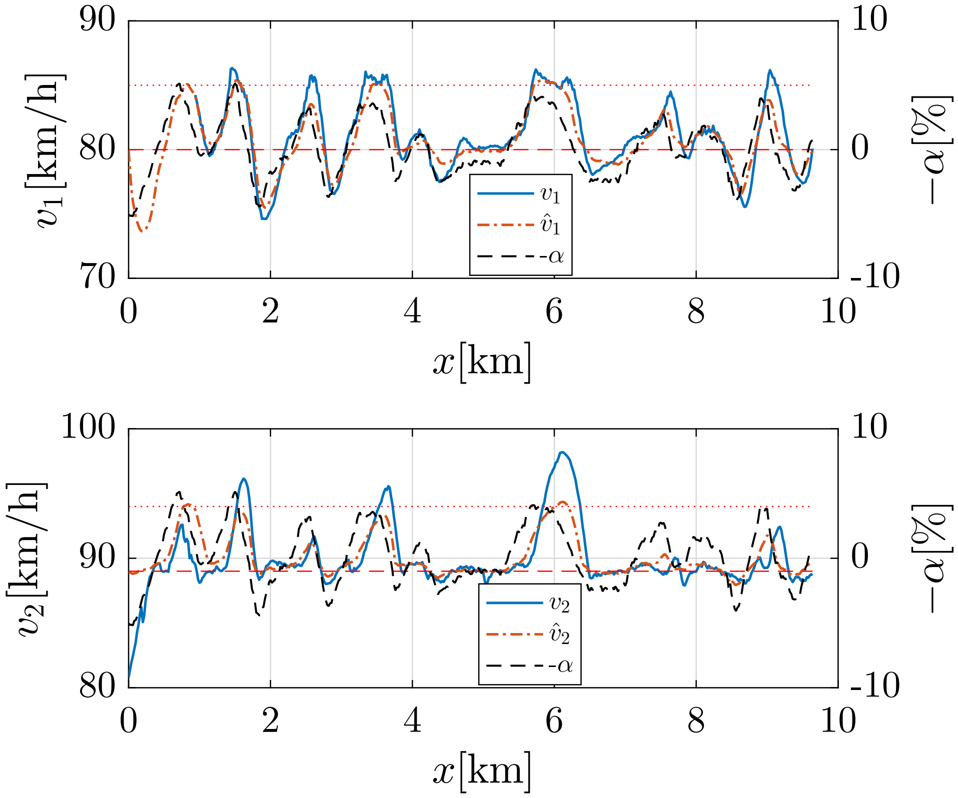

Figure 5.3: Predicted ($\hat{v}$) and measured (v) speed for the leader and the follower vehicle and negative road grade.

where

$$\hat{\tau}_{i,k+1} = \hat{\tau}_{i,k} + \frac{L}{\hat{v}_{i,k}},$$

assuming vehicle speeds will be approximately constant while driving on each road segment.

Finally, the vehicle speed prediction is calculated by initializing (5.10) with either $\hat{v}_{i,k_i(t)}(t) = v_i(t)$ or $\hat{v}_{i,k_i(t)}(t) = u_i(t)$, where $k_i(t)$ is the segment the vehicle is in at time t, $X_{k_i(t)} \leq x_i(t) < X_{k_i(t)+1}$ and recursing (5.10). We then use (5.11) in (5.4) to get

$$\hat{\chi}_i(\tau|t) = \hat{v}_{i,k_i(t)-1}\hat{\tau}_{i,k_i(t)} + \sum_{k=k_i(t)}^{K_i(\tau|t)} \left(\hat{v}_{i,k}\left(\hat{\tau}_{i,k+1} - \hat{\tau}_{i,k}\right)\right) + \hat{v}_{i,K_i(\tau|t)}(\tau - \hat{\tau}_{i,K_i(\tau|t)}),$$

where $k_i(t)$ and $K_i(\tau|t)$ are given by

$$X_{k_i(t)} \leq x_i(t) < X_{k_i(t)},$$
$$X_{K_i(\tau|t)} \leq x_2(t) + \chi_i(\tau|t) < X_{K_i(\tau|t)+1}.$$

The platoon merge time and position predictions are calculated according to (5.5). A comparison between the measured speeds and the speed prediction acquired this way, for a part of a test run, is shown in Figure 5.3.

Speed prediction model training

In the experiments [84] two HDVs were driving on an 11 km long stretch of public highway between Stockholm and Södertälje, namely between the Hallunda and Moraberg interchanges. Two standard Scania tractor trucks were used. The lead vehicle had a 480 hp engine and its total weight, including its trailer, was 37.5 tonnes. The follower vehicle had a 450 hp engine, had no trailer and weighed 15 tonnes. The road is fairly hilly, with road grades as high as $\pm 5\%$. The HDVs, initially apart, attempted to form a two-vehicle platoon by driving with different desired speed adaptive cruise control (ACC) settings. Three different desired speed pairs were considered, $(u_1, u_2) = (75, 85), (75, 89)$ and $(80, 89)$ km/h, where u_1 is the reference speed of the leader vehicle and u_2 of the follower. Downhill speed control was also active, with the offset of 5 km/h, allowing the vehicles to accelerate on downhill slopes and gain speed up to the set limit. The initial distance between the vehicles ranged from 400 m to 1300 m. The part of the experiment data that we used consist of periodical vehicle speed measurements and calculated distance between the vehicles, together with the information about road topography. Since we are primarily interested in the catch-up phase, we will consider the platoon merging completed when the distance between the vehicles is less than $d_p = 80$m, ignoring phenomena such as persistent drivers [84].

We used the vehicle speed data from the experiments to train the two proposed vehicle speed prediction models, the neural network approximation model (5.9)–(5.11) and the simple road grade moving average piecewise linear model (5.7). Roughly half of the experiment data was used for training and the rest was used for testing, and only the test runs which resulted in successful platoon formation were considered. Models for the leader and the follower vehicle speed prediction were trained independently.

Training the road grade moving average piecewise linear model consists of four linear regression equations of the form

$$\frac{v_{i,k} - u_i}{u_i} = k_{i,\alpha_\pm} \bar{\alpha}_k,$$

one for uphill (α_+) and one for downhill (α_-) slopes for each vehicle. Here, road grade is averaged over 400 meters and the calculated values of the regression parameters are $k_{1,\alpha_+} = -1.28$, $k_{1,\alpha_-} = -1.81$ for the leader and $k_{2,\alpha_+} = -0.32$,

$k_{2,\alpha_-} = -0.73$ for the follower vehicle. The speeds of both vehicles are more affected by downhill slopes than uphill slopes, and this effect is more pronounced on the leader vehicle, since it is significantly heavier than the follower vehicle. Uphill slopes have little effect on the follower vehicle speed, which could also be observed in experiment data (Fig. 5.1).

Before training the neural network speed model, it's necessary to select a structure for the neural network. Several structures were tested, and best results were acquired using a neural network with two hidden layers with five and three nodes and hyperbolic tangent sigmoid activation functions. This neural network is shown in Fig. 5.4. The output of the neural network is a nonlinear function of its inputs, $y_i(j) = f_{w,i}(x_i(j))$, parametrized by its weight matrices $W_i^{(l)}$, $l = 1, 2, 3$, which are trained using a back-propagation algorithm. The j-th sample input and target data for both neural networks are

$$
\begin{aligned}
x_i(j) &= \left[v_{i,j} - u_i \;\; \alpha_{j-1}\right]^\top, \\
y_i(j) &= \frac{v_{i,j}^2 - v_{i,j-1}^2}{2L} + g\alpha_{j-1}.
\end{aligned}
$$

By adopting this simple model, we assume that the behaviour of the vehicles only depends on local road topography. This allows us to use this model on any road segment whose topography is represented in the training data. Since highways in general follow similar topographic guidelines, most highways should be covered, except for road segments with long uphill or downhill slopes, which were not present in the training data. To enable generalization to these road segments, more data would need to be collected by running more experiments on different roads.

The training data from all three desired speed pair scenarios (u_1, u_2) was considered together, excluding data points if the distance between the vehicles is smaller than 200 m, vehicle speed differs from the goal speed by more than 10 km/h or

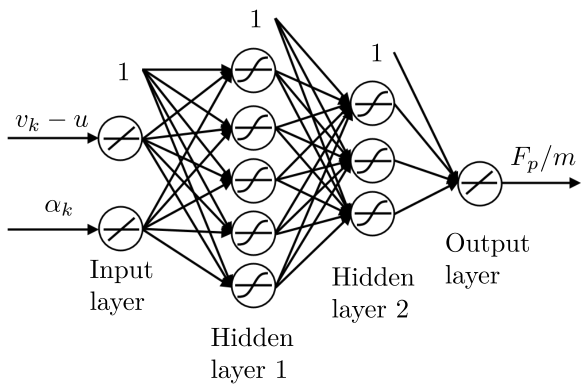

Figure 5.4: Structure of F_p/m neural networks.

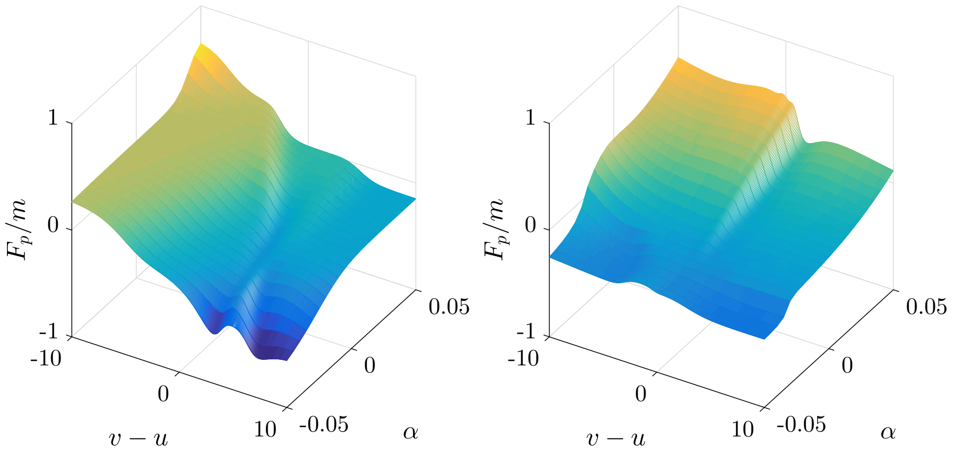

(a) Leader (b) Follower

Figure 5.5: F_p/m as a function of $v - v_{\mathrm{ref}}$ and α for the leader and the follower vehicle.

the distance from the start is less than 200 m. These data points are excluded in order to avoid speed changes that occur during the final platoon merging maneuver or if the vehicle is forced to brake, as well as to give the follower vehicle enough time to reach its goal speed. Finally, to reduce computational effort, the trained neural networks are implemented as look-up tables. Values of $F_{p,i}/m_i$ are shown in Fig. 5.5. In general, applied propulsive force will increase with road grade and vehicle speed deviation. This increase is faster around the origin ($v_i \approx u_i, \alpha \approx 0$) and it gets slower for larger speed discrepancies and road grades because the engine power is limited.

Experimental results

Platoon merging distance prediction based on the two proposed vehicle speed prediction methods is evaluated using the test data set. The comparison is summed up in Table 5.1 and box plots of relative errors are shown in Fig. 5.6. The relative error is defined as the ratio between the distance prediction error and the actual platoon merging position,

$$\tilde{\chi}_m^{rel} = \frac{\hat{\chi}_m(t) - \chi_m(t)}{\chi_m(t)}.$$

Also shown are naive estimates according to (5.6), assuming vehicle speed is constant. We can see that the neural network based approach shows consistently better results, with the smallest root mean square error and standard deviation.

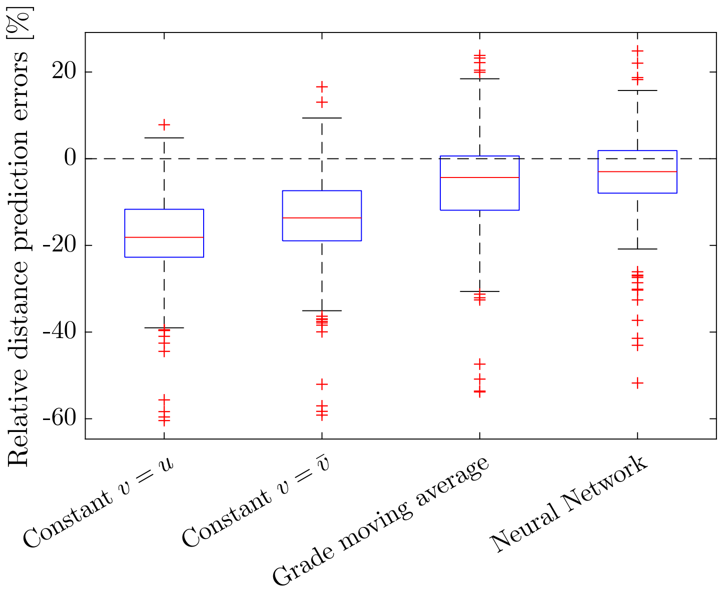

Figure 5.6: Box plots of relative platoon merge distance prediction errors.

Table 5.1: Comparison between the predicted merge distance errors for different speed prediction models.

	Constant $v = u$		Constant $v = \bar{v}$		Grade mov. avg.		Neural network	
	RMSE	STD	RMSE	STD	RMSE	STD	RMSE	STD
(75,85)	1492.65	704.58	1275.65	700.42	814.51	700.49	678.65	579.22
(75,89)	1386.28	948.91	1289.35	952.21	1060.23	956.22	865.83	829.03
(80,89)	1658.93	837.86	1287.53	870.10	975.07	861.52	835.46	786.28
Total	1516.22	855.45	1284.41	851.30	959.11	846.51	800.49	741.33

Once the future speed profile is predicted, it is easy to adopt some empirical criterion for recalculating the platoon merge distance predictions. This enables us to only recalculate speed profile predictions when the measured speed deviates from its predicted value due to some disturbances or model mismatch, instead of recalculating them periodically. The results of applying one such recalculation criterion for one test run are shown on Fig. 5.7. Here, recalculations were done at most once per 400 m, when speed deviations are more than 3 km/h. The speed of the follower vehicle will be recalculated twice, once at $x_2 = 600$ m and another time at $x_2 = 1020$ m. We can see that recalculating the speeds improves the platoon merging distance prediction, from approximately 393 m (4.12% of the current remaining distance) at the start of the test run to 170 m (1.9%) after 600 m, and down to 70 m (0.8%) after another 420 m.

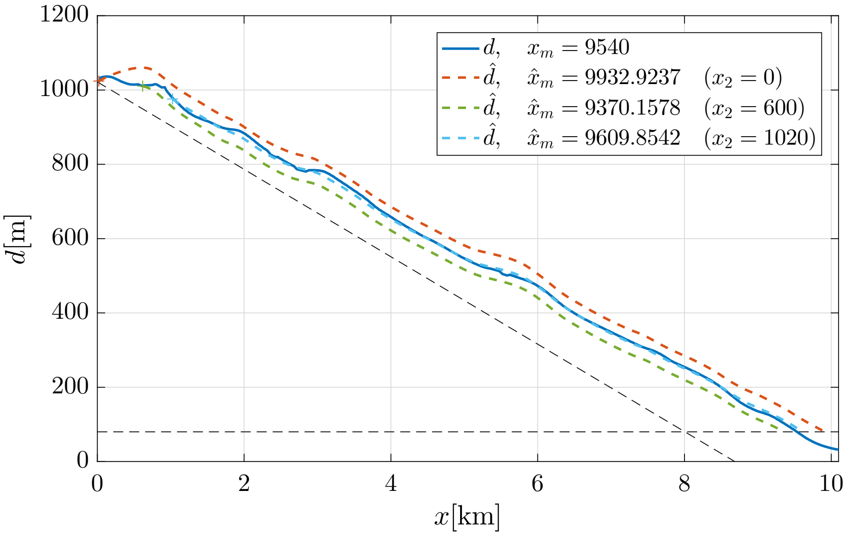

Figure 5.7: Recalculated merge distance predictions. The diagonal dashed black line shows the platoon catch-up phase if both vehicles would follow their reference speeds, and the horizontal dashed black line indicates distance d_p. The coloured dashed lines show the prediction of the distance between the vehicles, calculated when $x_2 = 0$, $x_2 = 600$ and $x_2 = 1020$.

The neural network model predicts nominal vehicle speeds reasonably well in nominal conditions (Fig. 5.3). However, the vehicles will often deviate from their nominal behaviour, resulting in larger discrepancies between the predicted and actual speed and causing outliers in merging distance prediction. Most often, we cannot be sure what caused the deviation. In a number of test runs, the cruise control goal speeds were set wrong, and a vehicle drove slower or faster than intended. The nominal downhill speed control offset, set to 5 km/h, was exceeded in some test runs (clearly visible on Fig. 5.3), and in some other test runs, the offset was reduced to 3 km/h. Apart from these situations, the traffic conditions are the most likely cause of larger deviations from nominal vehicle behaviour, especially when the nominal speed of the vehicles was close to the speed limit.

The box plots (Fig. 5.6) show that the mean error for all methods is negative, i.e., all methods on average predict that the platoon will merge sooner than it actually does. The neural network speed model gives the smallest median and mean relative errors, -3% and -4%, respectively. In general, the influence of the surrounding traffic conditions on the trucks is hard to see from truck speed measurements when the speed of the truck is much lower than the average speed on the road. In the first test-scenario, the follower vehicle was driving with nominal speed of 85 km/h, while the speed limit on the road was 100 km/h, and the road grade was the main cause of its speed deviation. In two other scenarios, the influence of traffic conditions was much more apparent, resulting in larger root mean square errors (835.46 and 865.83 versus 678.65).

5.4 Energy-optimal platoon catch-up in traffic

The second subproblem considered in this chapter is calculating energy-optimal speeds for vehicles attempting to merge to a platoon. These speeds will be given as reference speeds u_1 and u_2 that the vehicles will attempt to follow. We will assume these speeds are constant, unless something in the environment changes from the time they were calculated. Whereas in the previous section, the focus was solely on the catch-up phase, we now also have to take into account the platooning phase, during which the vehicles drive together and achieve fuel savings through air drag reduction.

We denote by x_f the end of the common road segment, i.e. the position at which the platoon will split, with vehicles continuing their separate ways afterwards. Without loss of generality, we will set d_p to zero in this section. Although in reality, vehicles might have some degree of flexibility with regard to timing, by only considering one fixed t_f, we ensure that the comparison between different pairs of speeds (u_1, u_2) is fair. In order to negate the ostensible energy saving by simply reducing the speed of a vehicle, in turn causing it to be delayed, we assume that both vehicles need to be at position x_f at some specified time t_f. This is trivially satisfied in case the vehicles did form a platoon, but even if we chose for the vehicles not to attempt to catch-up and form a platoon, we can use this assumption while calculating optimal speeds. While calculating the optimal catch-up speeds at time instant t, we will be using the relative coordinate system similar to the one used in the previous section, and

$$\tau_f(t) = (t_f - t)T,$$
$$\chi_f(t) = x_f - x_2(t).$$

For readability, we omit writing t wherever this time instant is irrelevant or obvious. If the calculated speeds are such that the vehicles merge into a platoon very close to x_f, we will know that is not beneficial to attempt forming a platoon, and the vehicles can proceed driving according to their own plans.

Another way of dealing with this issue is by including delay into the cost function. However, this would lead to a more complicated optimization problem and

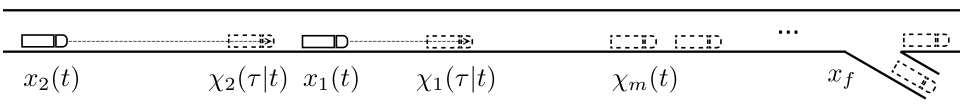

Figure 5.8: Platoon catch-up problem.

necessitate ad-hoc combination of two heterogeneous terms. To keep the optimization problem consistent and simple, we will therefore use the former approach and take t_f so that it satisfies the most stringent constraints the two vehicles have.

Energy-optimal catch-up problem

We focus on reducing the total work required to overcome the resistive forces acting on the vehicles. The three major external forces acting on vehicles are air drag, rolling resistance and gravity. Since we are generating reference speed profiles, we assume that road grade is zero. In reality, varying road grade will be handled by some form of look-ahead control. This assumption allows us to focus solely on reducing air drag, since the contribution of rolling resistance will be the same whether or not the vehicles adjust their speeds and attempt to merge into a platoon.

Ideally, the metric that we would like to use to evaluate the optimality of chosen catch-up speeds would be fuel consumption. However, getting accurate fuel consumption models can be very difficult, and will depend on the properties of the vehicles in question. Instead, we focus on reducing the total work required to overcome the resistive forces acting on the vehicles, which yields more general results.

Based on the air drag model described in 5.1, the cost function related to this component of the overall resistive force can therefore be written

$$J = \int_0^{\tau_m} v_1^3(\tau) + v_2^3(\tau) d\tau + \phi \int_{\tau_m}^{\tau_f} v_p^3(\tau) d\tau, \tag{5.12}$$

where by ϕ we denote the total air drag coefficient of the platoon. In order for the vehicles to obey the timing and platoon merge constraints, we require that

$$\int_0^{\tau_m} v_2(\tau) - v_1(\tau) d\tau = \chi_0, \tag{5.13a}$$

$$\int_0^{\tau_m} v_1(\tau) d\tau + \int_{\tau_m}^{\tau_f} v_p(\tau) d\tau = \chi_f - \chi_0, \tag{5.13b}$$

$$\int_0^{\tau_m} v_2(\tau) d\tau + \int_{\tau_m}^{\tau_f} v_p(\tau) d\tau = \chi_0, \tag{5.13c}$$

$$u_{\min} \leq v_1 \leq u_{\max}, \tag{5.13d}$$

$$u_{\min} \leq v_2 \leq u_{\max}, \tag{5.13e}$$

$$u_{\min} \leq v_p \leq u_{\max}. \tag{5.13f}$$

Here constraint (5.13a) ensures that $\chi_1(\tau_m) = \chi_2(\tau_m)$, constraints (5.13b) and (5.13c) ensure that $\chi_1(\tau_f) = \chi_f$ and $\chi_2(\tau_f) = \chi_f$, and constraints (5.13d), (5.13e) and (5.13f) give the admissible ranges for speeds v_1, v_2 and v_p.

Assume first that the vehicles were able to follow their desired speeds, $v_i(\tau) = u_i$ and $v_p(\tau) = u_p$. We will denote the platoon merging time and position for this case by τ_{m_0} and χ_{m_0}. Then, consistently with the conditions (5.13a)-(5.13c), τ_{m_0} and χ_{m_0} are given by (5.3), and the speed of the merged platoon is

$$v_p(\tau) = u_p = \frac{\chi_f - \chi_{m_0}}{\tau_f - \tau_{m_0}}.$$

Then the cost function (5.12) becomes

$$J_0(u) = (u_1^3 + u_2^3)\tau_{m0} + \phi\frac{(\chi_f - \chi_{m_0})^3}{(\tau_f - \tau_{m_0})^2}.$$

This cost function is parametrized by χ_0, χ_f, τ_f and ϕ, and we seek to minimize it by choice of u_1 and u_2.

Denote by $u_{10} = \frac{\chi_f - \chi_0}{\tau_f}$ and $u_{20} = \frac{\chi_f}{\tau_f}$ the constant speeds individual vehicles should keep in order to reach χ_f at τ_f, and assume this is possible without violating the constraints on minimum and maximum speed. Note that, although possible, it will never be beneficial for the leader to go faster than $u_{10} \leq u_{\max}$ nor for the follower to go slower than $u_{20} \geq u_{\min}$. Therefore, we can further tighten the constraints to $u_{\min} \leq u_1 \leq u_{10}$ and $u_{20} \leq u_2 \leq u_{\max}$. The minimization problem that we solve to calculate optimal u_1 and u_2 then becomes

$$\begin{aligned} \underset{u_1,u_2}{\text{minimize}} \quad & \frac{(u_1^3 + u_2^3)\chi_0}{u_2 - u_1} + \phi\frac{(\chi_f(u_2 - u_1) - u_2\chi_0)^3}{(u_2 - u_1)(\tau_f(u_2 - u_1) - \chi_0)^2} \\ \text{subject to} \quad & u_{\min} \leq u_1 \leq u_{10} \\ & u_{20} \leq u_2 \leq u_{\max} \end{aligned} \tag{5.14}$$

This is a convex problem and can easily be solved numerically.

However, since we assumed no interference from traffic and other extraneous factors that might render it impossible for the follower vehicle to maintain its optimal speed, we might see discrepancies in behaviour that will make this solution suboptimal. In Fig. 5.9 we see the calculated optimal catch-up speeds and the average traffic speed upstream of the leader vehicle calculated in the moving bottleneck framework. The optimal speeds are given as a function of ϕ, ranging from 1 (the follower vehicle in a platoon experiences no air drag) to 2 (platooning does not reduce air drag at all). We can see that even for $\phi \approx 1.8$, we have $u_2 > \mathcal{V}(r_c(\sigma_b, u_1))$ (u_2 greater than the average traffic speed upstream of the leader vehicle), so the follower vehicle will not be able to maintain its optimal catch-up speed in face of congestion caused by the leader, and this discrepancy will cause the actual platoon merging to occur later. Consequently, the energy savings will be lower than expected and suboptimal, further motivating including the traffic conditions in the optimization problem.

The influence of traffic

We assume we can split the initial traffic conditions between them into two zones, $\rho(x, 0) \approx \rho_f,\ x < \chi_c$ and $\rho(x, 0) \approx \rho_c,\ x > \chi_c$, where χ_c is the minimal x for which

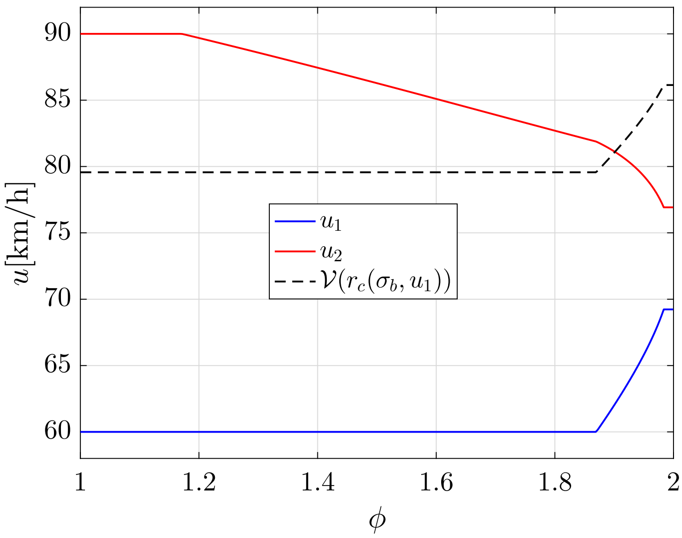

Figure 5.9: Optimal catch-up speeds for leader and follower vehicles and average traffic speed upstream of the leader vehicle.

$\mathcal{V}(\rho(\chi_c, 0)) < u_{\max}$. We calculate ρ_f and ρ_c as average values of ρ on $[0, \chi_c]$ and $[\chi_c, \chi_0]$ respectively. If $\mathcal{V}(\rho(x, 0)) \geq u_{\max}$ for all $x \in [0, \chi_0]$, we set $\chi_c = \chi_0$ and $\rho_c = \sigma$.

The follower vehicle can only be slowed down when it enters the zone of density ρ_c, or the zone of density $r_c(\sigma_b, u_1)$, originating from the leader vehicle. In further text, we denote $r_f(\sigma_b, u_2)$ as simply r_f and $r_c(\sigma_b, u_1)$ as r_c.

The solution to thus described composite Riemann problem for $\tau \approx 0$ is given by

$$\rho(x, \tau) = \begin{cases} r_f, & x < \lambda_{r_f \rho_f} \tau, \\ \rho_f, & \lambda_{r_f \rho_f} \tau < x < \chi_c + \lambda_{\rho_f \rho_c} \tau, \\ \rho_c, & \chi_c + \lambda_{\rho_f \rho_c} \tau < x < \chi_0 - W\tau, \\ r_c, & \chi_0 - W\tau < x, \end{cases}$$

where $\lambda_{\rho_- \rho_+} = \Lambda(\rho_-, \rho_+)$. This solution is valid until the first front interaction, when either the zone of density ρ_f disappears,

$$\lambda_{r_f \rho_f} \tau = \chi_c + \lambda_{\rho_f \rho_c} \tau \tag{5.15}$$

or the zone of density ρ_c disappears,

$$\chi_c + \lambda_{\rho_f \rho_c} \tau = \chi_0 - W\tau. \tag{5.16}$$

We denote the solution in τ to (5.15)

$$\tau_{\rho_f}(u) = \frac{\chi_c}{\lambda_{r_f\rho_f} - \lambda_{\rho_f\rho_c}},$$

and the solution in τ to (5.16)

$$\tau_{\rho_c}(u) = \frac{\chi_0 - \chi_c}{\lambda_{\rho_f\rho_c} + W}.$$

The times of following front interactions will be delineated by noting the order in which the zones of particular density vanished. For example, $\tau_{\rho_c\rho_f}$ denotes the time at which zone of density ρ_f vanishes in second front interaction, after zone of density ρ_c vanished in first front interaction.

The rest of the front interaction times are given by

$$\begin{aligned}
\tau_{\rho_f r_f} &= \tau_{\rho_f}\frac{\lambda_{r_f\rho_f} - \lambda_{r_f\rho_c}}{u_2 - \lambda_{r_f\rho_c}},\\
\tau_{\rho_f\rho_c} &= \frac{\chi_0 + \tau_{\rho_f}(\lambda_{r_f\rho_c} - \lambda_{r_f\rho_f})}{\lambda_{r_f\rho_c} + W},\\
\tau_{\rho_c\rho_f} &= \frac{\chi_0 - \tau_{\rho_c}(\lambda_{\rho_f r_c} + W)}{\lambda_{r_f\rho_f} - \lambda_{\rho_f r_c}},\\
\tau_{\rho_c r_c} &= \tau_{\rho_c}\frac{\lambda_{\rho_f r_c} + W}{\lambda_{\rho_f r_c} - u_1},\\
\tau_{t_1} = \tau_{\rho_f r_f\rho_c} &= \frac{\chi_0 + \tau_{\rho_f r_f}(v_{\rho_c}(u_2) - u_2)}{v_{\rho_c}(u_2) + W},\\
\tau_{t_2} = \tau_{\rho_f\rho_c r_f} &= \frac{\chi_0 - \tau_{\rho_f\rho_c}(\lambda_{r_f r_c} + W)}{u_2 - \lambda_{r_f r_c}},\\
\tau_{t_3} = \tau_{\rho_c\rho_f r_f} &= \tau_{\rho_c\rho_f}\frac{\lambda_{r_f\rho_f} - \lambda_{r_f r_c}}{u_2 - \lambda_{r_f r_c}},\\
\tau_{\rho_c\rho_f r_c} &= \frac{\chi_0 + \tau_{\rho_c\rho_f}(\lambda_{r_f r_c} - \lambda_{r_f\rho_f})}{\lambda_{r_f r_c} - u_1}
\end{aligned}$$

From the standpoint of cost function, there are four cases of traffic we need to consider based on the ordering of front interactions:

- **Case 0**: The follower is unaffected by traffic. This case typically happens in light traffic, when the zone of density ρ_c vanished first, $\tau_{\rho_c} < \tau_{\rho_f}$, and the zone of density r_c vanishes before the zone of density r_f, with either $\tau_{\rho_c\rho_f r_c} < \tau_{\rho_c\rho_f r_f}$ or $\tau_{\rho_c r_c} < \tau_{\rho_c\rho_f}$.

  This case was already discussed and corresponds to using J_0 as the cost function.

- **Case 1**: The zone of density ρ_f vanishes first, $\tau_{\rho_f} < \tau_{\rho_c}$, then the zone of density r_f, $\tau_{\rho_f r_f} < \tau_{\rho_f \rho_c}$. The follower vehicle first enters the zone of traffic of density ρ_c, and then of traffic density r_c at time τ_{t_1}.
- **Case 2**: The zone of density ρ_f vanishes first, $\tau_{\rho_f} < \tau_{\rho_c}$, then the zone of density ρ_c, $\tau_{\rho_f r_f} > \tau_{\rho_f \rho_c}$. The follower vehicle only enters the zone of traffic density r_c at time τ_{t_2}.
- **Case 3**: The zone of density ρ_c vanishes first, $\tau_{\rho_f} > \tau_{\rho_c}$, and the zone of density r_f vanishes before the zone of density r_c, with $\tau_{\rho_c \rho_f r_c} > \tau_{\rho_c \rho_f r_f}$ and $\tau_{\rho_c r_c} > \tau_{\rho_c \rho_f}$. The follower vehicle only enters the zone of traffic density r_c at time τ_{t_3}.

The latter three cases are shown on Figure 5.10. We denote the speed the follower vehicle maintains in traffic of density ρ, $v_\rho(u_2) = \min(u_2, \mathcal{V}(\rho))$. Finally, for traffic cases $i = 1, 2, 3$, the platoon merge will occur when the fronts corresponding to the leader and the follower vehicle intersect, at

$$\begin{aligned} \tau_{m_i} &= \frac{\chi_0 - \chi_{t_i} + v_{r_c}(u_2)\tau_{t_i}}{v_{r_c}(u_2) - u_1} \\ \chi_{m_i} &= \chi_0 + u_1 \tau_{m_i} \end{aligned}$$

where

$$\begin{aligned} \chi_{t_1} &= \chi_0 - W\tau_{\rho_f r_f \rho_c}, \\ \chi_{t_2} &= u_2 \tau_{\rho_f \rho_c r_f}, \\ \chi_{t_3} &= u_2 \tau_{\rho_c \rho_f r_f}, \end{aligned}$$

are the positions where the follower vehicle enters the traffic zone of density r_c.

Under the stated assumptions, the cost function (5.12) can be written as

$$J(u) = \begin{cases} J_0(u), & \tau_{\rho_f} > \tau_{\rho_c}, (\tau_{\rho_c \rho_f r_c} < \tau_{\rho_c \rho_f r_f} \vee \tau_{\rho_c r_c} < \tau_{\rho_c \rho_f}), \\ J_1(u), & \tau_{\rho_f} < \tau_{\rho_c}, \tau_{\rho_f r_f} < \tau_{\rho_f \rho_c}, \\ J_2(u), & \tau_{\rho_f} < \tau_{\rho_c}, \tau_{\rho_f r_f} > \tau_{\rho_f \rho_c}, \\ J_3(u), & \tau_{\rho_f} > \tau_{\rho_c}, \tau_{\rho_c \rho_f r_f} < \tau_{\rho_c \rho_f r_c}, \tau_{\rho_c \rho_f} < \tau_{\rho_c r_c}, \end{cases}$$

where

$$\begin{aligned} J_1(u) &= u_1^3 \tau_{m_1} + u_2^3 \tau_{\rho_f r_f} + u_{\rho_c}^3 (\tau_{t_1} - \tau_{\rho_f r_f}) + u_{r_c}^3 (\tau_{m_1} - \tau_{t_1}) + \frac{(\chi_f - \chi_{m_1})^3}{(\tau_f - \tau_{m_1})^2}, \\ J_2(u) &= u_1^3 \tau_{m_2} + u_2^3 \tau_{t_2} + u_{r_c}^3 (\tau_{m_2} - \tau_{t_2}) + \frac{(\chi_f - \chi_{m_2})^3}{(\tau_f - \tau_{m_2})^2}, \\ J_3(u) &= u_1^3 \tau_{m_3} + u_2^3 \tau_{t_3} + u_{r_c}^3 (\tau_{m_3} - \tau_{t_3}) + \frac{(\chi_f - \chi_{m_3})^3}{(\tau_f - \tau_{m_3})^2}. \end{aligned}$$

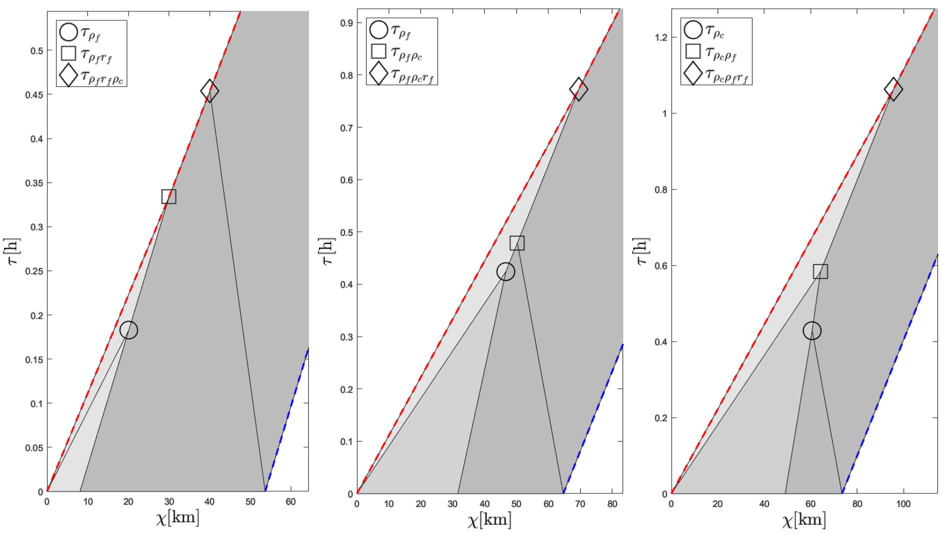

(a) $\tau_{\rho_f} < \tau_{\rho_c}$, $\tau_{\rho_f r_f} < \tau_{\rho_f \rho_c}$ (b) $\tau_{\rho_f} < \tau_{\rho_c}$,$\tau_{\rho_f r_f} > \tau_{\rho_f \rho_c}$ (c) $\tau_{\rho_f} > \tau_{\rho_c}$

Figure 5.10: Front tracking prediction of traffic between the leader (dashed blue) and the follower (dashed red).

To enforce speed and timing constraints on the vehicles, we add two additional barrier terms to J_i, corresponding to inequalities

$$\frac{\chi_f - \chi_{m_i}}{\tau_f - \tau_{m_i}} \leq u_{p,\max},$$
$$\tau_{m_i} \leq \tau_f,$$

where $u_{p,\max}$ is the maximum speed of the merged platoon, which could differ from $u_{\max}$. These two inequalities ensure that both vehicles will be able to reach position x_f at time t_f.

Finally, the optimization problem we want to solve in order of finding the energy-optimal catch-up speeds for two vehicles under constraints imposed by the surrounding traffic is

$$\begin{aligned} \underset{u_1,u_2}{\text{minimize}} \quad & J(u) \\ \text{subject to} \quad & u_{\min} \leq u_1 \leq u_{10} \\ & u_{20} \leq u_2 \leq u_{\max} \end{aligned} \tag{5.17}$$

This problem might not be convex, but it is unimodal.

Simulation results

Finally, we test the derived control laws in simulations. The metric we will be using is the percentage of energy saved, according to (5.12), compared to the case the vehicles would drive at a constant speed and arrive at x_f at time t_f. In total a 100 simulations were executed for each control law and traffic density range.

The simulation scenario in question is as follows:

1. $t < t_{10}$: The traffic is in free flow, with heterogeneous traffic density. The leader vehicle enters the road segment at $t = t_{10}$.

2. $t_{10} \leq t < t_{20}$: The leader vehicle travels at speed v_{01}, at which it would reach χ_f at time t_f. The follower vehicle enters the road segment at $t = t_{20}$.

3. $T_{20} \leq t < t_m$: The leader and the follower adjust their speeds according to the specified control law, until they merge into a platoon.

4. $t \geq t_m$: The newly merged platoon proceeds and adjusts its speed so that it reaches x_f at time t_f.

If the platoon merging fails for any of the control laws, or if the vehicles violate the timing constraint (not arrive at x_f by t_f), the vehicles proceed at their maximum speed until the end of the segment, and that simulation run is not counted in average cost calculations.

The initial background traffic conditions $\rho_i(0)$ and inflow into the first cell $q_0(t)$ are randomly generated heterogeneous free flow. We used three scenarios with different traffic density ranges, light traffic $[\sigma/5, \sigma]$, medium traffic $[\sigma/3, \sigma]$ and heavy traffic $[\sigma/2, \sigma]$, resulting in average traffic density of 0.6σ, 0.66σ and 0.75σ respectively.

We are comparing three different control laws:

- **Control law (1):** The optimal reference speeds are calculated by solving (5.14) once at $t = t_{20}$, ignoring traffic conditions.

- **Control law (2):** The optimal reference speeds are calculated by solving (5.14) periodically during the catch-up phase, ignoring traffic conditions,

- **Control law (3):** The optimal reference speeds are calculated by solving (5.17) periodically during the catch-up phase, taking traffic conditions into account.

We also considered the case when some disturbance is acting on the vehicles. Namely, at a random time instant between 5 and 10 minutes after the catch-up has begun, we decrease the speed of the follower vehicle by 20km/h for 10 minutes. This delays the platoon merging and would result in lower energy savings, so recalculating optimal speeds is required. Examples of simulation runs without and with follower speed disturbance are shown in Figure 5.11 and Figure 5.12. Vehicles forming a platoon are shown in traffic plots by red lines. Dashed black lines represent

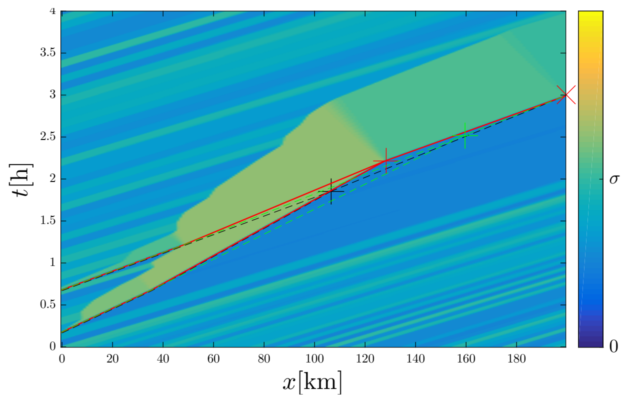

(a) Control law (2)

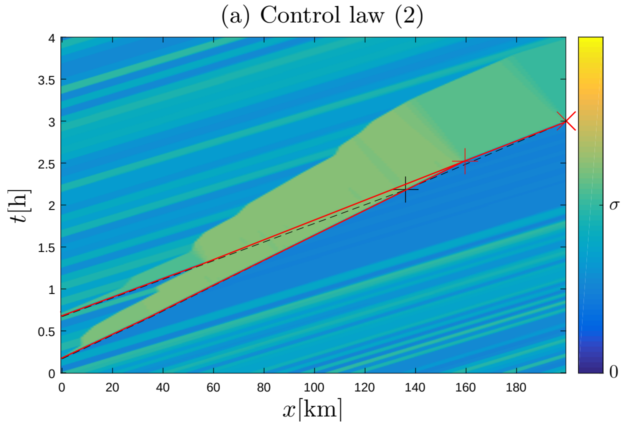

(b) Control law (3)

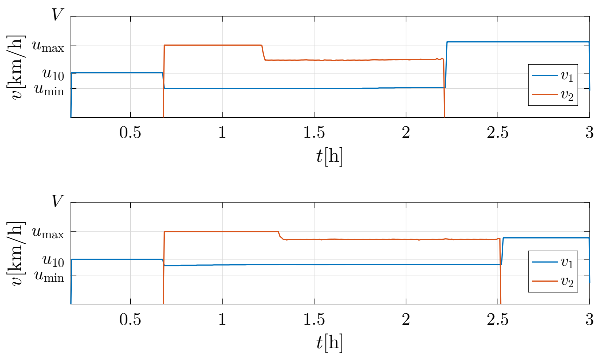

(c) Speed profiles under control law (2) (top) and (3) (bottom)

Figure 5.11: Traffic situation (subfigures (a) and (b)) and speed profiles (c) of one simulation run with no disturbances. Attempting to form a platoon using control law (2) led to an increase in energy cost by 0.71636%, whereas the control law (3) achieved energy savings of 0.50955%.

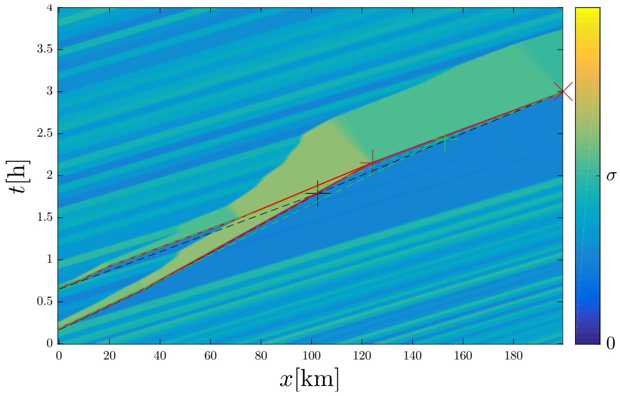

(a) Control law (2)

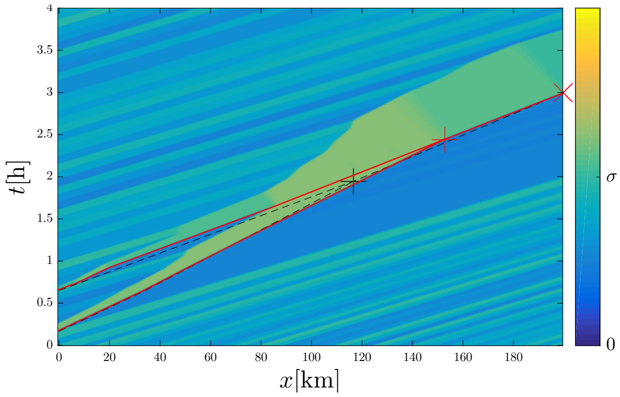

(b) Control law (3)

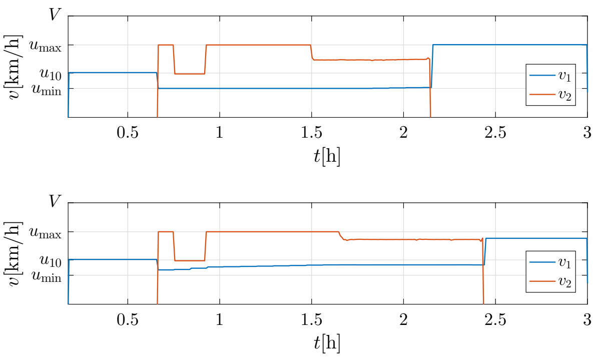

(c) Speed profiles under control law (2) (top) and (3) (bottom)

Figure 5.12: Traffic situation (subfigures (a) and (b)) and speed profiles (c) of one simulation run with follower speed disturbance. Attempting to form a platoon using control law (2) led to an increase in energy cost by 0.48012%, whereas the control law (3) achieved energy savings of 0.32183%.

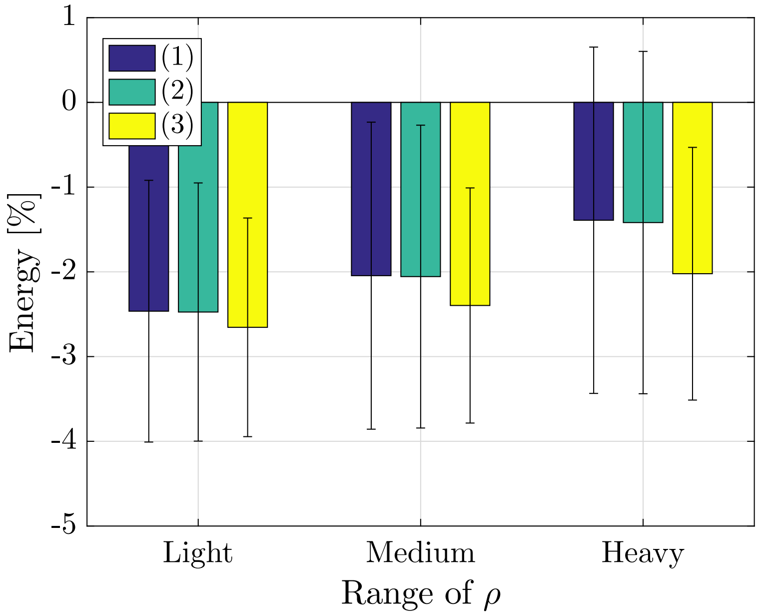

Figure 5.13: Relative energy consumption change with no disturbances.

ρ	(1)	(2)	(3)
Light	-2.4642%	-2.4741%	-2.6547%
Medium	-2.0452%	-2.0559%	-2.3969%
Heavy	-1.3909%	-1.4183%	-2.0220%

merging vehicles' trajectories if they would not be slowed down by the traffic, and dashed green lines in traffic plots for control law (2) represent the trajectories that would be followed if control law (3) was used instead. Crosses mark the position and time at which the platoon merge occurred.

The average energy savings are shown in Fig. 5.13 and Fig. 5.14. We can see that using control laws that take traffic conditions into consideration improves average energy savings, especially in heavy traffic.

In addition to calculating optimal catch-up speeds, this approach can also be used to predict when attempting to form a platoon is not beneficial. In Table 5.2 we see the number of "bad platooning attempts", i.e. in how many simulation runs the vehicles failed to reach the goal position in time, or had higher overall energy cost. If the calculated optimal catch-up speeds are such that platoon merging is predicted to occur very close to the end of the common road segment x_f, we know that attempting to form a platoon will not yield fuel savings, and may abandon the

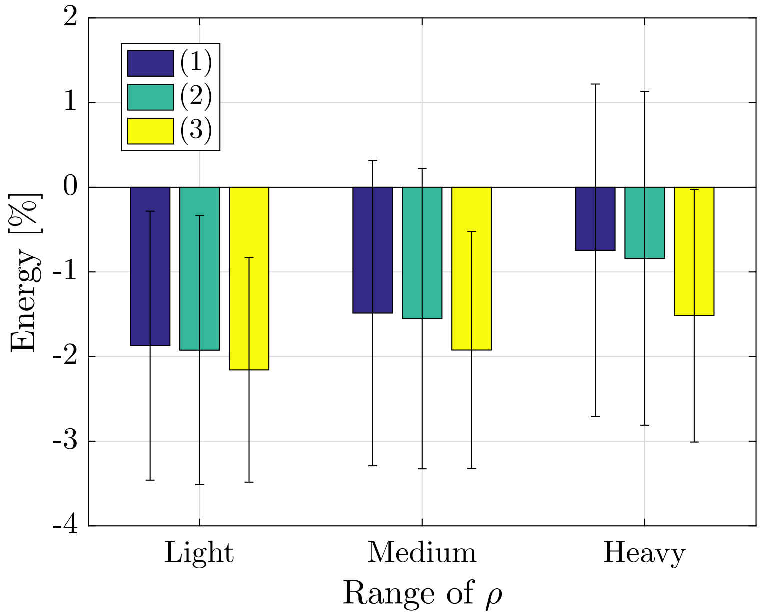

Figure 5.14: Relative energy consumption change with a disturbance.

ρ	(1)	(2)	(3)
Light	-1.8712%	-1.9245%	-2.1577%
Medium	-1.4860%	-1.5536%	-1.9228%
Heavy	-0.7458%	-0.8396%	-1.5171%

attempt at the start, instead continuing driving at vehicles' own optimal speeds. We also see the number of times the algorithm correctly predicted this outcome (true positive), which could be used to pre-emptively abort the platooning attempt, as well as the number of times the bad outcome was not predicted (false negative) and falsely predicted (false positive).

5.5 Summary

Optimal platoon formation coordination is a complex problem, even when considering only a single pair of vehicles attempting to catch-up and form a platoon. In this case, the difficulties come from a large number of potential disturbances from the environment that can disrupt the process.

Selecting correct catch-up speeds for the vehicles is important because failing to do so might result in higher fuel consumptions. Even deciding whether the vehicles

Table 5.2: Bad platooning attempt prediction.

	Light	Medium	Heavy
Total bad attempts	5	15	23
Correctly predicted	5	14	19
Not predicted	0	1	4
Falsely predicted	6	3	1

should attempt to platoon at all should be influenced by what kind of disturbances from the environment we might experience.

It is therefore important to have a good prediction model, for the merging vehicle trajectories in the catch-up process. Using this model, we tested different catch-up speed pairs and select the optimal one. Having predicted vehicle trajectories also enabled us to detect when the vehicles are deviating from the plan, and take appropriate actions to correct them.

It is clear that traffic conditions can play a significant role in the platoon catch-up phase, and that they cannot be ignored if we want to make a good prediction. By using the moving bottleneck framework, we were able to anticipate the effect the congestion formed upstream of the leader vehicle will have on the follower vehicle. This allowed us to calculate energy-optimal catch-up speeds, as well as to decide when platooning should be attempted.

Chapter 6

Conclusion and future work

Finally, in this chapter we conclude the thesis. In Section 6.1 we summarize and discuss the presented results, and in Section 6.2 outline some possible extensions and future work on the considered topic.

6.1 Conclusions

The central question of this thesis was how can we influence the overall traffic by using only a small portion of vehicles that we have direct control over. In accordance with that, the overarching theme of this thesis is dealing with mixed traffic consisting of some form of automated vehicles and human-driven vehicles in macroscopic framework. We studied how the interaction between these two classes of vehicles can be modelled, and what effects may arise from it. The situation of particular importance and interest was when the fraction of automated vehicles, that can be controlled from the infrastructure in some way, is small. This corresponds to the situation that we can expect to have in the near future, until autonomous vehicles achieve higher market penetration rate.

The question that this thesis aimed to answer is how to use these few directly controllable vehicles to improve the traffic situation, as well as how to take the influence of traffic into account when planning these vehicles' own operations. If we assume that the vehicles in question are moving slower than the rest of the traffic, one good way of modelling them macroscopically is to consider them moving bottlenecks. This assumption is well founded, since human drivers are inclined to try to maximize their speed, especially in congested traffic. By decreasing the speed of the directly controlled vehicle, we can create a controlled congestion, giving us the ability to control the traffic flow.

This effect was examined in the framework of PDE traffic models, and a way of including it into the cell transmission model (CTM) was proposed. Because of the correspondence between the CTM and the PDE model, the addition was done consistently, and without superfluous assumptions. Additionally, a multi-class

CTM was introduced and discussed, and then used to model vehicle platoons. This enabled us to use these platoons as moving bottlenecks, implementing a similar control law in this model as in the framework of CTM with moving bottlenecks. Even if platoons are not formed a priori, we can apply a different control law to first organize the vehicles into clusters, and then use them for traffic control as moving bottlenecks.

With such models available, we studied the problem of congestion wave dissipation and avoidance. From the perspective of the controlled vehicle, the control objective was to avoid the congestion wave with minimum delay, while also helping dissipate it quicker. The designed control law was shown to achieve good results, successfully avoiding the traffic jam with low delay, while also improving the overall traffic situation. The traffic density was made more homogeneous, with average total variation of traffic density reduced by over 5%, while the throughput was kept at a similar level, with total travel time increases by only 1%.

The CTM with moving bottlenecks also allowed us to take the influence of traffic into account when planning platoon formation while driving on the road. The simple case of two vehicles, one leading and one following, attempting to catch-up and form a platoon while driving on the road was studied. Since the leading vehicle has to slow down, it can cause a zone of congestion to form upstream of it, so the following vehicle is likely to encounter heavier traffic, which might render it impossible for it to follow its optimal calculated trajectory. Instead, the proposed model was used to take the traffic conditions, and this effect, into account, yielding a further reduction of energy cost of up to 0.5% in simulations compared to the case when we ignore the effect of traffic. This approach has an additional benefit of being able to indicate when attempting to form a platoon would not yield improvements in fuel consumption, and thus prevent unnecessary deviations from vehicles' individual plans. We are able to predict when attempting to form a platoon will result in no energy savings in approximately 80% of cases.

6.2 Future work

In the work presented in this thesis, we only used single vehicles as actuators. Considering multiple controlled vehicles, or even having direct control over a small portion of all vehicles participating in traffic is a logical next step. Platoons and moving bottlenecks can be represented in multi-class CTM in a way that is consistent with CTM with moving bottlenecks and PDE traffic models, as described in Chapter 3. It is straightforward to extend the results and control laws presented in Chapter 4 to this model. However, using the multi-class CTM offers additional possibilities for control, where the vehicles that can be controlled from the infrastructures are first consolidated into clusters, which are then used for control through the mechanism of moving bottlenecks. Because of its nonlinear nature, this approach suffers much less from low penetration rates of controllable connected vehicles, compared to control approaches that are based on linearized traffic models. The preliminary traffic control results using the multi-class CTM are promising and this research direction will be explored next.

Possible use of the multi-class CTM is not limited to this particular control strategy. By assuming we can assign reference speeds to some vehicles, we may be able to model many complex situations where controllable connected vehicles are used to improve the traffic situation. Many of such problems, e.g. vehicle trajectory optimization at a signalized intersection or bottleneck decongestion, have been approached in a microscopic traffic model setting, which may be problematic due to having to simulate and consider large number of individual vehicles. However, the solutions often lead to emergent behaviours with clear spatio-temporal patterns, which may be captured by macroscopic models. By adapting these solutions, we might be able to achieve similar results by applying a more general control action to all vehicles within a spatio-temporal region, instead of calculating separate control for all individual vehicles, thus greatly improving the tractability of the problem.

There are plenty of other ways this work can be continued and extended. First, the presented CTM with moving bottlenecks lends itself to other extensions, in order to cover a wider array of platooning maneouvres. One of the maneouvres that can be covered include reordering the vehicles in a platoon, where the vehicles will overtake each other, causing an even more severe disturbance in traffic. This maneouvre could be important in order to equalize the benefits that the platooning vehicles experience, since the first vehicle in a platoon usually benefits less from platooning than do the vehicles following it. Additionally, the control strategy for platooning is derived for an aggregated macroscopic traffic model, and it would be beneficial to test it in microscopic simulations. In this way, we might be able to look specifically at lane-changing behaviour around the controlled vehicles, though these effects could also be examined using multi-lane multi-class macroscopic traffic models. Additionally, more complicated control problems can be tackled, with the added complexity stemming from, for example, including uncertain traffic information, dissipating multiple traffic jams, explicitly minimizing some traffic performance metric, or having different constraints on traffic and controlled vehicles.

Bibliography

[1] European Commission, *Roadmap to a Single European Transport Area: Towards a Competitive and Resource Efficient Transport System: White Paper.* Publications Office of the European Union, 2011.

[2] M. Barth and K. Boriboonsomsin, "Real-world carbon dioxide impacts of traffic congestion," *Transportation Research Record: Journal of the Transportation Research Board*, no. 2058, pp. 163–171, 2008.

[3] D. J. Fagnant and K. Kockelman, "Preparing a nation for autonomous vehicles: opportunities, barriers and policy recommendations," *Transportation Research Part A: Policy and Practice*, vol. 77, pp. 167–181, 2015.

[4] K. Dresner and P. Stone, "Multiagent traffic management: A reservation-based intersection control mechanism," in *Proceedings of the Third International Joint Conference on Autonomous Agents and Multiagent Systems-Volume 2.* IEEE Computer Society, 2004, pp. 530–537.

[5] J. Walker, "The self-driving car timeline – predictions from the top 11 global automakers," *Tech Emergence*, 2018.

[6] F. Dressler, H. Hartenstein, O. Altintas, and O. Tonguz, "Inter-vehicle communication: Quo vadis," *IEEE Communications Magazine*, vol. 52, no. 6, pp. 170–177, 2014.

[7] T. Litman, *Autonomous vehicle implementation predictions.* Victoria Transport Policy Institute Victoria, Canada, 2017.

[8] S. Shladover, D. Su, and X.-Y. Lu, "Impacts of cooperative adaptive cruise control on freeway traffic flow," *Transportation Research Record: Journal of the Transportation Research Board*, no. 2324, pp. 63–70, 2012.

[9] L. D. Baskar, B. De Schutter, and H. Hellendoorn, "Optimal routing for automated highway systems," *Transportation Research Part C: Emerging Technologies*, vol. 30, pp. 1–22, 2013.

[10] R. Nishi, A. Tomoeda, K. Shimura, and K. Nishinari, “Theory of jam-absorption driving,” *Transportation Research Part B: Methodological*, vol. 50, pp. 116–129, 2013.

[11] Z. He, L. Zheng, L. Song, and N. Zhu, “A jam-absorption driving strategy for mitigating traffic oscillations,” *IEEE Transactions on Intelligent Transportation Systems*, vol. 18, no. 4, pp. 802–813, 2017.

[12] S. Shellenbarger, “One driver can prevent a traffic jam,” *Wall Street Journal*, 2016.

[13] C. Bergenhem, S. Shladover, E. Coelingh, C. Englund, and S. Tsugawa, “Overview of platooning systems,” in *Proceedings of the 19th ITS World Congress*, Vienna, Austria, 2012.

[14] A. Alam, B. Besselink, V. Turri, J. Martensson, and K. H. Johansson, “Heavy-duty vehicle platooning for sustainable freight transportation: A cooperative method to enhance safety and efficiency,” *IEEE Control Systems*, vol. 35, no. 6, pp. 34–56, 2015.

[15] M. Čičić and K. H. Johansson, “Traffic regulation via individually controlled automated vehicles: a cell transmission model approach,” in *21st IEEE International Conference on Intelligent Transportation Systems (ITSC)*, Maui, US, 2018.

[16] M. Čičić and K. H. Johansson, “Energy-optimal platoon catch-up in traffic in moving bottleneck framework,” in *European Control Conference (ECC)*, Naples, Italy, 2019, Submitted.

[17] L. Jin, M. Čičič, S. Amin, and K. H. Johansson, “Modeling the impact of vehicle platooning on highway congestion: A fluid queuing approach,” in *Proceedings of the 21st International Conference on Hybrid Systems: Computation and Control (part of CPS Week)*. ACM, 2018, pp. 237–246.

[18] M. Čičić, K.-Y. Liang, and K. H. Johansson, “Platoon merging distance prediction using a neural network vehicle speed model,” *IFAC-PapersOnLine*, vol. 50, no. 1, pp. 3720–3725, 2017.

[19] A. de Palma and R. Lindsey, “Traffic congestion pricing methodologies and technologies,” *Transportation Research Part C: Emerging Technologies*, vol. 19, no. 6, pp. 1377–1399, 2011.

[20] D. Ettema, J. Knockaert, and E. Verhoef, “Using incentives as traffic management tool: empirical results of the "peak avoidance" experiment,” *Transportation Letters*, vol. 2, no. 1, pp. 39–51, 2010.

[21] T. Roughgarden, "On the severity of braess's paradox: designing networks for selfish users is hard," *Journal of Computer and System Sciences*, vol. 72, no. 5, pp. 922–953, 2006.

[22] A. A. Kurzhanskiy and P. Varaiya, "Traffic management: An outlook," *Economics of Transportation*, vol. 4, no. 3, pp. 135 – 146, 2015.

[23] A. Keimer, N. Laurent-Brouty, F. Farokhi, H. Signargout, V. Cvetkovic, A. M. Bayen, and K. H. Johansson, "Information patterns in the modeling and design of mobility management services," *Proceedings of the IEEE*, vol. 106, no. 4, pp. 554–576, 2018.

[24] M. Papageorgiou, E. Kosmatopoulos, and I. Papamichail, "Effects of variable speed limits on motorway traffic flow," *Transportation Research Record: Journal of the Transportation Research Board*, no. 2047, pp. 37–48, 2008.

[25] M. Wang, W. Daamen, S. P. Hoogendoorn, and B. Van Arem, "Connected variable speed limits control and car-following control with vehicle-infrastructure communication to resolve stop-and-go waves," *Journal of Intelligent Transportation Systems*, vol. 20, no. 6, pp. 559–572, 2016.

[26] Y. Zhang and P. A. Ioannou, "Combined variable speed limit and lane change control for highway traffic," *IEEE Transactions on Intelligent Transportation Systems*, vol. 18, no. 7, pp. 1812–1823, 2017.

[27] M. Papageorgiou and A. Kotsialos, "Freeway ramp metering: An overview," *IEEE transactions on intelligent transportation systems*, vol. 3, no. 4, pp. 271–281, 2002.

[28] G. Gomes and R. Horowitz, "Optimal freeway ramp metering using the asymmetric cell transmission model," *Transportation Research Part C: Emerging Technologies*, vol. 14, no. 4, pp. 244–262, 2006.

[29] L. D. Baskar, B. De Schutter, J. Hellendoorn, and Z. Papp, "Traffic control and intelligent vehicle highway systems: a survey," *IET Intelligent Transport Systems*, vol. 5, no. 1, pp. 38–52, 2011.

[30] R. C. Carlson, I. Papamichail, M. Papageorgiou, and A. Messmer, "Optimal motorway traffic flow control involving variable speed limits and ramp metering," *Transportation Science*, vol. 44, no. 2, pp. 238–253, 2010.

[31] A. Hegyi, B. De Schutter, and H. Hellendoorn, "Model predictive control for optimal coordination of ramp metering and variable speed limits," *Transportation Research Part C: Emerging Technologies*, vol. 13, no. 3, pp. 185–209, 2005.

[32] X.-Y. Lu, P. Varaiya, R. Horowitz, D. Su, and S. Shladover, "Novel freeway traffic control with variable speed limit and coordinated ramp metering," *Transportation Research Record: Journal of the Transportation Research Board*, no. 2229, pp. 55–65, 2011.

[33] A. Festag, "Cooperative intelligent transport systems standards in europe," *IEEE communications magazine*, vol. 52, no. 12, pp. 166–172, 2014.

[34] K. Sjoberg, P. Andres, T. Buburuzan, and A. Brakemeier, "Cooperative intelligent transport systems in europe: current deployment status and outlook," *IEEE Vehicular Technology Magazine*, vol. 12, no. 2, pp. 89–97, 2017.

[35] A. Vinel, L. Lan, and N. Lyamin, "Vehicle-to-vehicle communication in C-ACC/platooning scenarios," *IEEE Communications Magazine*, vol. 53, no. 8, pp. 192–197, 2015.

[36] V. Milanés, S. E. Shladover, J. Spring, C. Nowakowski, H. Kawazoe, and M. Nakamura, "Cooperative adaptive cruise control in real traffic situations." *IEEE Transactions on Intelligent Transportation Systems*, vol. 15, no. 1, pp. 296–305, 2014.

[37] J. C. Herrera, D. B. Work, R. Herring, X. J. Ban, Q. Jacobson, and A. M. Bayen, "Evaluation of traffic data obtained via GPS-enabled mobile phones: The mobile century field experiment," *Transportation Research Part C: Emerging Technologies*, vol. 18, no. 4, pp. 568–583, 2010.

[38] C. De Fabritiis, R. Ragona, and G. Valenti, "Traffic estimation and prediction based on real time floating car data," in *11th International IEEE Conference on Intelligent Transportation Systems (ITSC)*. IEEE, 2008, pp. 197–203.

[39] T. Kim and K. Jerath, "Mitigation of self-organized traffic jams using cooperative adaptive cruise control," in *International Conference on Connected Vehicles and Expo (ICCVE)*. IEEE, 2016, pp. 7–12.

[40] A. Askari, D. A. Farias, A. A. Kurzhanskiy, and P. Varaiya, "Effect of adaptive and cooperative adaptive cruise control on throughput of signalized arterials," in *Intelligent Vehicles Symposium (IV)*. IEEE, 2017, pp. 1287–1292.

[41] M. Treiber and A. Kesting, "Traffic flow dynamics," *Traffic Flow Dynamics: Data, Models and Simulation, Springer-Verlag Berlin Heidelberg*, 2013.

[42] S. P. Hoogendoorn and P. H. Bovy, "State-of-the-art of vehicular traffic flow modelling," *Proceedings of the Institution of Mechanical Engineers, Part I: Journal of Systems and Control Engineering*, vol. 215, no. 4, pp. 283–303, 2001.

[43] A. Ferrara, S. Sacone, and S. Siri, *Freeway Traffic Modelling and Control*. Springer, 2018.

[44] F. van Wageningen-Kessels, H. Van Lint, K. Vuik, and S. Hoogendoorn, "Genealogy of traffic flow models," *EURO Journal on Transportation and Logistics*, vol. 4, no. 4, pp. 445–473, 2015.

[45] D. C. Gazis, R. Herman, and R. W. Rothery, "Nonlinear follow-the-leader models of traffic flow," *Operations research*, vol. 9, no. 4, pp. 545–567, 1961.

[46] P. G. Gipps, "A behavioural car-following model for computer simulation," *Transportation Research Part B: Methodological*, vol. 15, no. 2, pp. 105–111, 1981.

[47] M. Treiber, A. Hennecke, and D. Helbing, "Congested traffic states in empirical observations and microscopic simulations," *Physical review E*, vol. 62, no. 2, p. 1805, 2000.

[48] A. Kesting, M. Treiber, and D. Helbing, "Enhanced intelligent driver model to access the impact of driving strategies on traffic capacity," *Philosophical Transactions of the Royal Society of London A: Mathematical, Physical and Engineering Sciences*, vol. 368, no. 1928, pp. 4585–4605, 2010.

[49] F. Wu and D. B. Work, "Connections between classical car following models and artificial neural networks," in *21st IEEE International Conference on Intelligent Transportation Systems (ITSC)*, Maui, US, 2018.

[50] J. Barceló and J. Casas, "Dynamic network simulation with aimsun," in *Simulation approaches in transportation analysis.* Springer, pp. 57–98.

[51] M. Fellendorf, "Vissim: A microscopic simulation tool to evaluate actuated signal control including bus priority," in *64th Institute of Transportation Engineers Annual Meeting.* Springer, 1994, pp. 1–9.

[52] M. Behrisch, L. Bieker, J. Erdmann, and D. Krajzewicz, "Sumo–simulation of urban mobility," in *The Third International Conference on Advances in System Simulation (SIMUL), Barcelona, Spain*, vol. 42, 2011.

[53] S. Ossen and S. P. Hoogendoorn, "Heterogeneity in car-following behavior: Theory and empirics," *Transportation research part C: emerging technologies*, vol. 19, no. 2, pp. 182–195, 2011.

[54] S. Benzoni-Gavage and R. M. Colombo, "An n-populations model for traffic flow," *European Journal of Applied Mathematics*, vol. 14, no. 5, pp. 587–612, 2003.

[55] S. P. Hoogendoorn and P. H. Bovy, "Continuum modeling of multiclass traffic flow," *Transportation Research Part B: Methodological*, vol. 34, no. 2, pp. 123–146, 2000.

[56] M. W. Levin and S. D. Boyles, “A multiclass cell transmission model for shared human and autonomous vehicle roads,” *Transportation Research Part C: Emerging Technologies*, vol. 62, pp. 103–116, 2016.

[57] S. Logghe and L. H. Immers, “Multi-class kinematic wave theory of traffic flow,” *Transportation Research Part B: Methodological*, vol. 42, no. 6, pp. 523–541, 2008.

[58] J. Van Lint, S. Hoogendoorn, and M. Schreuder, “Fastlane: New multiclass first-order traffic flow model,” *Transportation Research Record: Journal of the Transportation Research Board*, no. 2088, pp. 177–187, 2008.

[59] S. Fan and D. B. Work, “A heterogeneous multiclass traffic flow model with creeping,” *SIAM Journal on Applied Mathematics*, vol. 75, no. 2, pp. 813–835, 2015.

[60] P. Bagnerini and M. Rascle, “A multiclass homogenized hyperbolic model of traffic flow,” *SIAM journal on mathematical analysis*, vol. 35, no. 4, pp. 949–973, 2003.

[61] M. Wright, G. Gomes, R. Horowitz, and A. A. Kurzhanskiy, “A new model for multi-commodity macroscopic modeling of complex traffic networks,” *arXiv preprint arXiv:1509.04995*, 2015.

[62] R. E. Stern, S. Cui, M. L. D. Monache, R. Bhadani, M. Bunting, M. Churchill, N. Hamilton, R. Haulcy, H. Pohlmann, F. Wu, B. Piccoli, B. Seibold, J. Sprinkle, and D. B. Work, “Dissipation of stop-and-go waves via control of autonomous vehicles: Field experiments,” *Transportation Research Part C: Emerging Technologies*, vol. 89, pp. 205 – 221, 2018.

[63] S. Cui, B. Seibold, R. Stern, and D. B. Work, “Stabilizing traffic flow via a single autonomous vehicle: Possibilities and limitations,” in *Intelligent Vehicles Symposium (IV)*. IEEE, 2017, pp. 1336–1341.

[64] Y. Sugiyama, M. Fukui, M. Kikuchi, K. Hasebe, A. Nakayama, K. Nishinari, S.-i. Tadaki, and S. Yukawa, “Traffic jams without bottlenecks–experimental evidence for the physical mechanism of the formation of a jam,” *New journal of physics*, vol. 10, no. 3, p. 033001, 2008.

[65] M. R. Flynn, A. R. Kasimov, J.-C. Nave, R. R. Rosales, and B. Seibold, “Self-sustained nonlinear waves in traffic flow,” *Physical Review E*, vol. 79, no. 5, p. 056113, 2009.

[66] J.-P. Lebacque, J. Lesort, and F. Giorgi, “Introducing buses into first-order macroscopic traffic flow models,” *Transportation Research Record: Journal of the Transportation Research Board*, no. 1644, pp. 70–79, 1998.

[67] C. Lattanzio, A. Maurizi, and B. Piccoli, “Moving bottlenecks in car traffic flow: a pde-ode coupled model,” *SIAM Journal on Mathematical Analysis*, vol. 43, no. 1, pp. 50–67, 2011.

[68] M. L. Delle Monache and P. Goatin, “A front tracking method for a strongly coupled pde-ode system with moving density constraints in traffic flow,” *Discrete and Continuous Dynamical Systems-Series S*, vol. 7, no. 3, pp. 435–447, 2014.

[69] M. D. Simoni and C. G. Claudel, “A fast simulation algorithm for multiple moving bottlenecks and applications in urban freight traffic management,” *Transportation Research Part B: Methodological*, vol. 104, pp. 238–255, 2017.

[70] J. C. Muñoz and C. F. Daganzo, “Moving bottlenecks: a theory grounded on experimental observation,” *15th International Symposium on Transportation and Traffic Theory*, pp. 441–462, 2002.

[71] C. F. Daganzo and J. A. Laval, “On the numerical treatment of moving bottlenecks,” *Transportation Research Part B: Methodological*, vol. 39, no. 1, pp. 31–46, 2005.

[72] A. Aw and M. Rascle, “Resurrection of" second order" models of traffic flow,” *SIAM journal on applied mathematics*, vol. 60, no. 3, pp. 916–938, 2000.

[73] M. Papageorgiou, J.-M. Blosseville, and H. Hadj-Salem, “Modelling and real-time control of traffic flow on the southern part of boulevard peripherique in paris: Part I: Modelling,” *Transportation Research Part A: General*, vol. 24, no. 5, pp. 345–359, 1990.

[74] G. Piacentini, P. Goatin, and A. Ferrara, “Traffic control via moving bottleneck of coordinated vehicles,” in *15th IFAC symposium on control in transportation systems*, 2018.

[75] E. Vinitsky, K. Parvatey, A. Kreidiehz, C. Wu, and A. Bayen, “Lagrangian control through deep-rl: Applications to bottleneck decongestion,” in *21st IEEE International Conference on Intelligent Transportation Systems (ITSC)*, Maui, US, 2018.

[76] H. L. Humphreys, J. Batterson, D. Bevly, and R. Schubert, “An evaluation of the fuel economy benefits of a driver assistive truck platooning prototype using simulation,” SAE Technical Paper, Tech. Rep., 2016.

[77] R. Horowitz and P. Varaiya, “Control design of an automated highway system,” *Proceedings of the IEEE*, vol. 88, no. 7, pp. 913–925, 2000.

[78] M. E. Khatir and E. J. Davison, “Decentralized control of a large platoon of vehicles using non-identical controllers,” in *Proceedings of the American Control Conference*, vol. 3. Portland, US: IEEE, 2004, pp. 2769–2776.

[79] V. Turri, B. Besselink, J. Mårtensson, and K. H. Johansson, "Fuel-efficient heavy-duty vehicle platooning by look-ahead control," in *53rd IEEE Conference on Decision and Control (CDC)*. Los Angeles, US: IEEE, 2014, pp. 654–660.

[80] J. Ploeg, D. P. Shukla, N. van de Wouw, and H. Nijmeijer, "Controller synthesis for string stability of vehicle platoons," *IEEE Transactions on Intelligent Transportation Systems*, vol. 15, no. 2, pp. 854–865, 2014.

[81] A. K. Bhoopalam, N. Agatz, and R. Zuidwijk, "Planning of truck platoons: A literature review and directions for future research," *Transportation Research Part B: Methodological*, 2017.

[82] S. van de Hoef, K. H. Johansson, and D. V. Dimarogonas, "Fuel-efficient en route formation of truck platoons," *IEEE Transactions on Intelligent Transportation Systems*, vol. 19, no. 1, pp. 102–112, 2018.

[83] K.-Y. Liang, J. Mårtensson, and K. H. Johansson, "When is it fuel efficient for a heavy duty vehicle to catch up with a platoon?" *IFAC Proceedings Volumes*, vol. 46, no. 21, pp. 738–743, 2013.

[84] K.-Y. Liang, J. Mårtensson, and K. H. Johansson, "Experiments on platoon formation of heavy trucks in traffic," in *19th IEEE International Conference on Intelligent Transportation Systems (ITSC)*, Nov 2016, pp. 1813–1819.

[85] M. Saeednia and M. Menendez, "Analysis of strategies for truck platooning: Hybrid strategy," *Transportation Research Record: Journal of the Transportation Research Board*, no. 2547, pp. 41–48, 2016.

[86] W. Zhang, E. Jenelius, and X. Ma, "Freight transport platoon coordination and departure time scheduling under travel time uncertainty," *Transportation Research Part E: Logistics and Transportation Review*, vol. 98, pp. 1–23, 2017.

[87] K.-Y. Liang, Q. Deng, J. Mårtensson, X. Ma, and K. H. Johansson, "The influence of traffic on heavy-duty vehicle platoon formation," in *Intelligent Vehicles Symposium (IV)*. Seoul, Korea: IEEE, 2015, pp. 150–155.

[88] M. J. Lighthill and G. B. Whitham, "On kinematic waves II. a theory of traffic flow on long crowded roads," *Proc. R. Soc. Lond. A*, vol. 229, no. 1178, pp. 317–345, 1955.

[89] P. I. Richards, "Shock waves on the highway," *Operations research*, vol. 4, no. 1, pp. 42–51, 1956.

[90] B. Greenshields, W. Channing, H. Miller *et al.*, "A study of traffic capacity," in *Highway research board proceedings*, vol. 1935. National Research Council (USA), Highway Research Board, 1935.

[91] C. F. Daganzo, "The cell transmission model: A dynamic representation of highway traffic consistent with the hydrodynamic theory," *Transportation Research Part B: Methodological*, vol. 28, no. 4, pp. 269–287, 1994.

[92] G. F. Newell, "A simplified theory of kinematic waves in highway traffic, part i: General theory," *Transportation Research Part B: Methodological*, vol. 27, no. 4, pp. 281–287, 1993.

[93] P. D. Lax, "Nonlinear hyperbolic equations," *Communications on Pure and Applied Mathematics*, vol. 6, no. 2, pp. 231–258, 1953.

[94] H. Holden and N. H. Risebro, *Front tracking for hyperbolic conservation laws.* Springer, 2015, vol. 152.

[95] C. F. Daganzo, "The cell transmission model, part ii: network traffic," *Transportation Research Part B: Methodological*, vol. 29, no. 2, pp. 79–93, 1995.

[96] J.-P. Lebacque, "The Godunov scheme and what it means for first order traffic flow models," *Proceedings of the 13th International Symposium on Transportation and Traffic Theory*, pp. 647–677, 1996.

[97] K. Fadhloun, H. Rakha, and A. Loulizi, "Analysis of moving bottlenecks considering a triangular fundamental diagram," *International journal of transportation science and technology*, vol. 5, no. 3, pp. 186–199, 2016.

[98] C. C. de Wit and A. Ferrara, "A variable-length cell road traffic model: application to ring road speed limit optimization," in *55th IEEE Conference on Decision and Control (CDC)*, 2016.

[99] A. Hegyi, S. Hoogendoorn, M. Schreuder, H. Stoelhorst, and F. Viti, "SPECIALIST: A dynamic speed limit control algorithm based on shock wave theory," in *11th IEEE International IEEE Conference on Intelligent Transportation Systems (ITSC).* IEEE, 2008, pp. 827–832.

[100] A. Alam, B. Besselink, V. Turri, J. Martensson, and K. H. Johansson, "Heavy-duty vehicle platooning for sustainable freight transportation: A cooperative method to enhance safety and efficiency," *IEEE Control Systems*, vol. 35, no. 6, pp. 34–56, Dec 2015.

[101] E. Hellström, M. Ivarsson, J. Åslund, and L. Nielsen, "Look-ahead control for heavy trucks to minimize trip time and fuel consumption," *Control Engineering Practice*, vol. 17, no. 2, pp. 245–254, 2009.

[102] V. Turri, B. Besselink, and K. H. Johansson, "Cooperative look-ahead control for fuel-efficient and safe heavy-duty vehicle platooning," *IEEE Transactions on Control Systems Technology*, vol. 25, no. 1, pp. 12–28, 2017.

[103] L. Guzzella, A. Sciarretta *et al.*, *Vehicle propulsion systems.* Springer, 2007, vol. 1.